NOAA Technical Report NOS OR&R 27

JOINT ANALYSIS GROUP, DEEPWATER HORIZON OIL SPILL:

REVIEW OF SUBSURFACE DISPERSED OIL AND OXYGEN LEVELS ASSOCIATED WITH THE DEEPWATER HORIZON MC252 SPILL OF NATIONAL SIGNIFICANCE

Silver Spring, Maryland

August 2012

U.S. Department of Commerce
National Oceanic and Atmospheric Administration
National Ocean Service

Mention of trade names or commercial products does not constitute endorsement or recommendation for their use by the United States Government.

Citation for this Report:

Joint Analysis Group, Deepwater Horizon Oil Spill (2012). Review of Subsurface Dispersed Oil and Oxygen Levels Associated with the Deepwater Horizon MC252 Spill of National Significance. NOAA Technical Report NOS OR&R 27, pp. 95. Joint Analysis Group, Deepwater Horizon Oil Spill.

Review of Subsurface Dispersed Oil and Oxygen Levels Associated with the Deepwater Horizon MC252 Spill of National Significance

NOAA Technical Report NOS OR&R 27

August 2012

U.S. DEPARTMENT OF COMMERCE
Rebecca M. Blank, Acting Secretary

National Oceanic and Atmospheric Administration
Dr. Jane Lubchenco
Under Secretary of Commerce for Oceans and
Atmosphere and NOAA Administrator

National Ocean Service
David Kennedy, Assistant Administrator for Ocean
Services and Coastal Zone Management

U.S. Department of Commerce
National Oceanic and Atmospheric Administration
National Ocean Service

Foreword

The National Incident Commander for the Deepwater Horizon Oil Spill established the Joint Analysis Group (JAG) for Surface and Subsurface Oceanography, Oil and Dispersant Data. Their mission was to examine the subsurface oceanographic data collected through the coordinated sampling efforts of vessels contracted for or owned by BP, the National Oceanic and Atmospheric Administration, and academic scientists. The JAG is comprised of scientists from the Environmental Protection Agency, the National Oceanic and Atmospheric Administration, the Bureau of Ocean Energy Management, and the White House Office of Science and Technology Policy, with additional information coordination and synthesis provided by BP and academic institutions.

The JAG performed three major tasks:

- Integrated the data both spatially and temporally to allow for their visualization and analysis
- Analyzed the data to describe the distribution of oil, the oceanographic processes that affected its transport, and its effect on subsurface oxygen levels.
- Issued periodic reports to the National Incident Command (NIC), the Unified Area Command, the public, and other researchers that included visualization, analysis, and synthesis products.

This Technical Report is one of a series of periodic reports released by the JAG.

Robert Haddad, Chief

NOAA National Ocean Service Assessment and Restoration

August 16, 2012

Executive Summary

The "Joint Analysis Group, Deepwater Horizon Oil Spill: Review Of Subsurface Dispersed Oil And Oxygen Levels Associated With The Deepwater Horizon MC252 Spill Of National Significance" provides the Federal OnScene Coordinator for the Deepwater Horizon MC252 Spill of National Significance with updated information on the location and transport of deep subsurface dispersed oil.

This report updates the reports previously published by the Deepwater Horizon Joint Analysis Group (JAG) using additional data gathered by researchers in the Gulf of Mexico from April 20 to November 12, 2010. Data collected from observations made in waters seaward of the continental shelf at depths >200 m were examined to determine the distribution and composition of deep subsurface dispersed oil, the oceanographic processes that affected its transport, and its impact on subsurface oxygen levels.

This report includes data from the following types of observations:

- In situ observations of conductivity, temperature, depth, and dissolved oxygen;
- In situ observations of fluorescence as measured by Colored Dissolved Organic Matter (CDOM) fluorometers and AQUAtracka fluorometers;
- In situ observations of ocean current speed and direction from Acoustic Doppler Current Profiler (ADCP) instruments;
- Laboratory chemical analysis of hydrocarbon levels in water samples collected concurrently with in situ observations.

The JAG accessed, compiled, and quality-controlled data collected under the auspices of the MC252 response from 1517 sampling stations used for in situ observations were obtained and from 6493 samples submitted for chemical analyses to produce a comprehensive, well-documented dataset available to the public in readily accessible formats. Those data are permanently archived and are available as documented in Appendix 1 of this report.

The JAG also considered physical and biochemical processes that affected MC252 oil transport and its fate in deep subsurface waters to provide a context for interpreting these data through detailed analysis, graphing, and mapping.

The analysis of data from observations and samples described in this report provides findings of interest to the Federal On-Scene Coordinator and others as they provide insight towards understanding the behavior of deep subsurface dispersed oil over the sampling period.

Key Findings

Data from the deep-water zone allowed the JAG to describe the horizontal and vertical extent of the deep subsurface dispersed oil and associated dissolved oxygen DO_2 depressions outside the immediate area of the well during the sampling period. These data were not adequate, however, to comprehensively characterize oil concentrations within the area where oil was found or to define the complex boundaries that delineated the horizontal extent of the oil.

Analyses of these data showed that the deep subsurface dispersed oil stayed mainly within one water layer as defined by density. Anomalies in DO_2 and oil measurements attributable to MC252 oil were found primarily between depths of 900 m and 1300 m. The oil components in this water layer contained both dissolved oil and small oil droplets. Measures of fluorescence and oil concentrations suggest that the deep dispersed oil did not experience significant buoyant rise or sinking beyond the initial release zone, but instead behaved as neutrally buoyant particles or as a dissolved material in the water.

The net movement of the deep dispersed oil was to the southwest away from the wellhead consistent with the prevailing currents at 900-m to 1300-m depths. The data considered in this report showed no evidence that these layers connected with the Florida Straits or with the shallower continental shelves along the Gulf of Mexico, suggesting that this oil remained within the deep basin of the Gulf.

Laboratory chemical analyses of oil in water samples were used to quantify the concentration and spatial extent of the deep subsurface dispersed oil. The analysis results allowed the JAG to assess the vertical and horizontal dimensions of the oil and to gain insight into concentration gradients created as the oil moved away from the wellhead. Volatile fraction hydrocarbons were found at significantly higher concentrations than semivolatile fraction hydrocarbons.

The highest concentration of volatile hydrocarbons detected in water between the depths of 900 m and 1300 m was 2112 parts per billion (ppb) found in a sample 1.2 km from the wellhead at Brooks McCall station 054. Beyond 20 km from the wellhead, volatile hydrocarbon concentrations were below 100 ppb and values beyond 100 km from the wellhead were below analytical method detection levels. The levels of semivolatile fraction hydrocarbons at depths between 900 m and 1300 m were primarily in the 1–10 ppb range at distances of >10 km from the well. The highest volatile hydrocarbon level in a water sample was 485 ppb also found at Brooks McCall station 054. Measurable amounts of semivolatile hydrocarbons were found 400 km from the wellhead; values above 10 ppb were found out to about 275 km.

The observed decreases in hydrocarbon concentrations were likely due to multiple factors, primarily dilution and biodegradation; other factors, such as particulate adsorption, could have also contributed to the decreases. The observations and analyses conducted as part of this effort were not sufficient to provide a quantitative estimate of the contribution that each process might have made to the observed oil concentrations.

Observations of DO_2 were useful for tracking deep subsurface dispersed oil. DO_2 were monitored from early in the response to address concerns about hypoxia (DO_2 levels of <1.4 mL/L or 2.0 mg/L) or anoxia resulting from biologically mediated oxidation of the deep subsurface oil. Depressions in DO_2 concentrations were associated with detected hydrocarbon concentrations. As distance from the wellhead increased and time passed, oil measurements from water sample analyses became less effective at detecting MC252 hydrocarbons in real time; however, the affected water mass could be followed by examining depressions in DO_2.

A DO_2 depression was consistently found in the waters between 900 m and 1300 m, but with the exception of one DO_2 profile, did not reach levels considered to be hypoxic. DO_2 depressions continued to be observed as distinct depressions at comparable magnitudes until mid-September 2010, even at hundreds of kilometers from the wellhead. A decrease in hydrocarbon concentrations associated with depressions in DO_2 concentrations was detected as distance from the wellhead increased. DO_2 anomalies did not decrease as quickly as the deep dispersed oil concentrations measured by both fluorescence and water sample analysis.

DO_2 observations—together with the presence of active hydrocarbon-consuming bacterial communities—suggested that biodegradation processes were actively consuming and mineralizing hydrocarbons. The JAG concluded that the oil underwent extensive oxidation, which was mediated by active hydrocarbon-consuming bacterial communities, with a simultaneous reduction in DO_2 at depth.

Acknowledgments

The JAG acknowledges the scientists, crews, and sponsors of the following ships and platforms for their efforts to collect the observations and samples supporting the data that are included in this report.

American Diver
M/V *Arctic*
R/V *Brooks McCall*
M/V *Bunny Bordelon*
R/V *Cape Hatteras*
Development Driller 3
Discoverer Enterprise
R/V *Endeavor*
R/V *Ferrel*
NOAA Ship *Gordon Gunter*
R/V *Gyre*
NOAA Ship *Henry Bigelow*
HOS Davis
R/V *Jack Fitz*
M/V *Meg L. Skansi*
NOAA Ship *Nancy Foster*
R/V *Ocean Veritas*
R/V *Pelican*
NOAA Ship *Pisces*
M/V *Rachel Bordelon*
Ram-Powell
Ryan Chouest
R/V *Seward Johnson*
Specialty Diver
NOAA Ship *Thomas Jefferson*
R/V *Walton Smith*
M/V *Wes Bordelon*

Contents

Joint Analysis Group: Review of Subsurface Dispersed Oil and Oxygen Levels Associated with the Deepwater Horizon MC252 Spill of National Significance

1 Introduction

This report is one of a series of documents published by the Joint Analysis Group (JAG). The purpose of these reports was to examine the location and transport of deep subsurface dispersed oil at the site of the Deepwater Horizon drilling rig explosion at the Macondo Prospect located in Mississippi Canyon Block 252, Well #1 (MC252), in the Gulf of Mexico (Joint Analysis Group, 2010a–d). Figure 1 depicts the site of the drilling rig in relation to the surrounding bathymetric features.

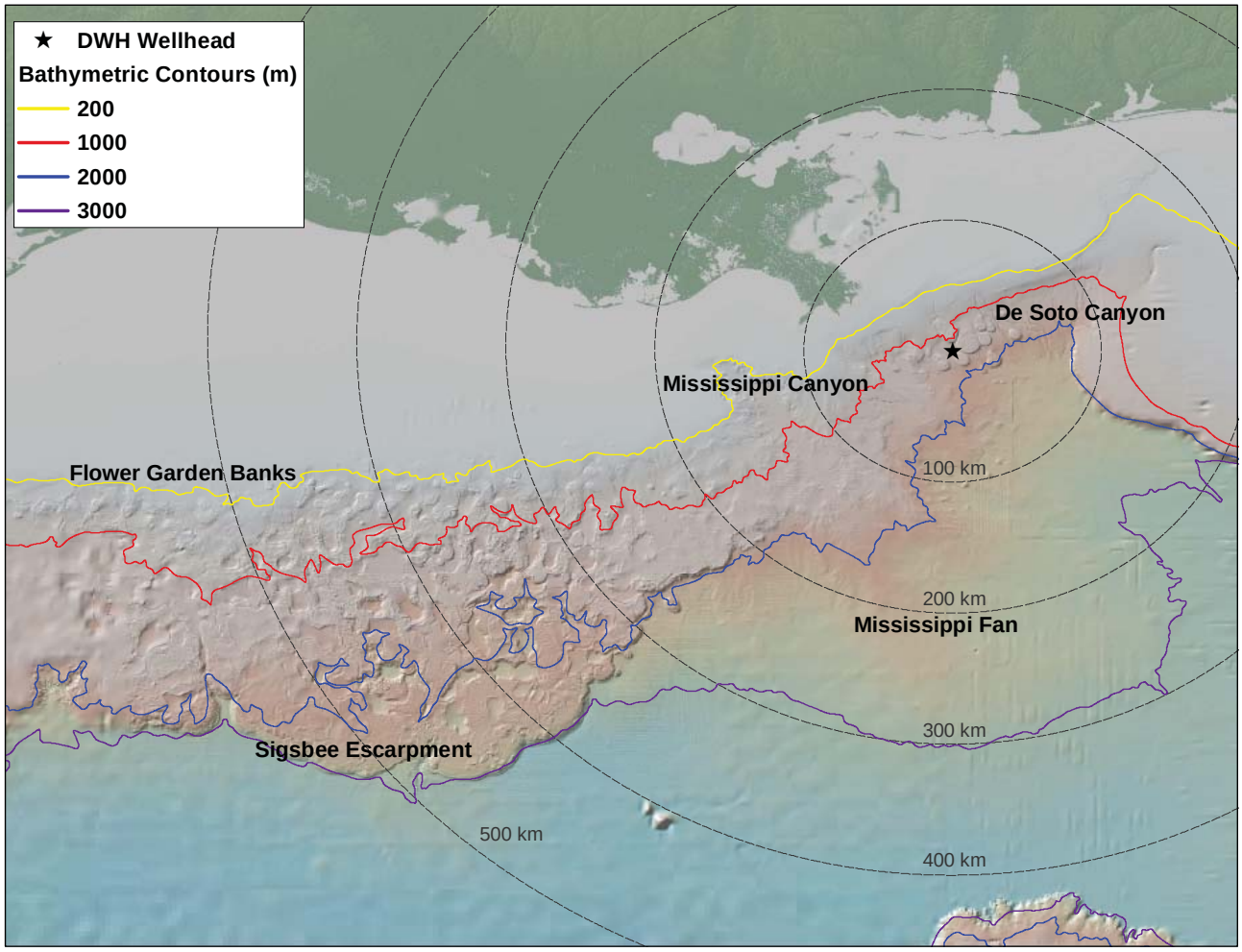

Figure 1. The site of the MC252 drilling rig is depicted as a black star, major geographic features in the region are also shown. Distances from the wellhead are shown in kilometers out to 500 km.

The JAG previously published reports and updates (Joint Analysis Group, 2010a–d) on various aspects of deepwater subsurface monitoring data. On March 11, 2011, the Federal On-Scene Coordinator gave approval for the JAG to extend their previous efforts by examining unreported data and completing a comprehensive report on deep subsurface dispersed oil. Previous reports addressed data collected and available to the JAG

between April 20 and July 15, 2010. This report extends analysis provided in previously published JAG reports including both data collected under the auspices of the response between April 20 and July 15, 2010, but not previously available and data collected between July 15, 2010 and November 12, 2010.

The JAG examined these new data in the context of previous JAG reports and reports by other researchers. Observations made in waters seaward of the continental shelf with depths >200 m were considered. This specific area was defined as the "deepwater" in the National Incident Commander "Strategic Plan for Sub-Sea and Sub-Surface Oil and Dispersant Detection, Sampling and Monitoring" (Zukunft, 2010).

This report includes data from the following types of observations:

- In situ observations of temperature, salinity, oxygen, and fluorescence as detected by CDOM (Colored or Chromophoric Dissolved Organic Matter) fluorometers and Chelsea Technologies AQUAtracka fluorometers deployed late in the sampling period.
- In situ analysis of dissolved oxygen (DO_2) levels;
- In situ observations of ocean currents from Acoustic Doppler Current Profiler (ADCP) instruments; and
- Laboratory chemical analysis of water samples collected concurrently with in situ observations.

The depth and behavior of the MC252 release, the complexity of local bathymetry and currents, and limitations of sampling, laboratory analysis, and data integration make it difficult to fully characterize the location and transport of oil in the deepwater areas. This report, rather than relying on any single type of measure, considers each of the available measures in conjunction with each other to provide a more comprehensive evaluation of deep subsurface dispersed oil conditions.

This report focuses on data collected below the naturally occurring oxygen minimum zone, which generally occurred between 350 m and 450 m in the northern and central Gulf of Mexico and between 550 m and 650 m in the southeast Gulf (see Jochens et al., 2005, their Table 4.5). In addition to the main report Appendices 1–6 list: (1) Data Accessibility, (2) Methods Used in Data Processing and Analysis, (3) Cruises with Water Chemistry Data and Associated Databases, (4) MC252 Reservoir Oil Composition, (5) Methods Used to Analyze Specific Compounds, and (6) Results of Comparisons of Field Duplicates from the Scribe Databases.

This report does not address samples collected in "nearshore" or "offshore" areas as defined in the National Incident Commander Sub-Sea and Sub-Surface Monitoring Strategy. The Operational Science Advisory Team (OSAT) previously reported on these data (Operational Science Advisory Team, 2010). This report does not consider data on oil in deepwater sediments, which were previously reported on by the OSAT (Operational Science Advisory Team, 2010).

2 Background

2.1 Well Release

The explosion and subsequent failure of the Deepwater Horizon drilling rig resulted in the release of a multiphase flow of oil and gas for 87 days until the well was successfully shut-in on July 15, 2010. The volume and characteristics of the flow from the well were subject to change over time—due in part to efforts to remove the damaged riser. Table 1 is a timeline of key events at the wellhead, based on U.S. Department of Energy information (Department of Energy, 2010).

Table 1. MC252 Selected Events Based on U.S. Department of Energy Key Events Timeline, July 28, 2010.

20 April	Explosion and fire; oil and gas flow up riser to ocean surface.
22 April	Rig sinks; oil and gas continue flowing into ocean from sunken riser on ocean bottom.
30 April	Subsea dispersant application begins.
05 May	One of three leaks stopped on broken riser.
08 May	Cofferdam containment system fails.
16 May	Riser Insertion Tube Tool (RITT) operational for recovering oil from riser to surface ship.
25 May	RITT removed.
26 May	Top Kill begins including pumping drilling mud into the well.
29 May	Top Kill ends, without success.
01 June	First shear cut to remove riser.
03 June	Second shear cut removes top of riser. Top Hat #4 in place.
04 June	First gas and oil to surface from Top Hat #4, received onboard the *Discoverer Enterprise*.
23 June	Temporary suspension of Cap containment operations.
10 July	Top Hat #4 Removed.
12 July	Flange removed - Spool Flange installed. 3-Ram Capping Stack landed/secured.
13 July	Shut-in operations initiated (1600). Shut-in terminated due to leak in choke line of stacking cap flow diverted to kill side of stack only (1748).
15 July	Subsea dispersant application ends. Well shut-in complete.

The Flow Rate Technical Group (FRTG) estimated that 4.9 million barrels of liquid petroleum hydrocarbon (pentane and higher molecular weight hydrocarbons) were released from the well (liquid petroleum fraction is hereafter referred to as “oil”) (McNutt et al., 2011). The FRTG also estimated that containment activities recovered 0.8 million barrels of oil before it was released into the Gulf of Mexico. The FRTG further investigated the ratio of liquid petroleum to natural gas (natural gas, condensates, and nonhydrocarbon gases) in the release (natural gas fraction is hereafter referred to as “gas”).

As part of the FRTG’s work, the Woods Hole Oceanographic Institution sampled flow at the wellhead on June 20, 2010, and found that the oil fraction comprised 43.7% of the bulk flow by volume (McNutt et al., 2011).

The dispersion of liquid oil at the wellhead was altered by the application of 18,364 barrels of chemical dispersant to the flow at the wellhead between April 30 and July 15 (Federal Interagency Solutions Group,

2010). The Oil Budget Calculator Science and Engineering Team estimated that 1.3 million barrels[1] of oil from the leaking well were horizontally distributed in deep subsurface waters as a result of natural dispersion and the added chemical dispersants.

Figure 2 uses estimates from the Oil Budget Calculator Science and Engineering Team to show the daily volumes of oil released into the Gulf of Mexico, the estimated fraction of oil dispersed in deep subsurface waters, and the volume of subsurface dispersant applied (Federal Interagency Solutions Group, 2010). A significant drop in the daily estimate of oil released into the environment can be seen between June 1 and June 8, 2010, which corresponded to the time when the riser was removed and Top Hat #4 was installed.

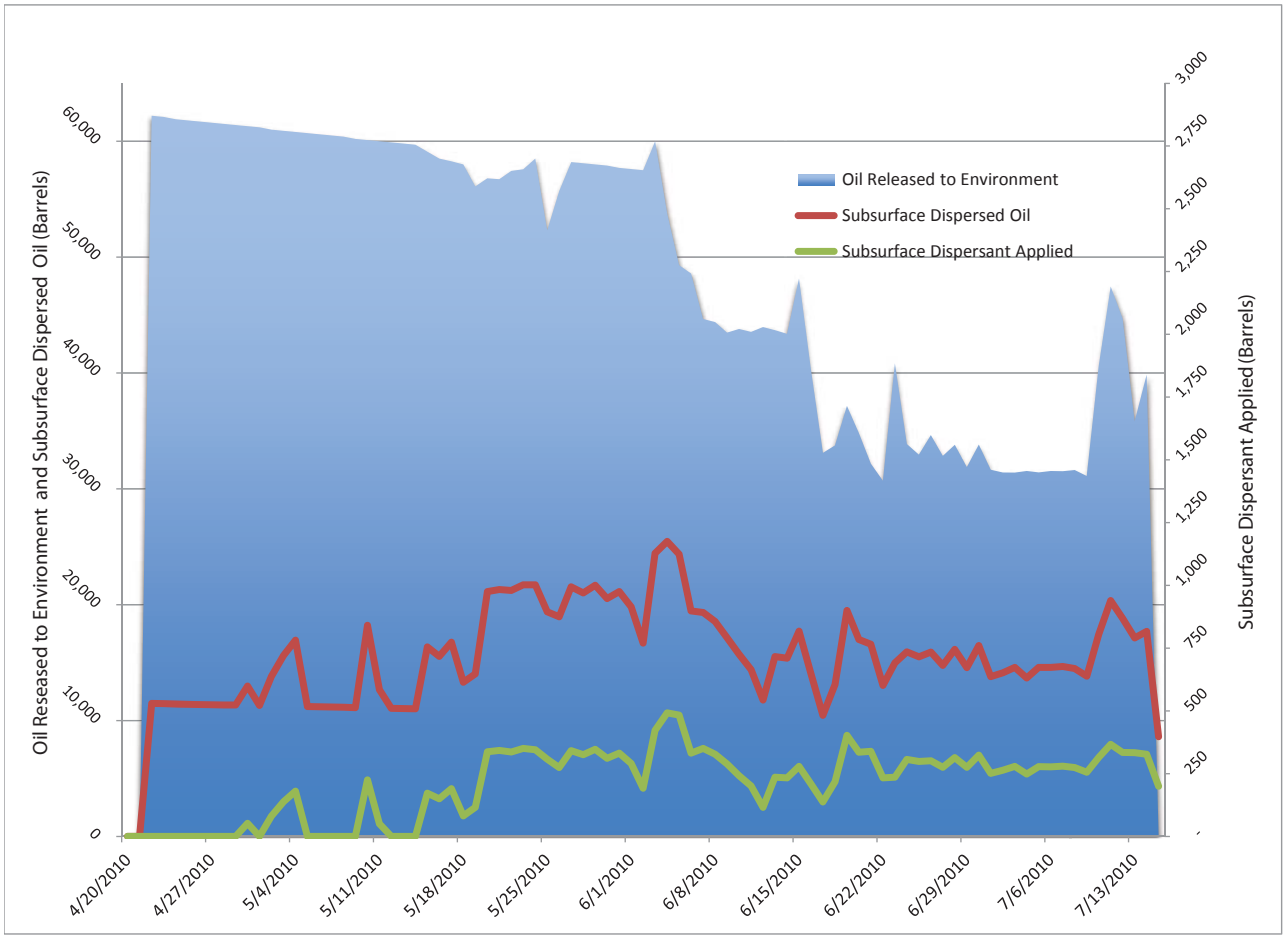

Figure 2. Daily volumes of net oil released, subsurface dispersed oil, and subsurface dispersant applied, based on estimates of the Oil Budget Calculator Science and Engineering Team (Federal Interagency Solutions Group, 2010).

1 Calculated as $V_{DB}(t) = V_{DC}(t) + V_{DN}(t)$, where V_{DB} is subsurface oil volume dispersed, V_{DC} is subsurface oil volume dispersed chemically, and V_{DN} is subsurface oil dispersed naturally on day t *(Federal Interagency Solutions Group, 2010)*.

2.2 Nature of MC252 Oil

The specific nature of the source oil dictates how the oil behaves when released in the environment. In particular, the oil's physical and chemical properties help to explain this behavior. Chemical composition is key to understanding how a specific sensor used in these analyses may or may not detect weathered oil. With this in mind, some of the salient properties of the Macondo Oil (MC252) are presented.

Using chemical separation techniques coupled with Iatroscan analyses (thin liquid chromatography/flame ionization detection; TLC/FD), the oil can be separated and quantified in terms of:

- *Saturates*: alkanes (e.g., hexane and decane), isoalkanes (e.g., isobutane and pristane), saturated cycloalkanes (e.g., cyclohexane and decalin).
- *Aromatics*: mono aromatic hydrocarbons (e.g., benzene), polycyclic aromatic hydrocarbons (e.g., naphthalene).
- *Resins*: high molecular weight highly condensed hydrocarbons (residual oil).
- *Asphaltenes*: larger high molecular weight highly condensed hydrocarbons (residual oil).

This analysis provides information on the gross oil composition and a coarse means of distinguishing among oils from different sources and reservoirs. To more completely assess the chemistry of the MC252 oil, gas chromatography coupled with mass spectrometry (GC/MS) was also used to quantify specific compounds from the oil present in the C3-C40+ carbon range. The lighter components (~C3-C12) of MC252 oil as described here were quantified using the EPA SW846 8260 analyte list. The heavier components (~C10-C40+) were quantified using the EPA SW846 8270 analyte list. These oil samples of MC252 oil were collected and analyzed before the Deepwater Horizon spill.[2] Consistent with the high gas-to-liquid ratios is the high percent composition of the low molecular weight alkanes/aromatics in these oil samples. The specific composition of MC252 samples analyzed is as follows:

- Saturates: 64–73%
- Aromatics: 21–29%
- Resins: 4–7%; Asphaltenes: 0–1%

Compared to other crude oils, such as the North Slope Crude Oil involved in the Exxon Valdez spill, MC252 oil is lower in polycyclic aromatic hydrocarbons (PAHs). The MC252 pre-spill reservoir fluid oil samples are also notable due to their very high gas-to-liquid ratios (>2.8 scf/stb).[3] Consistent with the high gas-to-liquid ratios is the high percent composition of the low molecular weight saturates to aromatics in these oil samples. This higher percentage of lower molecular saturates suggests that the MC252 oil could provide a good substrate for microbial oxidative respiration. Because of this, oxygen measurements were an important indicator of the presence of the oil being weathered and consumed by oxidative biodegradation processes.

The detailed composition of the MC252 aromatic fraction is particularly important because this fraction of the oil was primarily responsible for the MC252's fluorescence signals. The water-soluble aromatic fractions, including the BTEX (benzene, toluene, ethylbenzene and total xylenes) and the naphthalene, alkyl naphthalene fractions of the aromatics were most abundant in this oil. These component aromatics could be present either dissolved in the seawater or as part of the liquid oil-droplet phase. In either case, these aromatics would contribute to the fluorescence signals being generated at depth. The ability to detect these fluorescence signals depends on the sensitivity of the instrument being used. Resins and asphaltenes

2 Reservoir fluid composition is presented from the analyses of samples of the MC252 oil in Appendix 4.

3 Standard cubic feet/stock tank barrel.

can also exhibit fluorescence signals; however, MC252 source oil has a relatively small proportion of these compounds. Because of their extreme low water solubility, resins and asphaltenes are believed to be mostly associated with the large oil droplets that rose relatively rapidly to the surface from the well.

3 Physical and Biochemical Processes

3.1 Conceptual Model for Analysis

The composition of oil and gas flowing from the well, the well control activities, and the subsurface application of chemical dispersants all influenced the amount of MC252 hydrocarbons found in deep subsurface waters. This section describes the physical and biochemical processes affecting MC252 oil transport and fate in deep subsurface waters.

A simple conceptual model of the physical and biochemical processes operating on the deep subsurface naturally and chemically dispersed oil provides a framework for interpreting the monitoring data contained in this report. First, the multiphase flow rising from the wellhead formed two main features; a surface/near-surface spill, and deep subsurface dispersed oil. The deep subsurface dispersed oil was consistently seen between 900 and 1300 m and was initially composed of dispersed oil droplets, less than 70-100 μm in diameter (Federal Interagency Solutions Group, 2010), and dissolved hydrocarbons. Over time as the deep dispersed oil was observed farther from the wellhead, its composition changed as discussed below.

Processes driven by flow from the wellhead governed the deep oil's formation. It was carried with the ambient flow along density surfaces, extending downstream from the wellhead. Other processes govern the oil's long-term concentration, extent, and fate. We can distinguish two regions of the deep subsurface dispersed oil where the dynamics differ considerably, the near-field and the far-field as defined below.

The *near-field* is the region that begins where the hot single-phase momentum hydrocarbon jet transitions into a mixture of liquid and gas phases, which rise due to the buoyancy of the hot oil/gas mixture (Yapa et al., 1999; Johansen, 2003; and Socolofsky et al., 2011). The transition to the *far-field* occurs at the dynamic point, where the gas bubbles and oil droplets separate: the gas bubbles and largest droplets rise quickly upward toward the surface. Oil droplet rise velocity is proportional to droplet diameter. The smallest droplets may take weeks to rise to the surface, initially creating a nearly neutrally buoyant feature of small droplets and dissolved gases. The near-field region was not sampled in the dataset being considered; response activities in the immediate vicinity of the wellhead precluded the entry of sampling vessels into the area. Nevertheless, it was the dynamics of the near-field region that determined the source material in the deep dispersed oil that was sampled farther away. Several events in the near-field must be considered to appreciate the time-varying nature of the source, including the following.

- Changes in the riser configuration.
- Changing rate of flow from the wellhead.
- Subsurface dispersant application.
- Oil recovery efforts at the wellhead.

Each of these events influences the momentum, droplet-size distribution, and buoyancy of the ejected fluids.

Before the riser was cut, there were two main leaks: one from the kink above the riser well, and one from the end of the riser. These two leaks were almost 9 m apart vertically and ~225 m apart horizontally. Observations suggest that these two leaks resulted in a wider combined oil field than would have been expected from the widths of the individual leaks.

After the riser was cut, the single source point at the well was ~23 m below the removed kink leak. The oil was found at lesser densities (shallower depths) after the riser was cut (Socolofsky et al., 2011, and in Sect. 4.2 of this report), potentially due to the change in the near-field dynamics. The cut riser provided a smooth

exit point for the jet, and the reduced friction at the well's release point could have allowed the deep dispersed oil to rise higher in the water column before reaching the dynamic point.

Also important is the ambient current at the wellhead. The character of the near-field can change from a buoyancy-dominated feature to one dominated by the ambient flow if the current is large enough (estimated by Socolofsky et al., 2011, to be 0.16 m/s). Any variations in the blowout hydrocarbon source or in the magnitude of the currents will impact the quantity of dispersed oil, the range of densities over which this occurs, and the initial concentration and composition of the dispersed oil.

The *far-field* is the region beyond the dynamic point, typically during the MC252 oil spill more than a few hundred meters above and away from the wellhead, where the changes in concentration and spatial distribution of the dispersed oil can be expressed by an advection–diffusion balance. This balance is most easily cast in a frame of reference moving with the dispersed oil (an advective, or Lagrangian reference frame), and expressed as the time rate of the change of concentration being equal to the net effect of physical processes that cause the oil to mix with ambient fluid, biodegradation associated with microbial processes, and scavenging by plankton fecal pellets and sediment particles that fall through the water column. A brief explanation of the terms and processes is provided below, followed by a brief discussion of how observing in a fixed or Eulerian reference system complicates interpretation.

Concentration refers to the total volume or weight of oil per volume or weight of seawater, both in droplets and dissolved in seawater. Oil will remain at depth only if the droplet size is small enough that lift due to buoyancy is no larger than drag on the droplets. Components of oil will also dissolve in seawater. Observed particle diameters in the deep dispersed oil were 2.5–100 μm (Federal Interagency Solutions Group, 2010) and it is likely that droplets smaller than 2.5 μm measurement limit were present. The composition of the oil—in particular, the relative contribution of specific molecular weight compounds to the total concentration—will change over time. Saturates are expected to be metabolized most readily, and the composition may shift over time to be dominated by more refractory compounds (e.g. aromatics, resins and asphaltenes), as discussed in Section 2.2. The presence of deep subsurface dispersed oil was measured indirectly by fluorescence (initially measured primarily with a WET Labs ECO fluorometer optimized for CDOM analysis, but later with Chelsea AQUAtracka hydrocarbon-tuned fluorometry—see Sect. 4.2), and concentration was measured directly through laboratory analysis of discrete water samples using gas chromatography/mass spectrometry.

Turbulent mixing is the physical process of dilution of the dispersed oil with ambient seawater, typically represented as turbulent mixing coefficients that quantify the rate at which mixing occurs. These coefficients are scale-dependent quantities (the magnitude depends on the scales of fluid motion explicitly measured). However, for oceanic flows resolved at kilometer scales, it is well known that horizontal mixing rates far exceed vertical mixing rates (because density stratification reduces vertical exchange, and because of the aspect ratio of the flow, 1-km deep but hundreds of kilometers in the horizontal). It is expected that:

- Turbulent mixing processes act equally on all molecular weight components of the oil; and
- Horizontal mixing rates will be 10,000 to 1,000,000 times greater than the vertical mixing rates (i.e., horizontal mixing coefficients K_h~0.1–10 m^2/s, vertical mixing coefficients K_v~10^{-5} m^2/s, e.g., Sundermeyer and Ledwell, 2001).

For example, a horizontal mixing rate of 1 m^2/s results in relatively rapid dilution and spreading of the oil. Assuming Fickian-type diffusion acting on a Gaussian spatial distribution in the horizontal direction perpendicular to the main flow direction, the peak concentration would fall to <1/100 of its initial value in 10 days, and the width would increase by more than a factor of 10. Mixing rates are most often determined from the rate at which concentration decreases in magnitude and spreads out spatially over time.

Consumption (*biodegradation*) is the breakdown of oil components by microbes in seawater. For the purposes of this analysis, we are focusing on biologically mediated oxidative degradation and thus evaluating the deficits in seawater DO_2 as a proxy indicator of these processes. The rate of *biodegradation* is expected to vary strongly with molecular weight, with low molecular weight components likely to be degraded more rapidly than high molecular weight components. Thus, over time, we expect the composition of the oil to shift from its initial composition to one that is dominated by higher molecular weight components. Details on biodegradation processes are provided in Section 3.3.

Scavenging, in the present context, means adsorption of oil molecules or droplets onto particulate matter that sinks through the water column. A variety of biological and abiotic processes in the upper ocean produce particles (e.g., fecal pellets, "marine snow", etc.) that are denser than seawater and sink slowly to the seafloor. The size of the particles can be hundreds to thousands of micrometers or more, and therefore are large when compared to the estimated size of the dispersed oil droplets. Oil droplets can attach to the particles as they pass through the deep dispersed oil and be carried to the seafloor. The rate at which this process removes dispersed oil from the layer of neutrally buoyant material is dependent on the concentration and reactivity of particles, the concentration of oil droplets, and the fall rate. There were no direct observations of these processes considered by this report; however, oil-rich surface sediment, which was fingerprinted as MC252 oil and measured in quantities exceeding EPA's aquatic life benchmarks, was found within ~3 km of the wellhead (see Figs. 5.2 and 5.7 in the OSAT-1 [2010] report).

An important consideration when interpreting the observations is the frame of reference. In a frame of reference moving with the fluid (Lagrangian), the change in oil concentration with time is relatively straightforward. Each of the processes listed above acts to decrease the concentration of the deep dispersed oil over time and, with estimates of the magnitude of the terms, the expected decrease in concentration over time can be assessed. Conversely, having observed the concentration changes, the rates of the processes could be inferred. However, the response monitoring was not conducted in a fashion that tracked the movement of the deep dispersed oil and water. Monitoring conducted from early May until early August confirmed the existence of the deep dispersed oil by sampling within a few tens of kilometers of the wellhead. Monitoring conducted from August through October sought to establish the spatial extent of the subsurface oil and surveyed a broad spatial area at varying times over several months. We must therefore interpret the monitoring observations in a frame of reference that is fixed in space and from varying points in time. In this case, the position of the fluid parcels over time must be known to utilize the advection-diffusion balance.

To develop an understanding of how to interpret the monitoring observations in the context of an advection-diffusion balance, consider two simple examples: steady-state flow and time-varying flow. If the flow field is steady and has a relatively constant speed and direction, then the position of the deep dispersed oil is simply defined as the time since release from the wellhead multiplied by the speed in the direction of flow. Figure 3 is a graphic representation of how this situation would appear. It is a useful way to consider how conditions within the deep dispersed oil vary with position. Figure 3 illustrates that changes in DO_2 and the fluorescence signature of oil occur over tens of kilometers.

Near the wellhead, the concentration of dispersed oil was relatively high and appeared as a large anomaly in the fluorescence signal. The deep dispersed oil seen by Camilli et al. (2010) was roughly 1 km wide at a distance of 16 km away from the wellhead. As the oil is carried away from the wellhead, ambient turbulence mixes oil free seawater with the seawater containing oil; increasing its dimensions over time, and resulting in a decrease in the oil concentration. The combination of mixing, biodegradation, and scavenging acts to decrease the concentration of the oil.

DO_2 is consumed as the microbial community metabolizes components of the oil. As a result, DO_2 levels are initially expected to be unaffected, but over time the levels would exhibit anomalously low values as a

consequence of the aerobic respiration of oil components. In this case of a simple flow field and steady release from the wellhead, distance from the wellhead is directly related to time since release from the well.

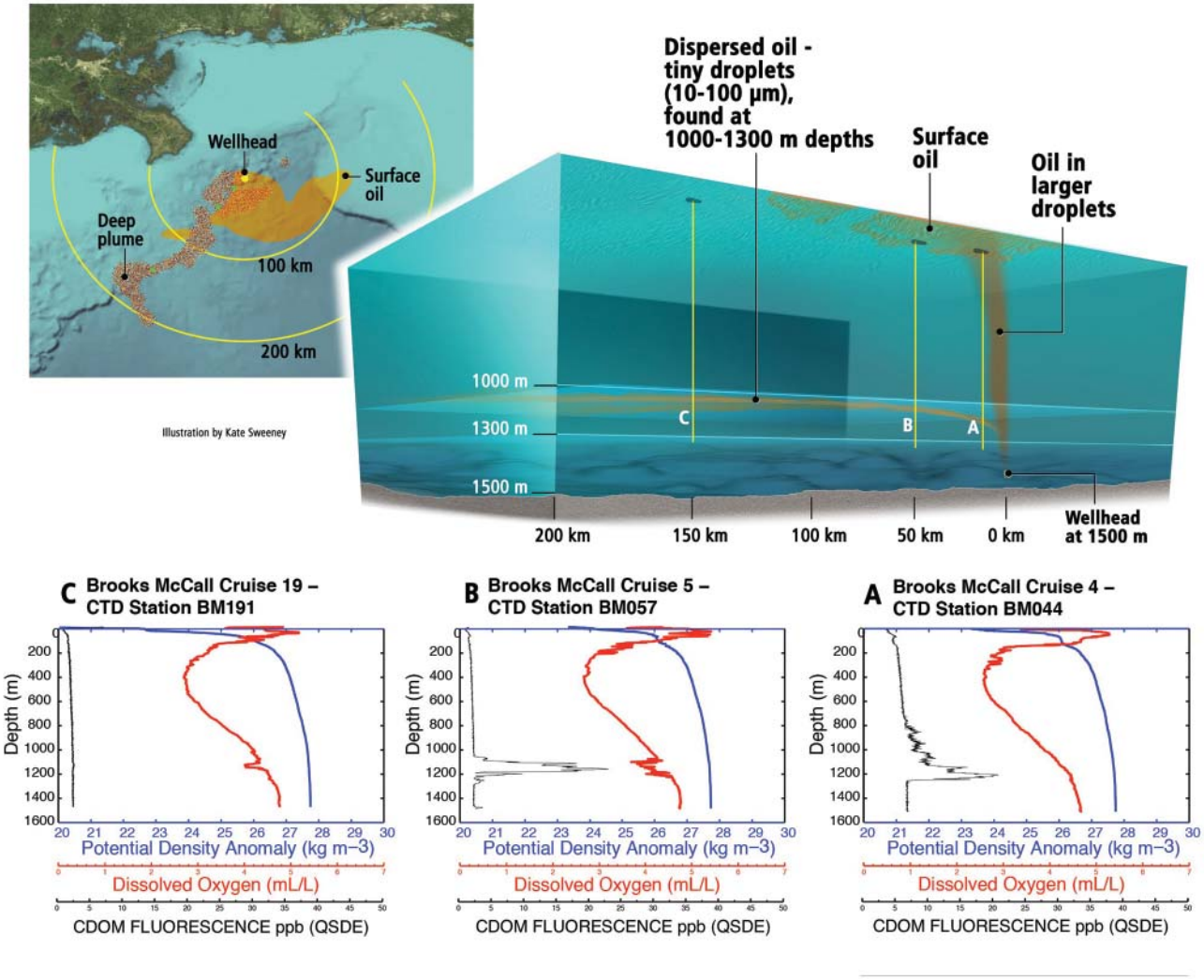

Figure 3. Representation of the oil spill as it existed just before the wellhead was shut–in on July 15, 2010. The map view shows the surface plume (based on the NOAA forecast of 7/13/2010) and an estimate of the position of the deep dispersed oil. The perspective view illustrates the vertical position of the deep plume at an approximate depth of 1100 m. The three profiles illustrate how fluorescence as measured by CDOM fluorometers and DO_2 vary as the plume is carried away from the wellhead by a mean west–southwest current. The approximate positions of the profiles are indicated on both the map view and the perspective view.

A second example stems from the knowledge that (1) currents at the wellhead were not steady over time and (2) the flow varied in both strength and direction while oil was flowing from the wellhead. Although the currents at the wellhead were observed on average to flow toward the west-southwest at 0.02–0.05 m/s, roughly following the bathymetry, currents were at times as large as 0.3 m/s and in nearly all directions (see Sect. 4.4). The time-varying flow field makes the relationship more complicated between time since oil left the wellhead and its spatial position relative to the wellhead; the position of oil released at any given time is the net motion of the fluid from the release up to the time of interest (the integral of the velocity of the fluid parcel).

In the time-varying flow example, a simple relationship between position and time since release no longer exists. A flow reversal can cause the deep subsurface dispersed oil to "double back" on itself, and in this case the concentration will no longer exhibit a monotonic decrease with distance from the wellhead because of multiple injections of "fresh" oil at a given position. When interpreting the observations, it is important to keep in mind that time-varying flow and source conditions complicate the spatial structure of the deep dispersed oil.

3.2 Oceanographic Baseline Conditions and Circulation in the Deep Gulf of Mexico

In the deep ocean, dissolved chemical tracers move with the water approximately along constant-density (isopycnal) surfaces, which are roughly horizontal. Therefore, the basin-scale, deep-ocean density structure, which was determined largely by the thermohaline arrangement of characteristic source water masses, was of particular interest in determining the transport and fate of the deep subsurface dispersed oil.

The largest anomalies in DO_2 and fluorescence attributable to MC252 hydrocarbons were primarily found centered between depths of 900 m and 1300 m, as detailed in Sections 4 and 5 of this report. This depth layer is roughly centered between the 1027.60 and 1027.70 kg/m^3 potential density surfaces (density referenced to the surface, 0 dbar). This section describes selected thermohaline and chemical characteristics of local subsurface waters within the Gulf of Mexico using historical and climatological oceanographic data along isopycnal surfaces and vertical sections near the well. Horizontal mixing in the ocean is thought to occur along surfaces with no exchange of heat with the surrounding water. These surfaces can be approximated using constant density (isopycnal) surfaces (e.g., Reid and Lynn, 1971). A water type is broadly defined by a point on a temperature–salinity diagram and a water mass by some idealized combination of water types (Worthington, 1981).

In the intermediate to deep (approximately >600-m depth) Gulf of Mexico, the large-scale water-mass structure is largely dominated by the input of remnant source waters ultimately formed in the Nordic (Norwegian and Greenland) Seas, the Labrador Sea, the Mediterranean Sea, and the Southern Ocean (e.g., Warren, 1981; Schmitz and Richardson, 1991; Schmitz et al., 2005; and Nowlin et al., 2001). These deep cold-water masses travel slowly through the deep world ocean and into the Gulf of Mexico only through the Yucatan Strait (sill depth ~2040 m) from the Caribbean (Nowlin et al., 2001; Rivas et al., 2005).

The typical temperature–salinity relation in the deep Gulf of Mexico shows extrema that reflect the influence of upper North Atlantic Deep Water and Antarctic Intermediate Water. Each of these water masses is relatively cold (<5 °C), compared with the warm surface waters of the Gulf of Mexico. At a given salinity, cold water holds more DO_2 (solubility, e.g., Garcia et al., 2005a, 2005b; Keeling and Garcia, 2002; and Sarmiento et al., 1998). North Atlantic Deep Water is the most highly oxygenated water mass in the deep Gulf of Mexico,[4] based on the World Ocean Atlas (Garcia et al., 2010). During transport into the Gulf of Mexico, upward mixing brings the nutrient poor and oxygen rich North Atlantic Deep Water into the overlying relatively nutrient rich and oxygen poor Antarctic Intermediate Water. Dissolved nutrients and oxygen are not conservative constituents, and their relative concentrations result from (1) advection and mixing of waters with varied preformed or initial concentrations, and (2) biogeochemical processes.

Water-mass characteristics near the ocean surface help us to understand constraints on the movement of the deep subsurface dispersed oil. Along the Louisiana–Texas continental shelf, the high salinity Subtropical Underwater is the deepest water mass to reach the base of that continental shelf (DiMarco et al., 2007). Subtropical Underwater is warm (20.4–22.2 °C) and salty (36.72–37.10) and forms in the North Atlantic (O'Connor et al., 2005). Along the West Florida Shelf, the coldest water to reach the continental shelf comes

4 See Figures 15–20.

from Loop Current eddies, which bring water with temperatures <13 °C up and onto the shelf (Paluszkiewicz et al., 1983). A more detailed discussion of these analyses of water masses as related to the response to the MC252 oil spill can be found in Beegle-Krause et al. (2011).

Within the world ocean, some dissolved chemicals become tracers of water movement; for example, see Broecker et al. (1982). Research experiments have used deliberate injection of tracers specifically to provide information on processes over a few years (e.g., Ledwell and Hickey, 1995; Ledwell and Bratkovich, 1995; and Ledwell et al., 1993) or longer. These studies show that in the deep ocean, dissolved chemical tracers move with the water approximately along isopycnal surfaces. Therefore, large-scale analysis of the MC252 subsurface oil began with the conceptual model that as the deep circulation of the Gulf of Mexico[5] moved water over the well, (1) the water would pick up a signal from the MC252 oil spill, such as dissolved hydrocarbons;[6] and (2) the water could be identified by chemical or fluorescent measurement of those hydrocarbons or from anomalously low oxygen values (DO_2 depression)

Figure 4 shows the average spring climatological depth (pressure) of the 1027.60 kg/m^3 density layer in the Gulf of Mexico based on the World Ocean Atlas (1/4° grid extended depth climatology, experimental). This layer is just above the depth where we see the largest anomalies in DO_2 and fluorescence. The contours of Figure 4 represent the pressure of the density surface in decibars, which approximate water depth in meters. Looking at the nominal depth of the 1027.60 kg/m^3 density surface across the Gulf of Mexico, this isopycnal surface does not reach shallower than a depth of about 850 m against the continental slope. Gray areas are locations where the local bathymetry is equal to or shallower than the nominal depth of this isopycnal surface. We have no evidence that this layer connects with the Florida Straits.

Figures 5 and 6 show the average depth of the 1027.65 kg/m^3 and 1027.70 kg/m^3 surfaces, respectively from the World Ocean Atlas for the spring season (April–June). These figures show that the waters found within this density range (1027.6–1027.7 kg/m^3) lie well offshore in the northern and eastern Gulf of Mexico continental shelf. We also have no evidence that these deep layers could reach up onto the continental shelf (depth <200 m).

Figures 7 and 8 show the average difference in depth among these three density surfaces. The upper (1027.6 kg/m^3) and middle (1027.65 kg/m^3) density surfaces are separated by ~50 m near the continental slope and 150 m offshore in the deep Gulf of Mexico domain. Conversely, the upper and lower (1027.7 kg/m^3) density levels of the water layer are nominally thicker with values between ~150 and 250 dbar (or approximately in 150-250 m) thick. During the MC252 operational sampling, there was no evidence that these water layers connected with either the Florida Straits or with the shallower continental shelves along the Gulf of Mexico, suggesting that the deep subsurface dispersed oil remained within the deep basin of the Gulf of Mexico.

5 See, for example, Figure 43.

6 See Figures 44 and 45.

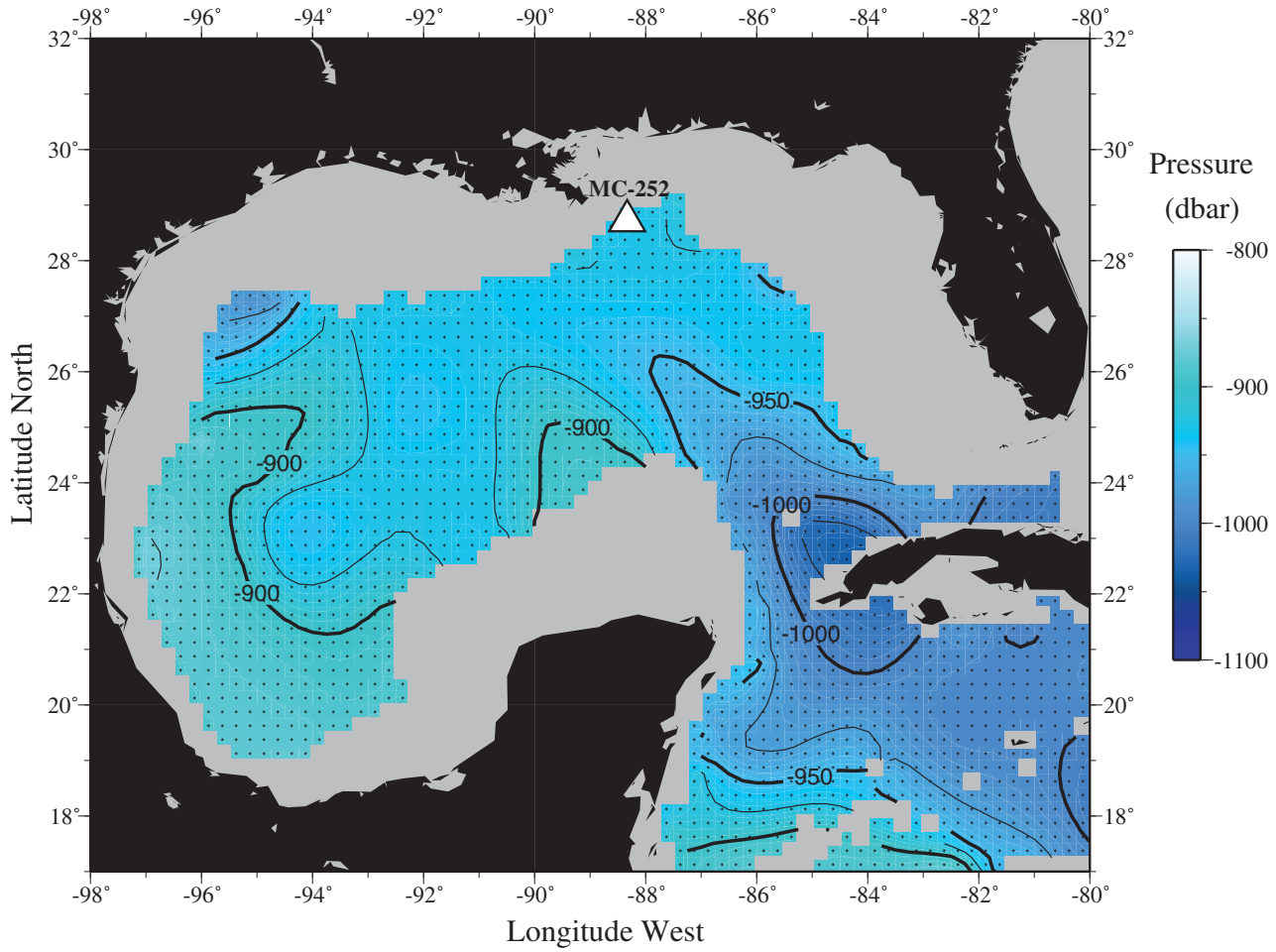

Figure 4. Climatological average spring (April-June) pressure (dbar) of the sigma-θ 1027.60 kg/m^{3}surface based on the NODC World Ocean Atlas (1/4° grid extended depths). Gray areas are locations where the local bathymetry is equal to or shallower than the nominal depth of this isopycnal surface. The climatological field is an experimental data product that has not been fully quality-controlled and may contain erroneous values. Ocean Climate Laboratory, NODC, NESDIS, NOAA.

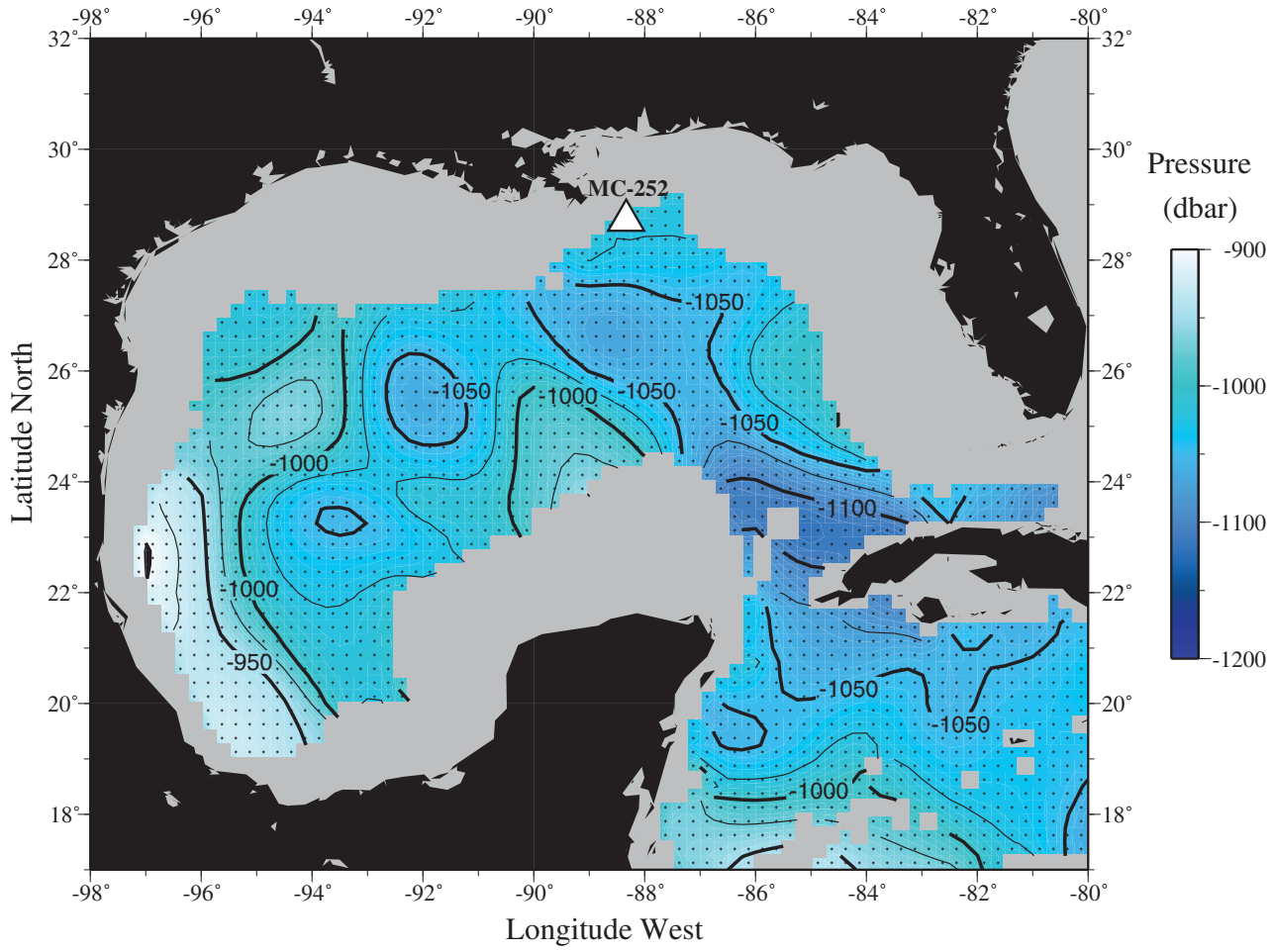

Figure 5. Climatological average spring (April-June) pressure (dbar) of the sigma-θ 1027.65 kg/m^3 surface based on the NODC World Ocean Atlas (1/4° grid extended depths). Gray areas are locations where the local bathymetry is equal to or shallower than the nominal depth of this isopycnal surface. The climatological field is an experimental data product that has not been fully quality-controlled and may contain erroneous values. Ocean Climate Laboratory, NODC, NESDIS, NOAA.

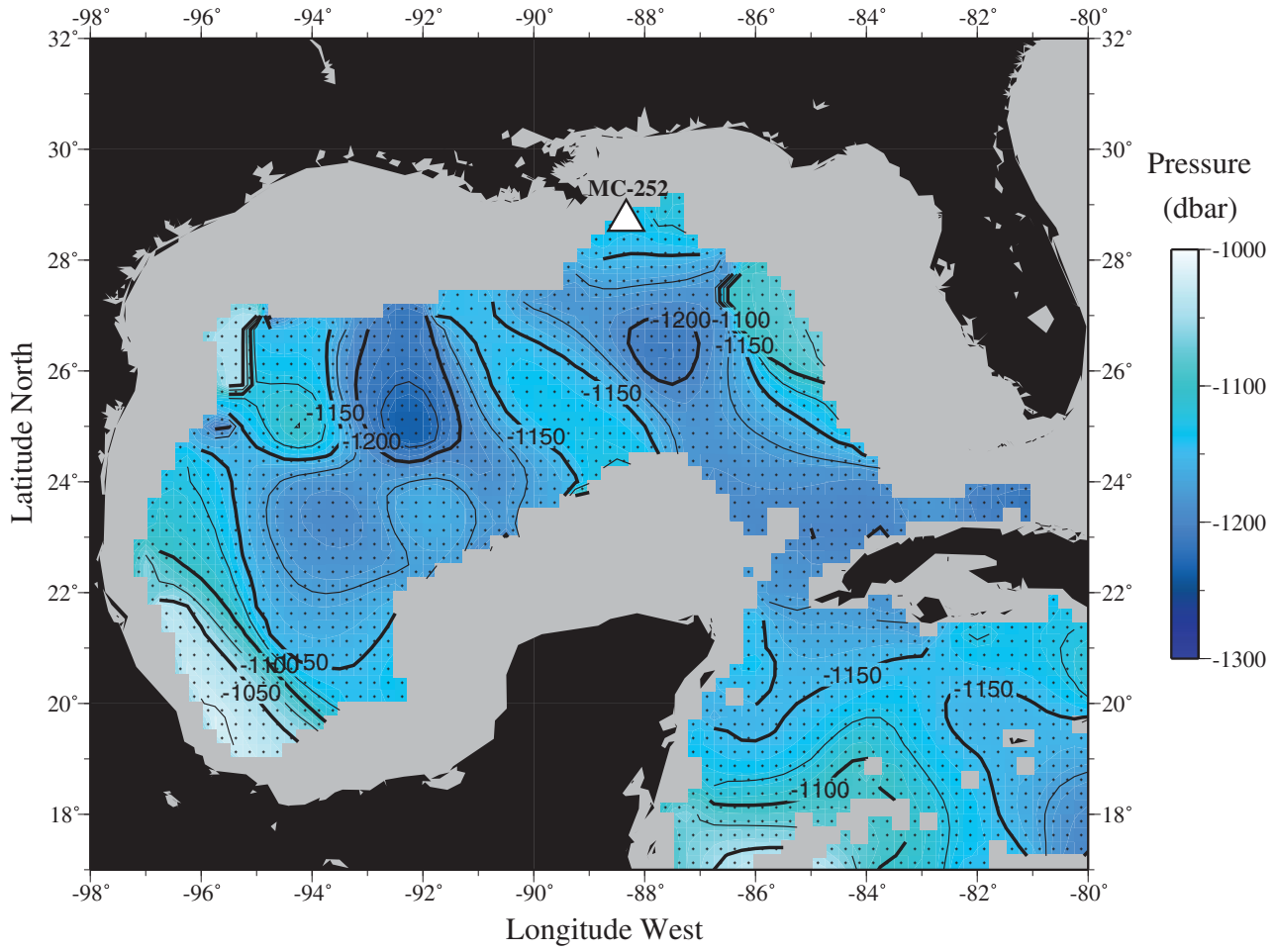

Figure 6. Climatological average spring (April-June) pressure (dbar) of the sigma-θ 1027.70 kg/m^3 surface based on the World Ocean Atlas (1/4° grid extended depths). Gray areas are locations where the local bathymetry is equal to or shallower than the nominal depth of this isopycnal surface. The climatological field is an experimental data product that has not been fully quality-controlled and may contain erroneous values. Ocean Climate Laboratory, NODC, NESDIS, NOAA.

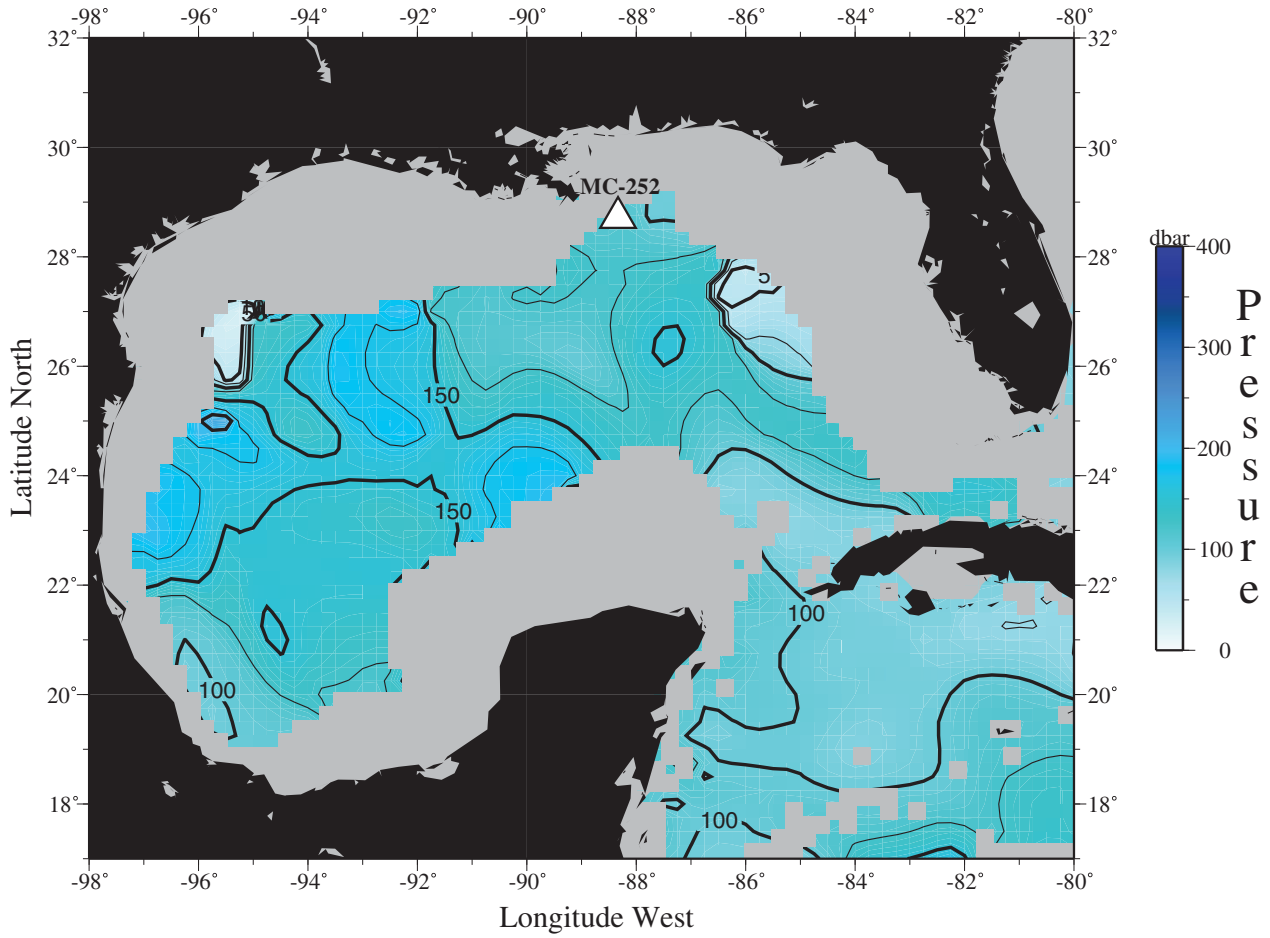

Figure 7. Climatological average spring (April-June) pressure difference (dbar) of the sigma-θ 1027.65 to 1027.60 kg/m^3 surfaces based on the World Ocean Atlas (1/4° grid extended depths). Gray areas are locations where the local bathymetry is equal to or shallower than the nominal depth of the 1027.65 kg/m^3 isopycnal surface. The climatological field is an experimental data product that has not been fully quality-controlled and may contain erroneous values (Ocean Climate Laboratory, NODC, NESDIS, NOAA).

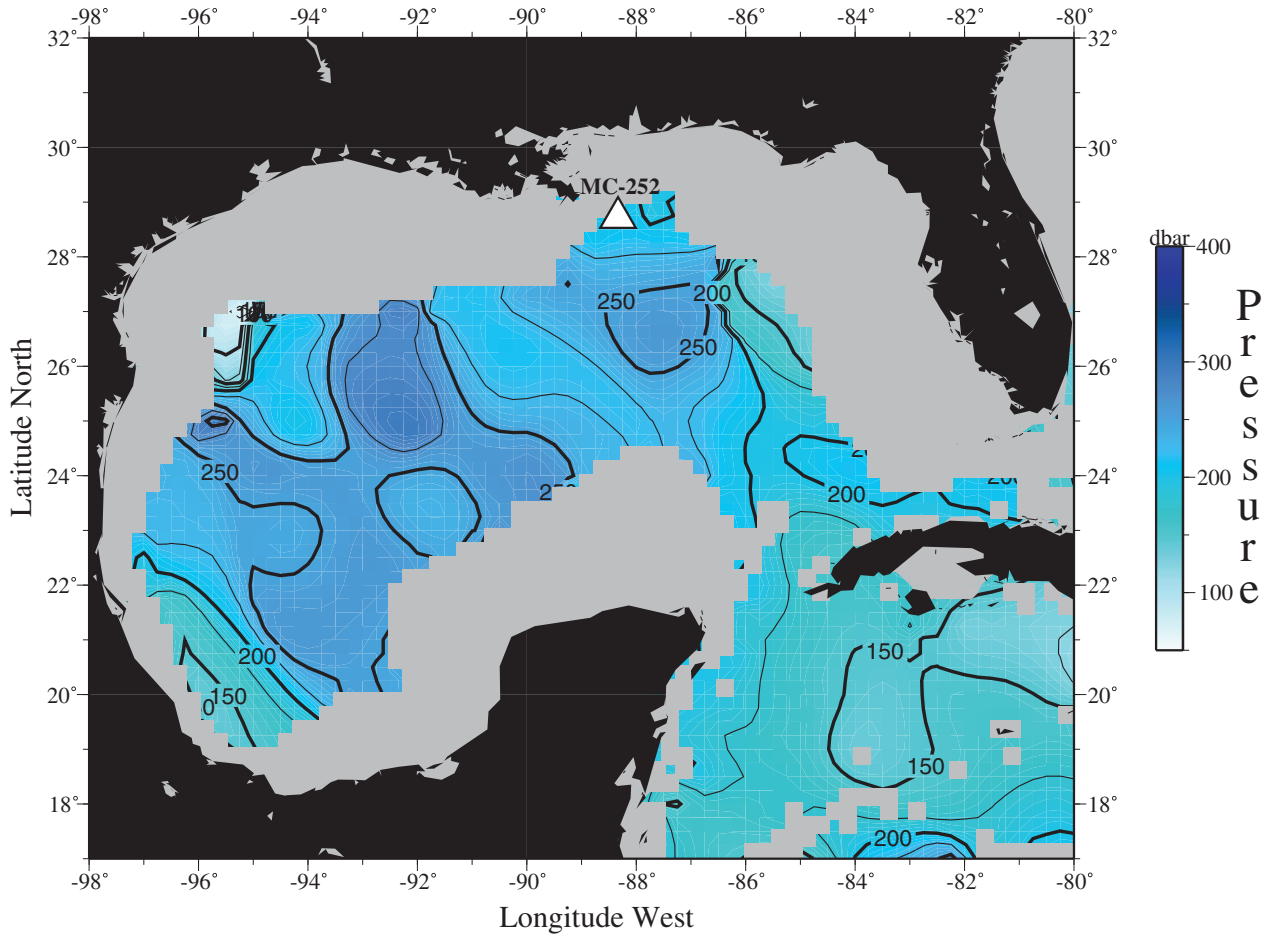

Figure 8. Climatological average spring (April-June) pressure difference (dbar) of the sigma-θ 1027.70– 1027.60 kg/m^3 surfaces based on the World Ocean Atlas (1/4° grid extended depths). Gray areas are locations where the local bathymetry is equal to or shallower than the nominal depth of the 1027.70 kg/m^3 isopycnal surface. The climatological field is an experimental data product that has not been fully quality-controlled and may contain erroneous values (Ocean Climate Laboratory, NODC, NESDIS, NOAA).

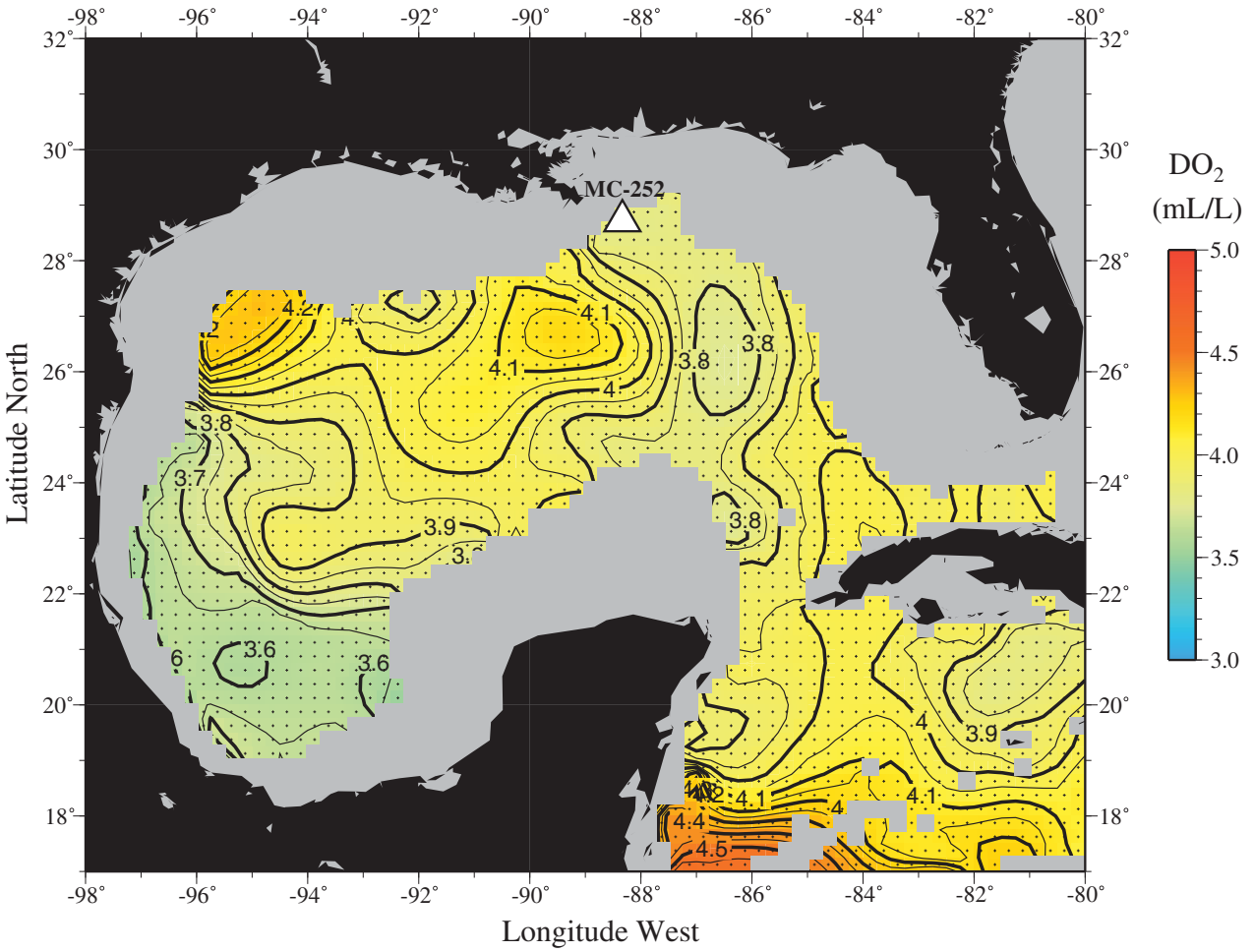

Figure 9. Climatological average spring (April-June) DO_2 concentration (mL/L) distribution along the sigma-θ 1027.60 kg/m^3 surface based on the World Ocean Atlas (1/4° grid extended depths). Gray areas are locations where the local bathymetry is equal to or shallower than the nominal depth of this isopycnal surface. The climatological field is an experimental data product that has not been fully quality-controlled and may contain erroneous values (Ocean Climate Laboratory, NODC, NESDIS, NOAA).

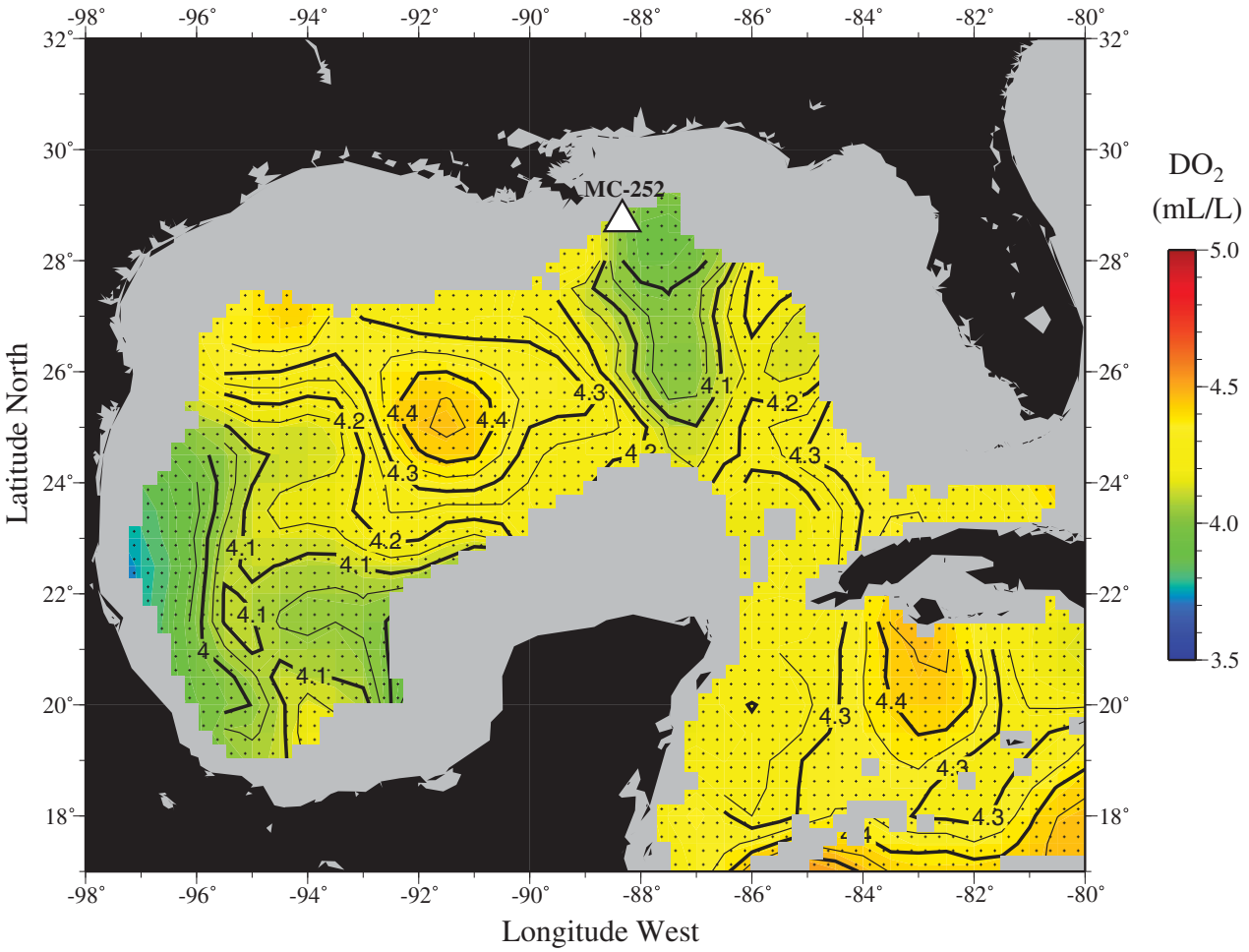

Figure 10. Climatological average spring (April–June DO_2 concentration (mL/L) distribution along the sigma-θ 1027.65 kg/m^3 surface based on the World Ocean Atlas (1/4° grid extended depths). Gray areas are locations where the local bathymetry is equal to or shallower than the nominal depth of this isopycnal surface. The climatological field is an experimental data product that has not been fully quality-controlled and may contain erroneous values (Ocean Climate Laboratory, NODC, NESDIS, NOAA).

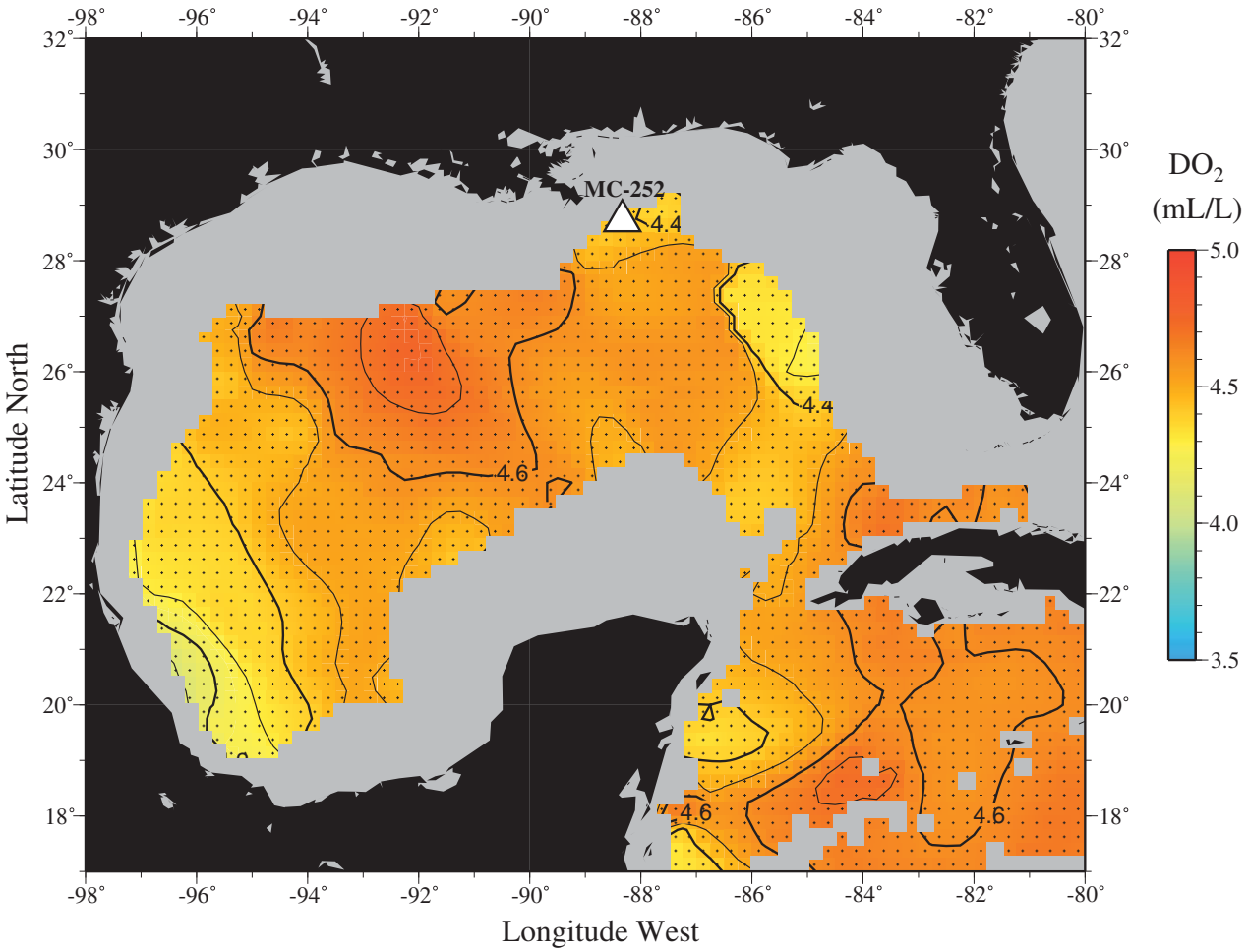

Figure 11. Climatological average spring (April-June) DO_2 concentration (mL/L) distribution along the sigma-θ 1027.70 kg/m^3 surface based on the World Ocean Atlas (1/4° grid extended depths). Gray areas are locations where the local bathymetry is equal to or shallower than the nominal depth of this isopycnal surface. The climatological field is an experimental data product that has not been fully quality-controlled and may contain erroneous values (Ocean Climate Laboratory, NODC, NESDIS, NOAA).

Climatological oceanographic data based on quality-controlled historical oceanographic data can also provide information on the mean DO_2 concentrations typically found in the Gulf of Mexico. This information is important for understanding how the observed DO_2 anomalies resulting from oxidation of MC252 hydrocarbons can be distinguished from climatological values. Figure 9 shows the climatological average spring DO_2 (mL/L) along the sigma-θ 1027.60 kg/m^3 surface based on the World Ocean Atlas (1/4° grid extended depth climatology, experimental). The average spring DO_2 level along the upper density level ranges from about 3.6 mL/L in the southwestern Gulf of Mexico to >4 mL/L in the northern Gulf of Mexico, the Yucatan channel, and the northern Caribbean Basin. The DO_2 concentration levels along the 1027.65 kg/m^3 density surface range from about 4.1 to 4.4 mL/L in the northern Gulf of Mexico (Fig. 10). The lowest DO_2 values are found in the southwestern Gulf of Mexico against the continental slope. DO_2 concentration values along the lower (1027.70 kg/m^3) density level range from about 4.0 to 4.7 mL/L in the northern Gulf of Mexico (Fig. 11).

Zonal (east–west) and meridional (north–south) sections of climatological DO_2 illustrate spring average top-to-bottom concentration gradients near the well. Figures 12–14 show the zonal gradient progressing from north of the well to south of the well. Figure 12 shows DO_2 levels along a zonal section in shallower water

just north of the wellhead (~29.6° N). The average DO_2 minimum zone (<3 mL/L) begins at an approximate depth of 180 m. Note that water types at or deeper than the upper (1027.60 kg/m^3) density surface layer described earlier are much deeper than waters found on the continental shelf.

In Figure 13, a zonal west–east section along the wellhead nominal latitude (~28.6° N) shows the DO_2 minimum layer to be between about 250 m and 600 m depth. DO_2 levels in the deeper layer of interest (~900–1200 m) are a mixture of the less dense and relatively DO_2-poor Antarctic Intermediate Water and the denser and DO_2-rich North Atlantic Deep Water. Figure 13 shows that the depths of the 1027.60 and 1027.70 kg/m^3 isopycnal surfaces discussed earlier are found well below the DO_2 minimum depth zone.

Figure 14 represents a zonal west–east section just south of the wellhead's nominal latitude (~27.6° N) and shows increasing DO_2 concentrations as a function of depth and relatively smaller east–west DO_2 horizontal gradients. The depth of the lower density surfaces nearly coincides with waters that have DO_2 concentrations greater than ~4.5 mL/L (Figure 14).

For comparison, Figures 15–17 show meridional views of spring average DO_2 concentrations along three sections, progressing from slightly west (~89.1° W) of the well to slightly east (~87.1° W) of the well. These meridional sections of DO_2 concentration distribution near the well support the observation that the overall mean deep circulation in the Gulf of Mexico is generally westward along the continental slope (Sturges and Kenyon, 2008). Lower overall DO_2 levels are expected in the west where more DO_2 is being consumed (or less ventilation) as a result of oxidation of labile organic matter. The black dotted lines in these figures bound the approximate depth where the vast majority of fluorescence and DO_2 anomalies discussed in this report were found.

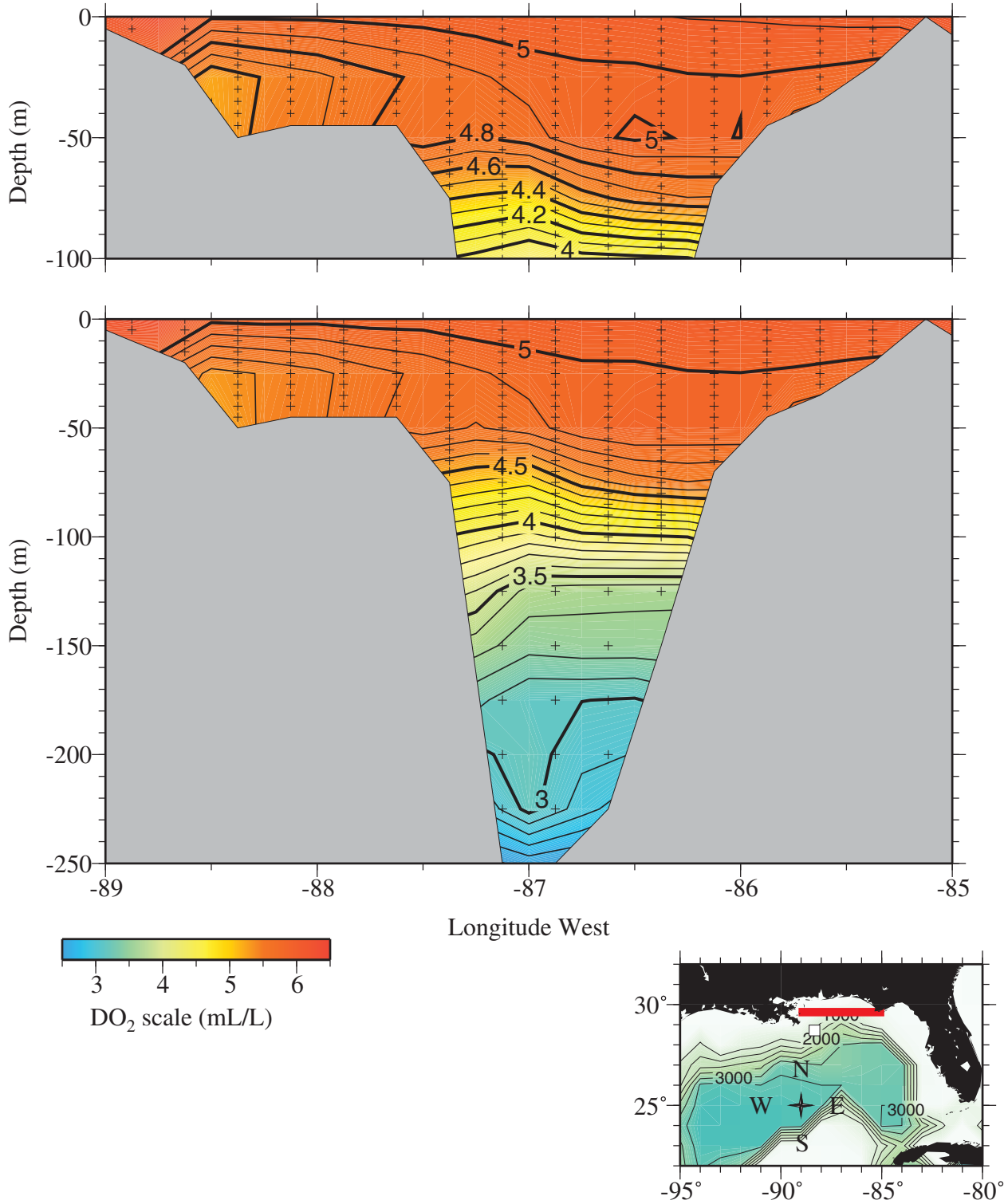

Figure 12. Zonal (east–west) section along about 29.625° N (just north of the well) of climatological average spring (April-June). DO_2 concentration (mL/L) distribution based on the World Ocean Atlas (1/4° grid extended depths). Gray areas represent the approximate local bathymetry. The climatological field is an experimental data product that has not been fully quality-controlled and may contain erroneous values (Ocean Climate Laboratory, NODC, NESDIS, NOAA).

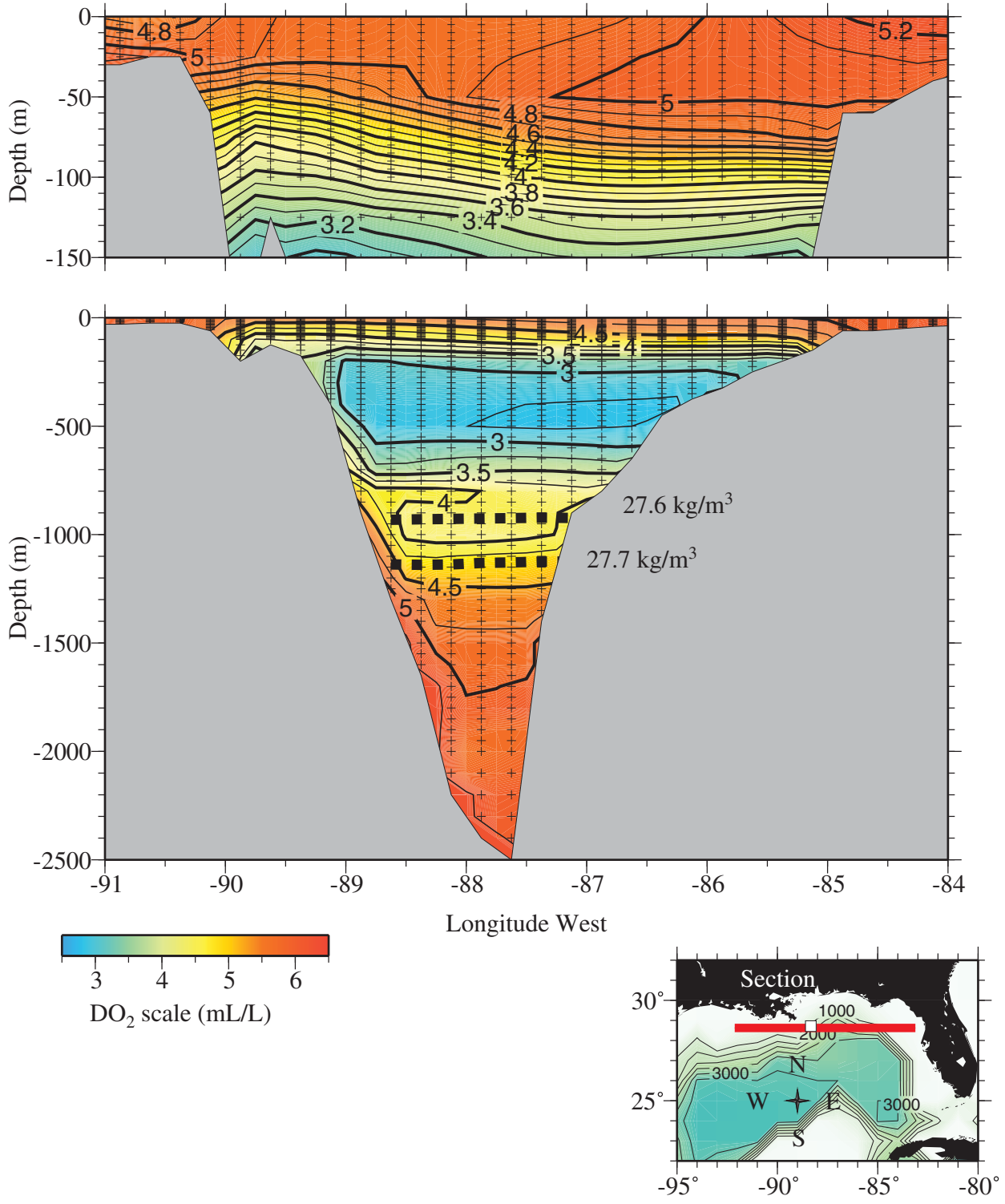

Figure 13. Zonal (east–west) section along about 28.625° N (near the well) of climatological average spring (April-June). DO_2 concentration (mL/L) distribution based on the World Ocean Atlas (1/4° grid extended depths). Gray areas represent the approximate local bathymetry. The black dotted lines in these figures bound the approximate depths of the 1027.60 and 1027.70 kg/m^3 isopycnal surfaces where the vast majority of fluorescence and DO_2 anomalies discussed in this report were found. The climatological field is an experimental data product that has not been fully quality-controlled and may contain erroneous values (Ocean Climate Laboratory, NODC, NESDIS, NOAA).

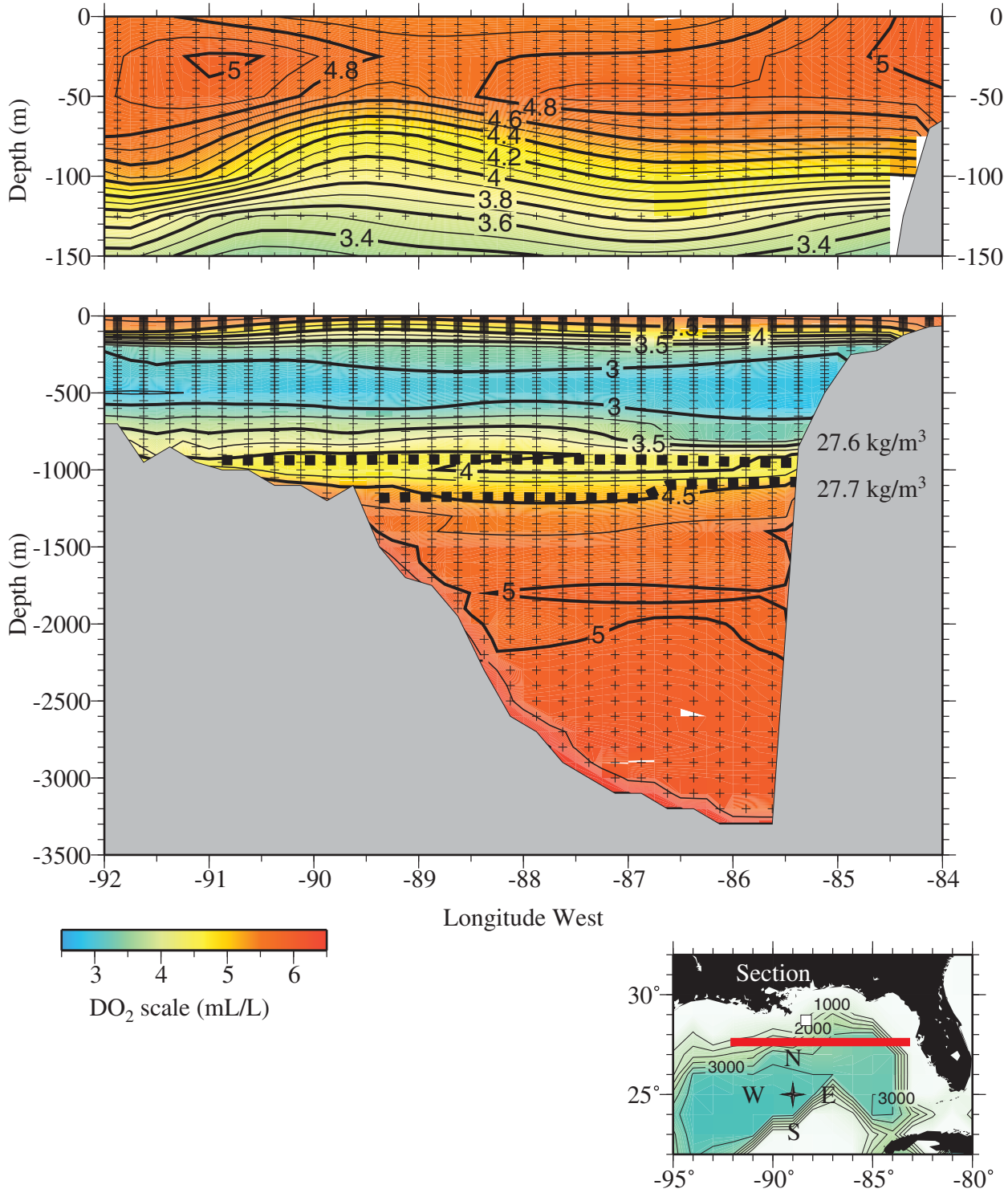

Figure 14. Zonal (east–west) section along about 27.625° N (just south of the well) of climatological average spring (April-June). DO_2 concentration (mL/L) distribution based on the World Ocean Atlas (1/4° grid extended depths). Gray areas represent the approximate local bathymetry. The black dotted lines in these figures bound the approximate depths of the 1027.60 and 1027.70 kg/m³ isopycnal surfaces where the vast majority of fluorescence and DO_2 anomalies discussed in this report were found. The climatological field is an experimental data product that has not been fully quality-controlled and may contain erroneous values (Ocean Climate Laboratory, NODC, NESDIS, NOAA).

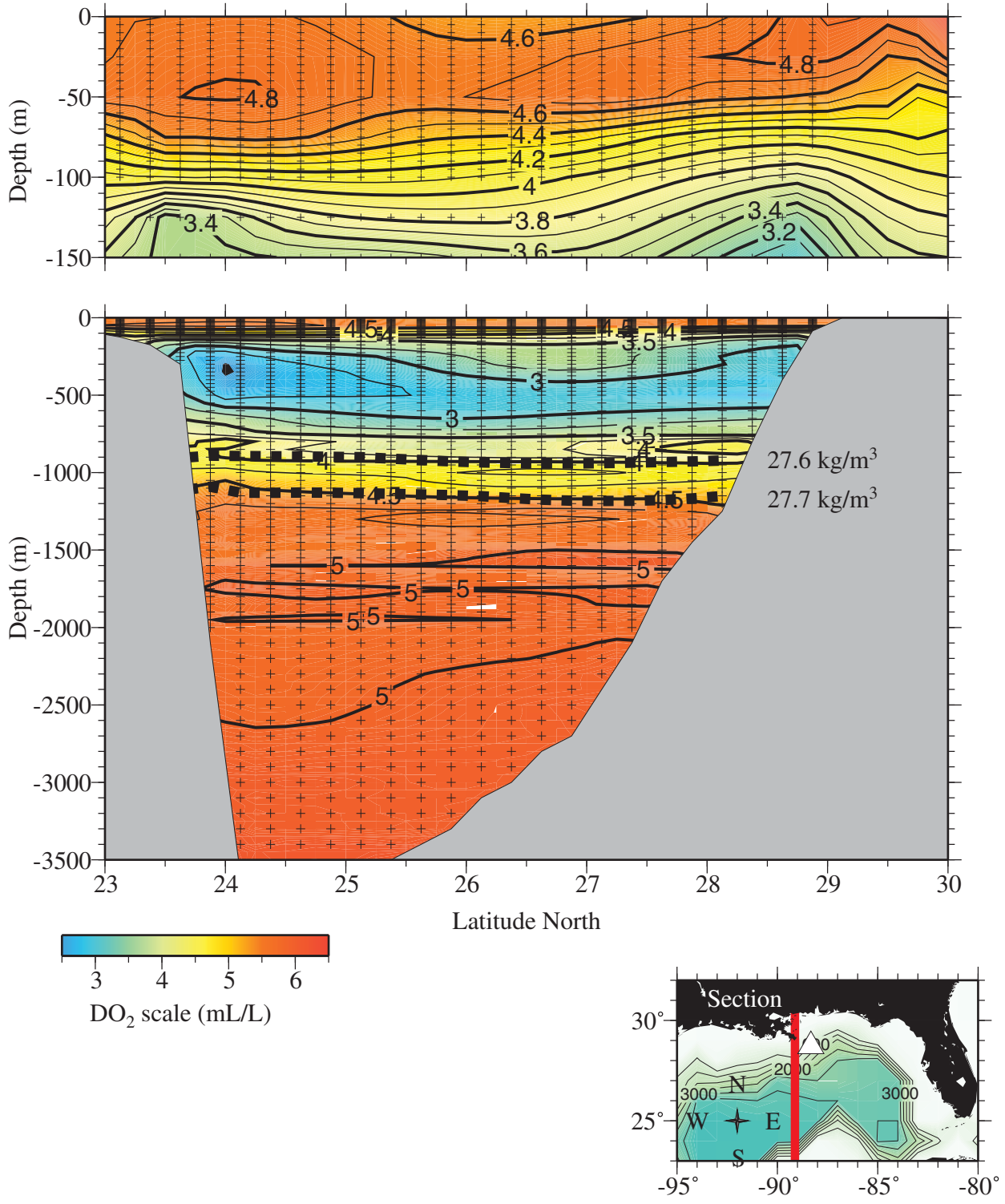

Figure 15. Meridional (north–south) section along about 89.125° W (just west of the well) of climatological average spring (April-June). DO_2 concentration (mL/L) distribution based on the World Ocean Atlas (1/4° grid extended depths). Gray areas represent the approximate local bathymetry. The black dotted lines in these figures bound the approximate depths of the 1027.60 and 1027.70 kg/m^3 isopycnal surfaces where the vast majority of fluorescence and DO_2 anomalies discussed in this report were found. The climatological field is an experimental data product that has not been fully quality-controlled and may contain erroneous values (Ocean Climate Laboratory, NODC, NESDIS, NOAA).

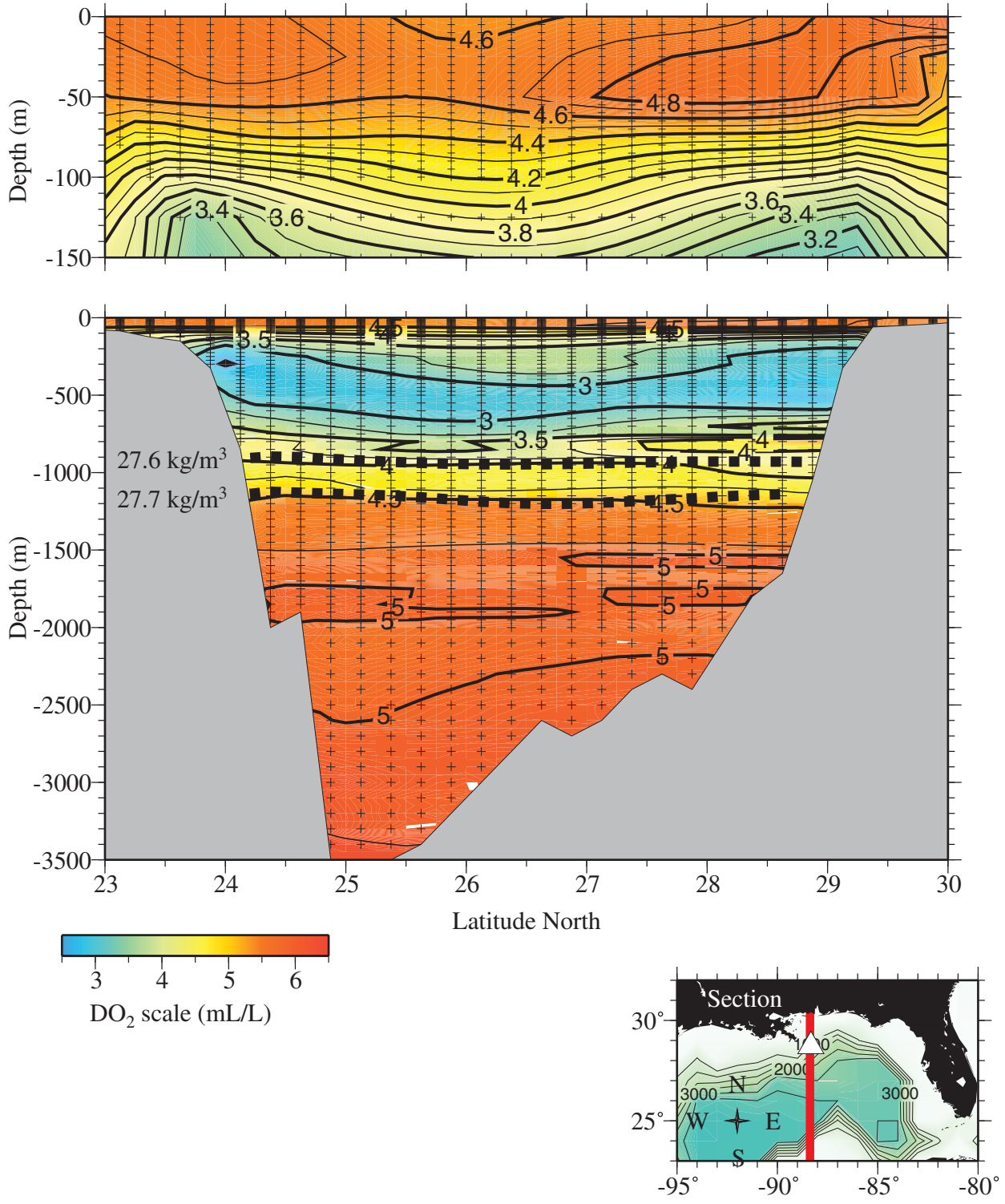

Figure 16. Meridional (north–south) section along about 88.375° W (near the well) of climatological average spring (April-June). DO_2 concentration (mL/L) distribution based on the World Ocean Atlas (1/4° grid extended depths). Gray areas represent the approximate local bathymetry. The black dotted lines in these figures bound the approximate depths of the 1027.60 and 1027.70 kg/m^3 isopycnal surfaces where the vast majority of fluorescence and DO_2 anomalies discussed in this report were found. The climatological field is an experimental data product that has not been fully quality-controlled and may contain erroneous values (Ocean Climate Laboratory, NODC, NESDIS, NOAA).

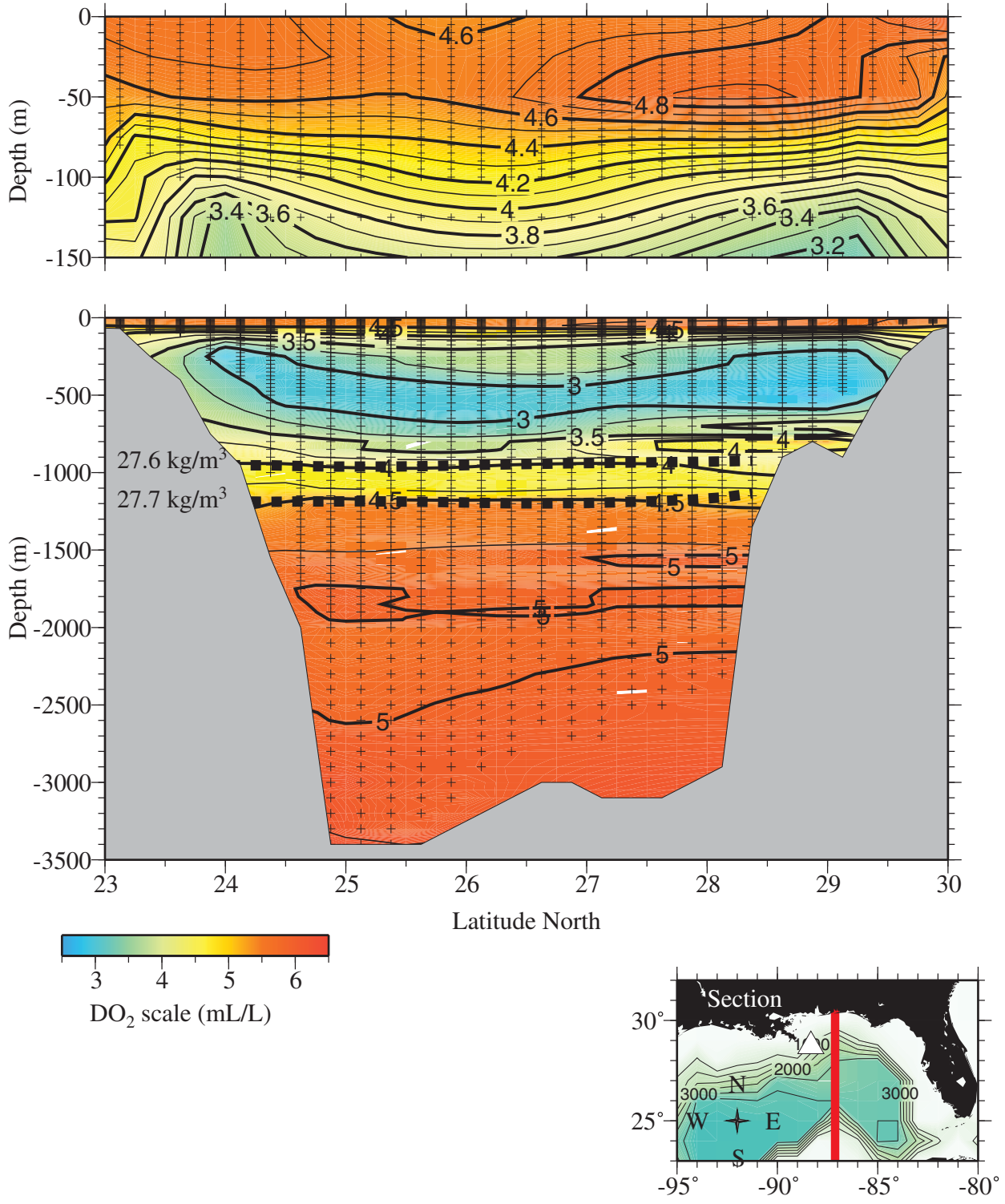

Figure 17. Meridional (north–south) section along about 87.125° W (just east of the well) of climatological average spring (April-June). DO_2 concentration (mL/L) distribution based on the World Ocean Atlas (1/4° grid extended depths). Gray areas represent the approximate local bathymetry. The black dotted lines in these figures bound the approximate depths of the 1027.60 and 1027.70 kg/m^3 isopycnal surfaces where the vast majority of fluorescence and DO_2 anomalies discussed in this report were found. The climatological field is an experimental data product that has not been fully quality-controlled and may contain erroneous values (Ocean Climate Laboratory, NODC, NESDIS, NOAA).

3.3 Microbial Degradation of Released Oil and Gas and the Associated Biochemical Oxygen Demand

The rationale for subsurface dispersant injection and surface application during the MC252 spill was fourfold:

1. If subsurface injection was successful in dispersing and keeping the oil in aqueous suspension, then exposure of responders aboard surface vessels to volatile organic compounds in oil that rose to the surface would be minimized;
2. Dispersing the oil into the water column would mitigate the likelihood of oil reaching the shoreline;
3. Dispersion would help to minimize exposure of sea birds to surface oil; and
4. When oil is chemically dispersed, the interaction between the oil and dispersant molecules would increase the surface area enhancing the ultimate biodegradation of the oil by microorganisms (Coastal Response Research Center, 2010).

Microorganisms metabolize the complex array of hydrocarbons in natural gas and petroleum into generally less toxic and more readily assimilated substrates, a process that substantially mitigates the environmental impacts of oil spills. The microbial capability for degrading or oxidizing hydrocarbons has been identified for over 30 genera of bacteria (Rosenberg, 2006) from natural aquatic and terrestrial habitats, and their numbers have been shown to increase in association with oil pollution (Walker and Colwell, 1975). The microbial metabolic process of degradation or oxidation of hydrocarbons is coupled to aerobic respiration, which consumes DO_2 from the water column.

Small particles offer greater available surface area for microbial colonization and degradative metabolism, as biodegradation takes place at the hydrocarbon–water interface (Atlas and Hazen, 2011). The injection of dispersants at the wellhead is presumed to have aided the dissociation of oil into small particles that resulted from mechanical processes. This assumption is based on evidence obtained from Laser In-Situ Scattering and Transmissometry (LISST) particle-size distribution and dual wavelength spectrofluorometry data collected in the field.[7]

Evidence was also provided from research studies in the laboratory using the Baffled Flask Test (Fig. 18). Baffled Flask Tests (Venosa et al., 2002) were conducted by the Centre of Offshore Oil Gas and Energy Research, Fisheries and Oceans Canada using MC252 source oil and Corexit® 9500 for various dispersant-to-oil ratios. Results of these tests showed that the addition of chemical dispersant resulted in a shift in particle-size distribution from larger sizes (Fig. 18C) to a distribution (Figs. 18A and 18B) that is predominantly smaller oil droplets (<70 μm). Since smaller particles facilitate biodegradation, the potential for DO_2 levels to decline to levels harmful to marine life (hypoxic conditions or DO_2 levels <1.4 mL/L or 2.0 mg/L) potentially increased with dispersant usage.

7 Results from these measurements were reported daily and made available on the Internet by the U.S. Environmental Protection Agency. See for example http://www.epa.gov/bpspill/dispersants/bp_20100721_lisst.pdf

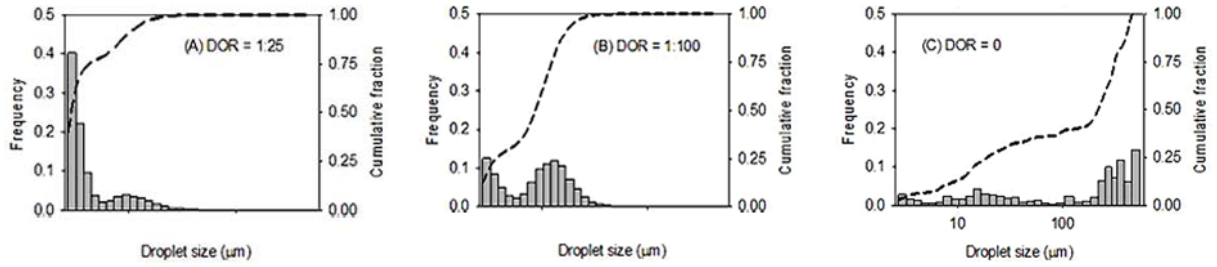

Figure 18. Dispersed oil droplet-size distribution at three DORs: (A) 1:25; (B) 1:100; (C) 0 (no dispersant control). Bars are volume size distribution frequency. Dashed lines denote the cumulative volume-size distribution.

Criteria were developed in the joint directives issued by the EPA and the U.S. Coast Guard (Environmental Protection Agency, 2010a–c) requiring responders to cease dispersant application if DO_2 levels became hypoxic. Microbial metabolism frequently depletes oxygen to hypoxic levels over the continental shelf in the northern Gulf of Mexico. Hypoxia there is associated with nutrient-laden Mississippi River inflow, high phytoplankton productivity, and seasonal stratification in the more westerly and shallow waters (<100 m) of the continental shelf (Rabalais et al., 2007). Although the spill occurred in the deep waters of the Gulf east of the Mississippi River outflow, there was concern that elevated levels of microbial degradation stimulated by oil would generate additional areas of hypoxia.

In the sea, the ability of naturally occurring bacteria to degrade hydrocarbons may be limited by the concentration of nutrients (nitrogen species, phosphate, and iron) available in the water column (Atlas and Hazen, 2011). The oil's composition also influences the rates of degradation. Among other factors, rates of degradation depend on temperature, the complexity of the oil, the surface area or particle size for microbial colonization, the composition of the microbial community, and the availability of oxygen, with aerobic degradation occurring considerably faster than degradation under anaerobic or hypoxic conditions.

The composition of the oil fraction from MC252 estimated by Reddy et al. (2011) from samples collected directly above the well indicated 74% saturated hydrocarbons, 16% aromatic hydrocarbons, and 10% polar hydrocarbons. (This composition differs to some extent from reservoir oil analysis identified in Sec. 2.2 and provided in App. 4). Many of these polar hydrocarbons are resistant to biodegradation. Gas chromatographic analysis for several monoaromatic compounds indicated BTEX concentrations that exceeded 50 $\mu g\ L^{-1}$ within the deep dispersed oil in June 2010 (Camilli et al., 2010). Estimates for hydrocarbon degradation in the deep dispersed oil range from 2 to 7 $\mu g\ L^{-1}d^{-1}$, which translates to an estimated half-life on the order of 1 month for petroleum hydrocarbons (Reddy et al., 2011). Methane was estimated to take longer to degrade. Kessler et al. (2011) estimated the oxidative lifetime of methane resulting from the spill to be 120 days.

The size and composition of the Gulf of Mexico microbial community were altered as microbes responded to the presence of MC252 oil. Bacterial cell densities were significantly higher in the deep subsurface dispersed oil, 10^5 cells/mL as compared to numbers outside the deep dispersed oil, which were 10^3 cells/mL (Atlas and Hazen, 2011). As the microbial community responded to the availability of oil, hydrocarbon degraders dominated, resulting in reduced community diversity.

DNA surveys for bacterial 16S rRNA genes from samples collected in June revealed dominance of the genera *Cycloclasticus* and *Colwellia*, likely degrading propane and ethane preferentially (Valentine et al., 2010; Kessler et al., 2011). Sixteen taxa of the γ- proteobacteria dominated by the order *Oceanospirillales* occurred in high numbers and dominated the community in the deep dispersed oil samples collected in the same time frame (Hazen et al., 2010). Among these were *Oliespira antarctica*, *Thalassolituus oleivorans*, and *Oliphilus messinensis*, bacteria known to be able to degrade hydrocarbons at the low temperatures that occur in the deep sea. Samples collected later (September) indicated a shift away from these hydrocarbon degraders to methanotrophs, including *Methylococcaceae*, *Methylophaga*, and *Methylophilaceae*. The enhanced abundance

of methanotrophs and bacteria containing the particulate methane monooxygenase gene (pmoA) indicated that methane was consumed later in the spill sequence by a different bacterial assemblage (Kessler et al., 2011).

Propane and ethane were degraded relatively rapidly and likely before alkanes >5 carbons in length (Valentine et al., 2010). The occurrence of natural seeps in the area of the spill may have supported the development and persistence of microbial communities capable of degrading hydrocarbons. Dissolved propane and ethane may promote rapid hydrocarbon degradation and low diversity communities that can degrade other hydrocarbons as the nature of remaining hydrocarbons changes. Hazen et al. (2010) estimated biodegradation rates for hydrocarbons in the deep dispersed oil based on observed concentrations of C13-C26 alkanes from samples collected near MC252 and from laboratory degradation studies at 5 °C. Based on these observations, degradation of alkanes was estimated to be 1.2–6.1 d^{-1}. Rapid rates of biodegradation may be expected for alkanes, the least recalcitrant fraction among the complex mixture of compounds that makes up Sweet Louisiana Crude oil. Rapid degradation rates reported for Sweet Louisiana Crude in the region of the MC252 oil spill may be related to its relatively light character, containing a large volatile component and a large fraction of alkanes, both of which are more amenable to degradation than heavier crude oil.

Valentine et al. (2010) estimated that 1.5×10^{12} g of oxygen may have been consumed in the deep subsurface dispersed oil, with roughly 15% of the consumption due to respiration of propane and ethane. To explore questions about the potential for hypoxia to occur, three additional scenarios were considered to determine the hypothetical length of time required for microbial degradation rates to cause hypoxia in the deep sea environment (Joint Analysis Group, 2010a–c). All three scenarios were conservative, assuming that no mixing took place in the region of the deep subsurface dispersed oil; mixing that would replenish the DO_2 in the water column. These scenarios predict that a minimum of 24 to 74 days would be required to reach the hypoxic state. Since hypoxia did not occur over the 87-day duration of the spill or in the months after the well was capped, these assumptions fortunately proved to be conservative.

3.4 Natural Hydrocarbon Seep Activity

Natural hydrocarbon seeps are found in the northern Gulf of Mexico, including the offshore zone where MC252 hydrocarbons have been documented. The Bureau of Ocean Energy Management (BOEM) used 3-D seismic data to map probable hydrocarbon seepage in this area. Two types of seismic amplitude anomalies were suggestive of ongoing seepage: high positive amplitude response inferred to be the result of low to moderate rate of hydrocarbon release and low positive amplitude response inferred to have rapid hydrocarbon flux. Some of these anomalies were confirmed by direct observation as active hydrocarbon seeps (Shedd et al., 2011).

Seep areas mapped by BOEM occur throughout the area covered by this report. In addition to the BOEM surveys, detailed acoustic surveys were conducted by NOAA in the area near the MC252. The sites were identified by the presence of gas bubble plumes that reflect sound from underwater acoustic instruments. This survey identified active gas seeps associated with salt domes that surrounded the well (many of which correspond to BOEM's seismic amplitude anomalies). Figure 19 shows active seeps near the MC252, assumed to be gas, as observed by the NOAA Ship *Okeanos Explorer* in September 2011. Seep locations were derived from a Konsberg EM302 multibeam echosounder.

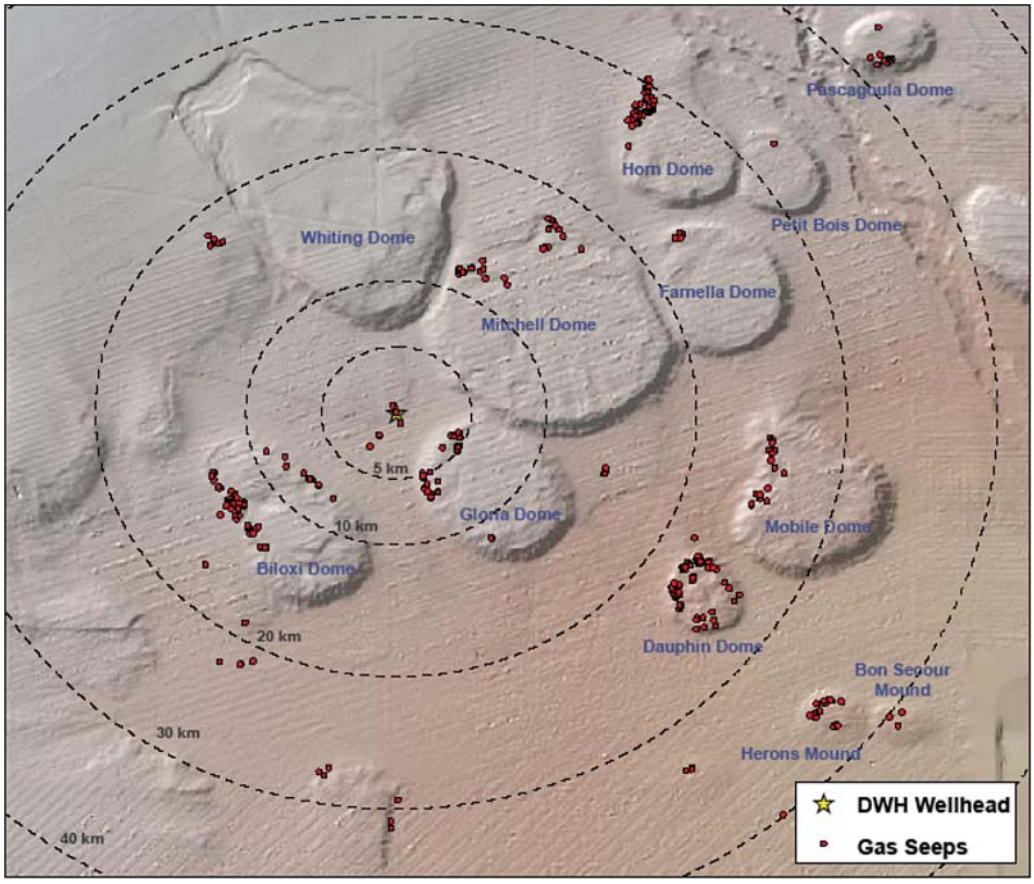

Figure 19. Areas of potential hydrocarbon seeps along the edges of salt domes near MC252. University of New Hampshire, Center for Coastal and Ocean Mapping, and NOAA Ship *Okeanos Explorer*, mapped September 2011.

Although it is important to recognize these seep sources when interpreting samples collected as part of the MC252 response, they are not likely a significant confounding factor in interpreting those data. The OSAT-1 (2010) report found that the vast majority of water samples collected in the offshore zone where oil was present in concentrations exceeding the chronic aquatic life benchmark either were indeterminate in origin (given lack of data) or were consistent with MC252 oil (OSAT 2010). Only one of these water samples was consistent with a seep source; this sample was collected on September 9 in 1450 m of water at a distance of 299 km from the wellhead, near a known natural seep area. Joye et al. (2011) found that the contribution of gas from natural seeps was small in comparison to the volume released by MC252, so the seeps would not be a significant source for microbial activity affecting oxygen levels. Jochens et al. (2005) reported that oxygen depressions in the water column associated with natural seeps were extremely localized, within a few centimeters of the sediment.

4 Description of Sampling, Measurement, Analysis, and Results

4.1 Definition of Observational Area

The data included in this report are based on stations located in water depths of >200 m, as detailed in Table 2. The number of stations sampled varied significantly each month. The greatest number of stations sampled was in August and September 2010 (Fig. 20). Figures 21–26 show the locations of conductivity-temperature-depth (CTD) station profiles by month.

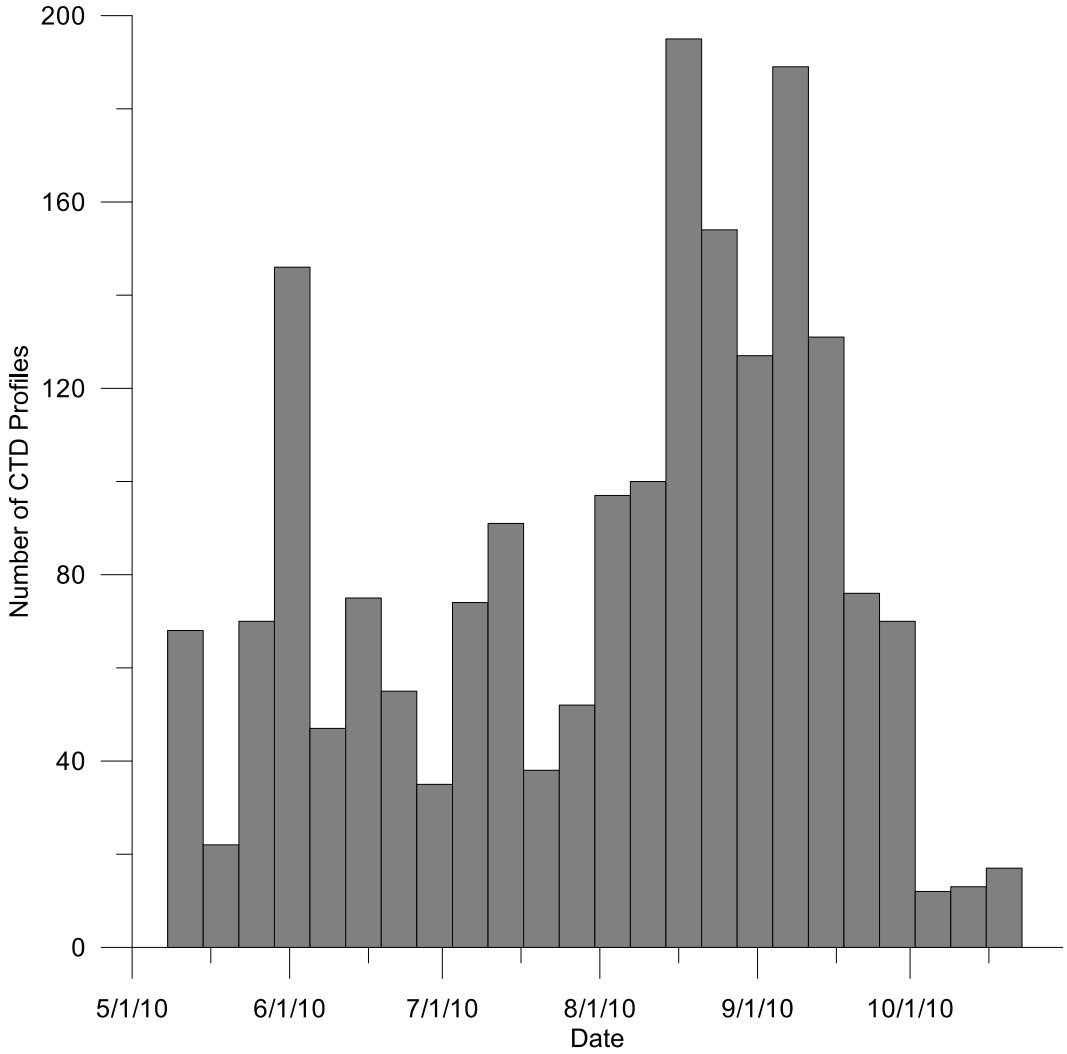

Figure 20. CTD station profiles as a function of time.

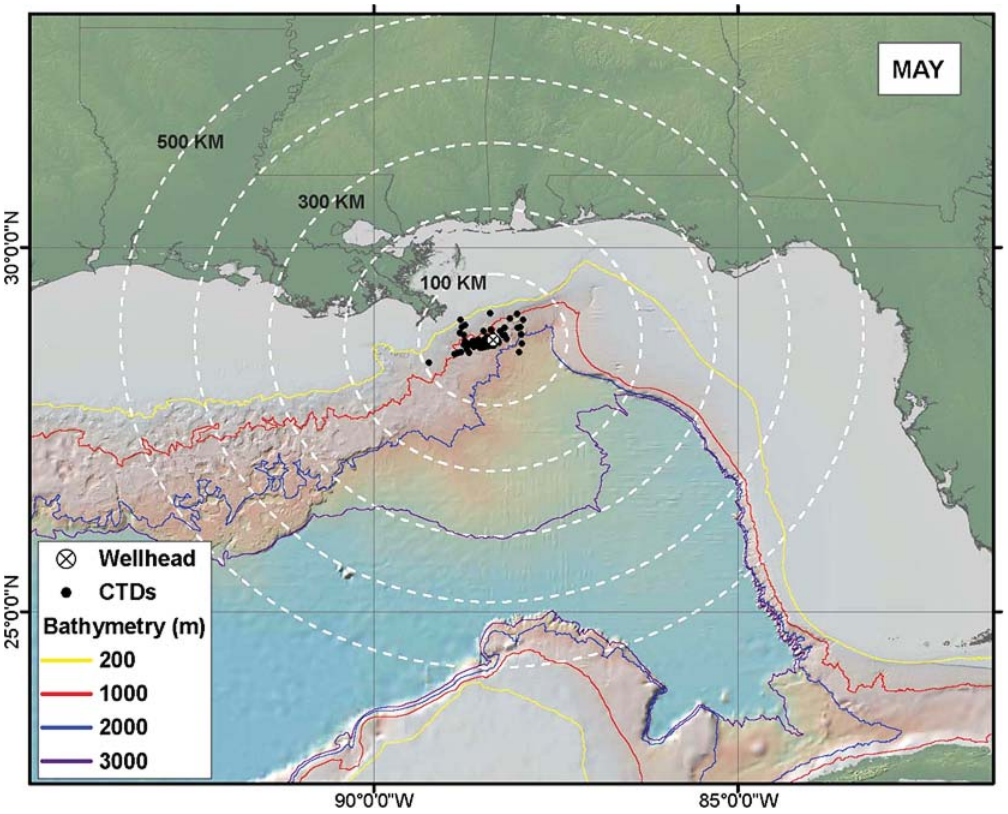

Figure 21. Map of CTD cast locations with a cast depth of ≥200 m for May 2010.

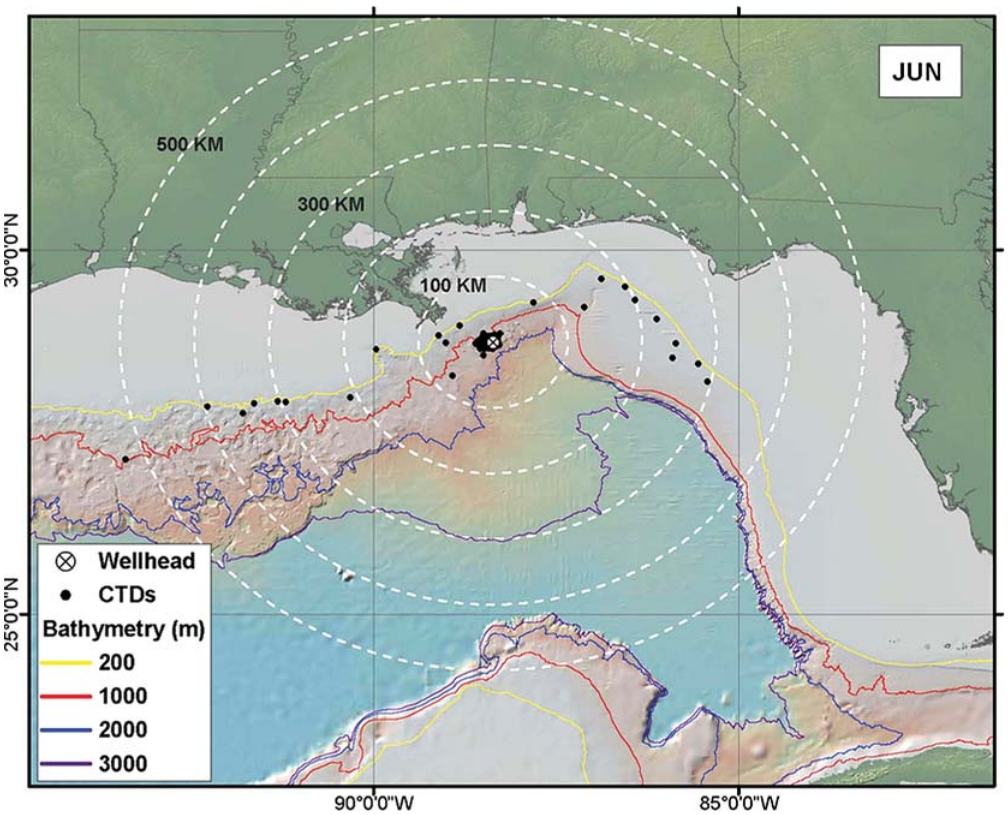

Figure 22. Map of CTD cast locations with a cast depth ≥200 m for June 2010.

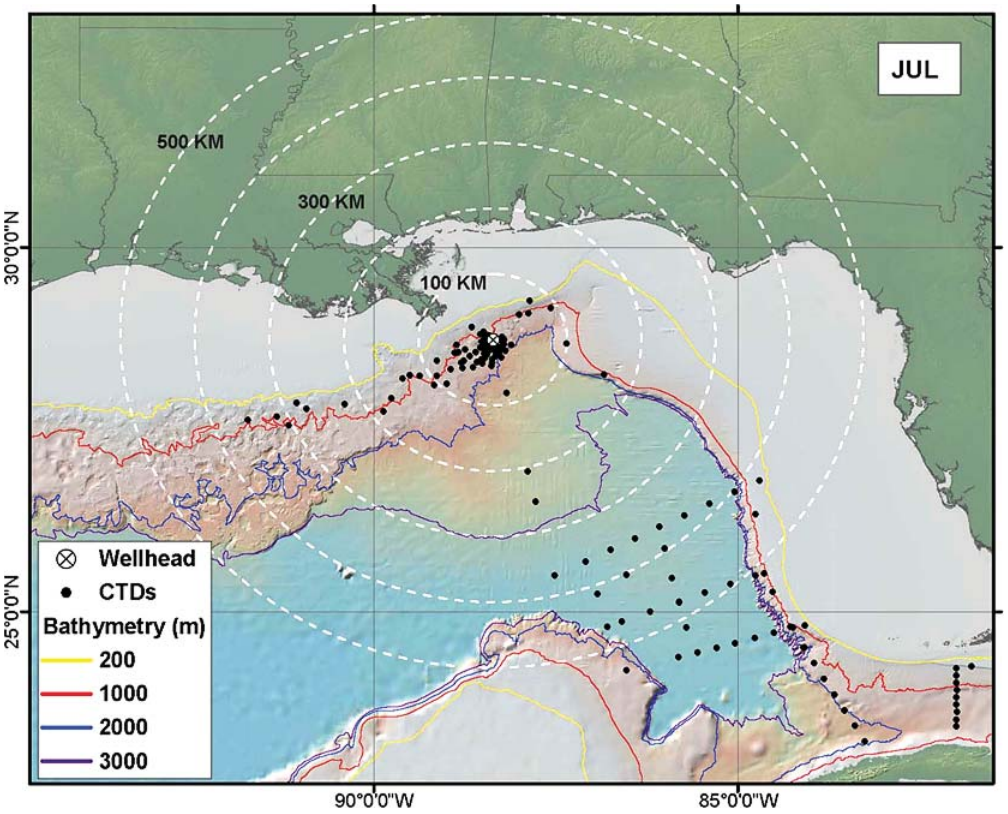

Figure 23. Map of CTD cast locations with a cast depth ≥200 m for July 2010.

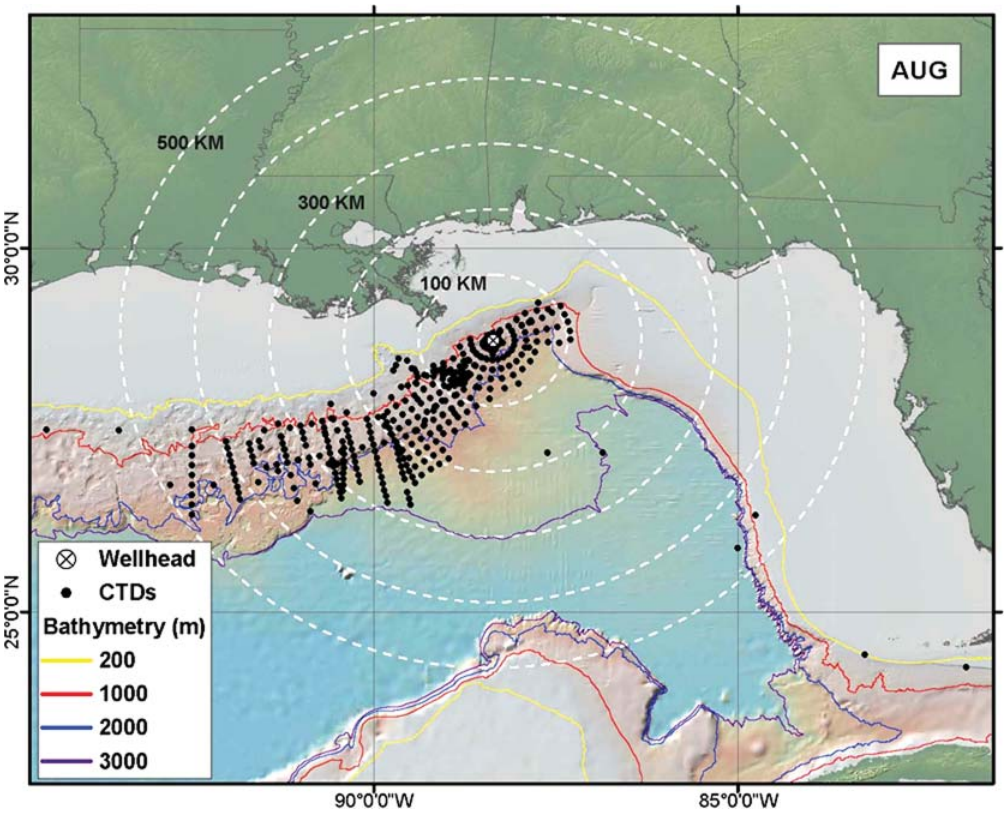

Figure 24. Map of CTD cast locations with a cast depth ≥200 m for August 2010.

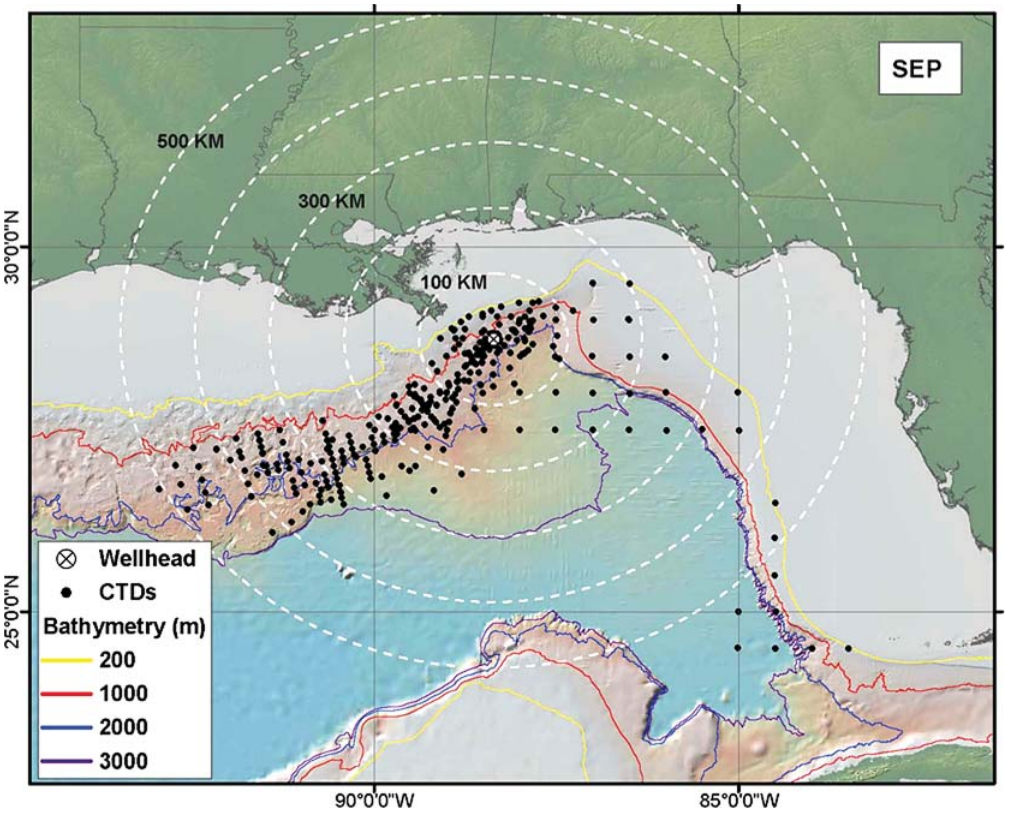

Figure 25. Map of CTD cast locations with a cast depth ≥200 m for September 2010.

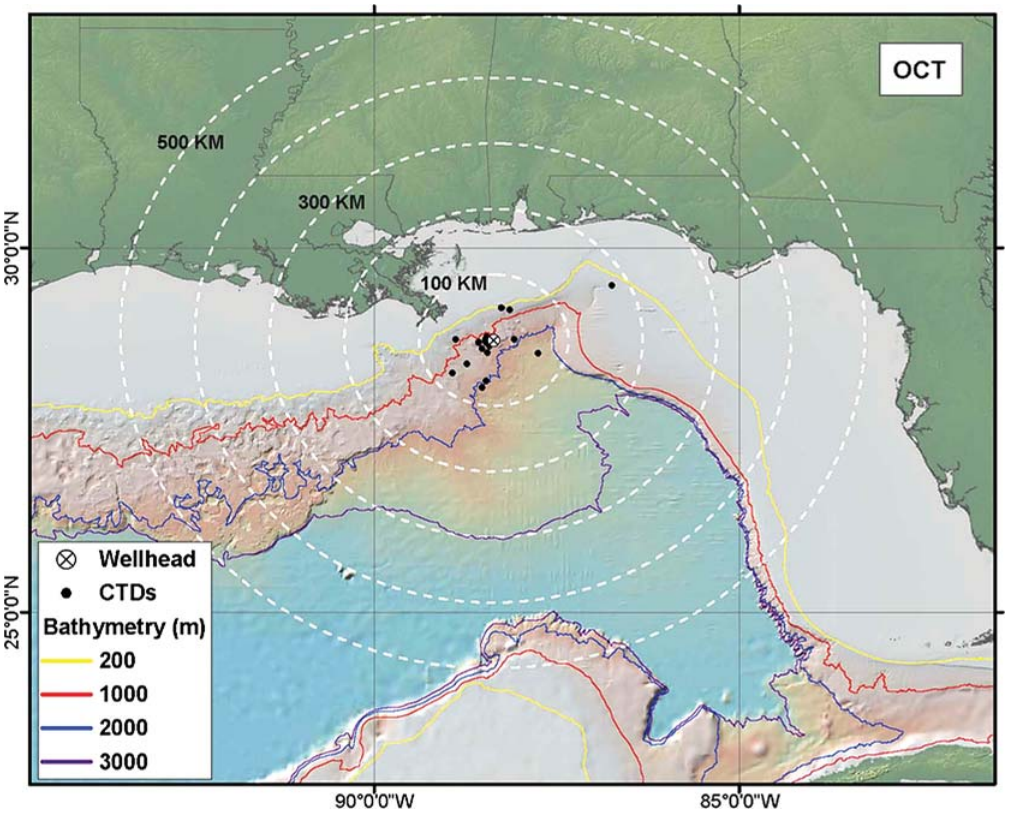

Figure 26. Map of CTD cast locations with a cast depth ≥200 m for October 2010.

A typical station during a cruise included data from in situ instruments mounted on a conductivity-temperature-depth (CTD) rosette and water samples collected from Niskin bottles triggered at discrete depths. Table 2 provides an overview of the types of observation methods, the variables measured for that method, and the dates and number of stations or locations sampled with that method. This report includes data from 1517 stations occupied during 76 cruises, including 6493 water samples. Appendix 3 provides a listing of each cruise, along with the database containing the results of the analytical chemistry.

Table 2. Summary of observations considered for use in this report: Number of observations, period of collection, and units for monitoring data used in this report. Note the absence of any direct observation of methane or other dissolved gases. Data access at NODC: http://www.nodc.noaa.gov/General/DeepwaterHorizon/support.html. Measurements in parts per billion are sometimes referred to as micrograms per liter (µg/L).

Observed Property	Measurement Method (Instrument or Equipment)	Observations	Period of Collection	Units of Measure
Dissolved Oil and/or Oil Droplets	CDOM Fluorometer (various manufacturers and models)	1423 casts	5/10/10–10/19/10	mg/m^3 QSDE
	Chelsea AQUAtracka Hydrocarbon Fluorometer	347 casts	8/16/10–10/03/10	µg/L Carbazole
Dissolved Oxygen	DO_2 sensor, SeaBird Electronics Model 43 (SBE43)	1516 casts	5/10/10–10/19/10	mL/L
Conductivity, Temperature, and Depth	SeaBird CTD (various models)	1517 casts	5/10/10–10/19/10	various
Current Speed and Direction	ADCP (38 kHz) Surface-Mounted	10-minute intervals	05/04/10–09/28/10	cm/s
	ADCP (75 kHz) Bottom-Mounted	20-minute intervals	04/04/10–09/09/10	cm/s
Hydrocarbon levels	Niskin Bottle (water sample)	76 cruises; 989 stations; 6493 samples (6308 whole water; 106 particulate; 79 field-filtered water)	4/20/10–9/2010	ppb, ppm

4.2 Measurement of Oil Fluorescence

Fluorescence is the emission of light by a molecule or a fluorophore after it absorbs photons at a shorter wavelength. All fluorophores have characteristic wavelengths for maximum absorption of light and characteristic wavelengths at which they emit light as fluorescence. Absorption and fluorescence can occur at either narrow or wide wavelength ranges depending on the chemistry and complexity of the fluorophores. A variety of naturally occurring fluorescent compounds occur in the ocean, from those with narrow wavelength ranges with sharp fluorescence peak maxima (plant pigments, such as chlorophyll, proteins, etc.)

to complex compound mixtures with wide diffuse peaks over long wavelength ranges (CDOM, oil). Sources of fluorescent organic materials can either be delivered to the ocean from rivers, groundwater or atmosphere (allochthonous) or produced in situ from aquatic biota (autochthonous). The dominant fluorescence signal in the ocean is from CDOM, comprised of humic and fulvic materials having both sources. It originates from organic material that has undergone remineralization over long time periods.

The fluorescence characteristics of complex mixtures can overlap if structurally similar compounds are shared. Such is the case with CDOM and the aromatic fraction of crude oils. Both are comprised of a variety of organic molecules and both exhibit complex, three-dimensional excitation and emission matrix spectra. In general, crude oils have a broad excitation peak centered in the ultraviolet spectrum (<300 nm) and two emission peaks, one centered in the ultraviolet spectrum around 350 nm and a much larger and broader peak in the visible around 450 nm (Bugden et al., 2008). These peaks result from the single ring benzene derivatives and the "polynuclear aromatic" fraction that are particularly susceptible to ultraviolet excitation wavelengths. Resins and asphaltenes may also contribute to the fluorescence signal, although they are in particularly low concentration in MC252 oil.

Given that oil fluoresces, its presence can be detected with a fluorometer. During the response, vertical profiles of fluorescence were initially obtained from CDOM fluorometers. The CDOM fluorometers were attached to the CTD instrumentation package along with temperature, salinity, and DO_2 sensors. This method allowed responders to identify where the oil was in the water column.

The ability of any fluorescence sensor to detect oil is a function of how well the sensor matches the excitation and emission wavelengths of the oil (including bandwidth of the wavelength filters), the power or the light source, and the sensitivity of the detector. CDOM fluorometers were used to detect oil during the response because of their accessibility and because these sensors are appropriate to detect oil as overlap exists in the fluorescence peak wavelengths for CDOM and oil fluorescence. Typical CDOM fluorometer sensors have light sources that excite at wavelengths slightly longer than peak absorption by hydrocarbons and emitted light in the visible part of the spectrum.

The most common CDOM fluorometer used in the response, a WET Labs' ECO CDOM fluorometer, employs filters centered on excitation (Ex) and emission (Em) wavelengths at 370 and 460 nm (ExEm370/460 nm). Although the center wavelength of the filters does not capture the peak of the oil fluorescence signal, the wide bandwidth of the emission filters (120 nm Full Width at Half Max) and the broad nature of the fluorescence peaks provides this CDOM sensor with the capability to detect a portion of the visible fluorescence signal due to oil.

A second type of in situ fluorometer, the Chelsea Technologies AQUAtracka, was also used in monitoring subsurface oil after the well was capped. The AQUAtracka fluorometer employs filters centered on excitation and emission wavelengths at 230 and 360 nm (ExEm239/360 nm) which are capable of capturing the peak fluorescence due to the aromatic fractions of petroleum hydrocarbons. Additionally, the AQUAtracka uses a xenon lamp for a light source and a photomultiplier tube (PMT) for detection, both increasing the sensitivity and the signal-to-noise ratio of the sensor. Conversely, the ECO uses a less powerful LED light source and a photodiode for detection. As a result, at low concentrations of oil the AQUAtracka sensor was considered at the time to be capable of detecting oil fluorescence at locations where the CDOM fluorometer sensors might not. This consideration was due in part due to the nature of the MC252 oil: it has a small fraction of highly fluorescing molecules, except at relatively higher concentrations of the oil (>1 ppm).

To allow for valid comparisons among the vessels, cruises, and instruments from which data have been drawn, fluorescence data from the CDOM fluorometers presented in this report were normalized using the method described in Appendix 2B. Figure 27a and 27b show normalized fluorescence as detected by CDOM

fluorometers vs. date, color-coded for distance from the wellhead, with figure 27b plotting fluorescence on a log scale. Due to the differences in shipboard configuration (e.g., Analog Scaling Factor selected) and instrument responses, varying degrees of noise existed in profiles. A threshold of 50 ppb Quinine Sulfate Dihydrate Equivalent (QSDE) * m was selected as the floor for detect/non-detect in displaying data from among all sensors/platforms.[8] Figure 28 maps fluorescence detected by CDOM fluoromters within 30 km of the well and to the furthest survey distance. Points below the 50 ppb threshold are show as an "x" in Figure 28. Figures 27b and 28 show that the CDOM fluorometers were able to detect a signal above the 50 ppb QSDE threshold out to approximately 300 km from the wellhead. This value was measured by the R/V Cape Hatteras at station 16-01 on August 26, 2010.

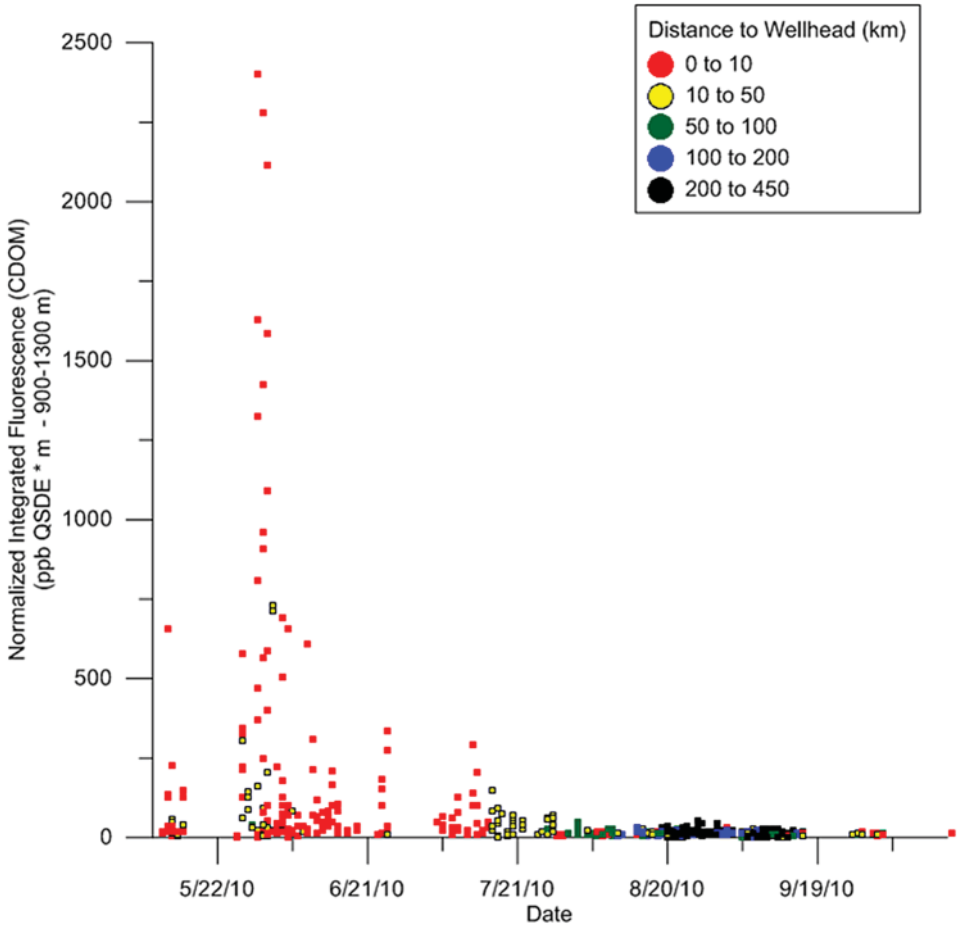

Figure 27a. Normalized integrated fluorescence as detected by CDOM fluorometers (mean 900–1300 m) vs. date and distance from the wellhead (km).

8 See Appendix 2b for a complete explanation of how this threshold was established.

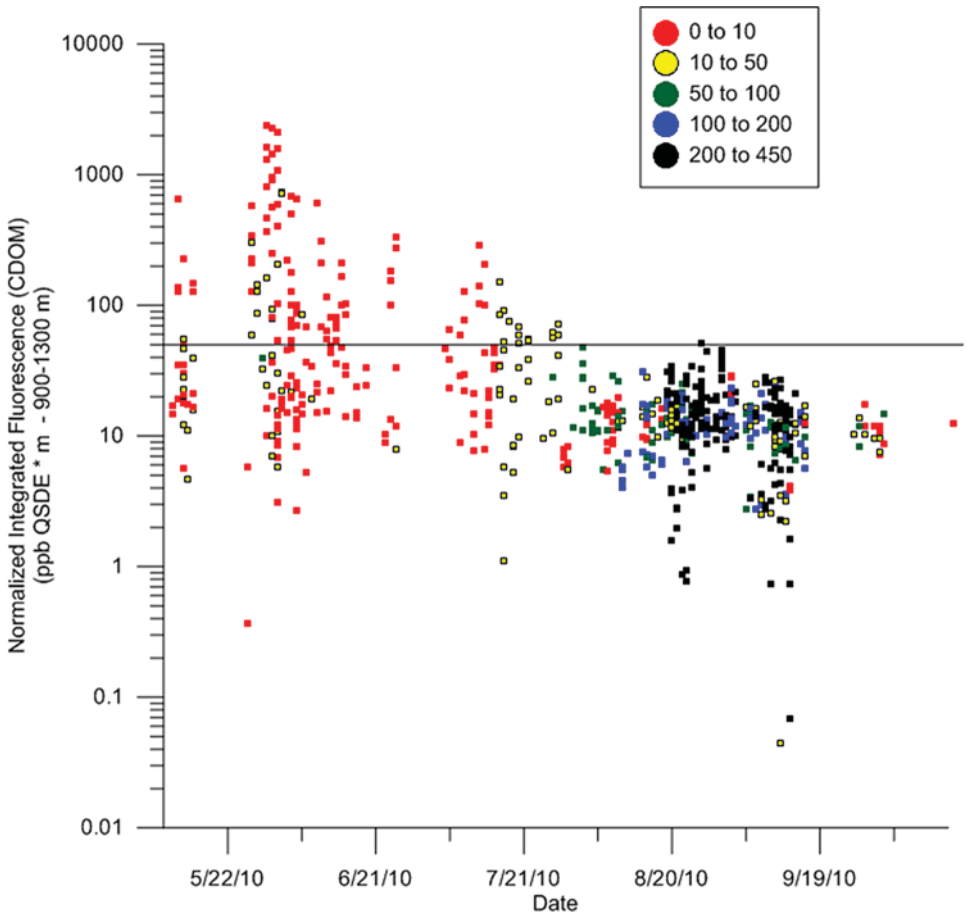

Figure 27b. Normalized integrated fluorescence as detected by CDOM fluorometers plotted using a log scale. The line at 50 ppb*m indicates nominal integrated values for no fluorescence anomaly threshold. Colors correspond to distance from the wellhead.

Where relatively high levels of MC252 petroleum hydrocarbons were observed in the chemical analysis of discrete water samples, strong fluorescence signals were also observed, providing evidence that the CDOM fluorometer was detecting MC252 oil.

Figure 29 shows a significant transition in the fluorescence signal as measured by the CDOM fluorometers within 10 km of the wellhead after about June 1 when removal of the riser began. Before June 1-3, when the riser was being cut, the fluorescence signal was more intense and was found at a higher potential density water layer (deeper depth). After that period, the signal was found at lesser densities (shallower depths), potentially because of the change in the near-field dynamics. As previously discussed, this finding is likely due to a change in the depth of the discharge and character of blowout dynamics due to the riser-cutting operation. Before the riser was cut, three release points were distributed both horizontally and vertically. After the riser was cut, only one release point remained (see Sect. 3.1).

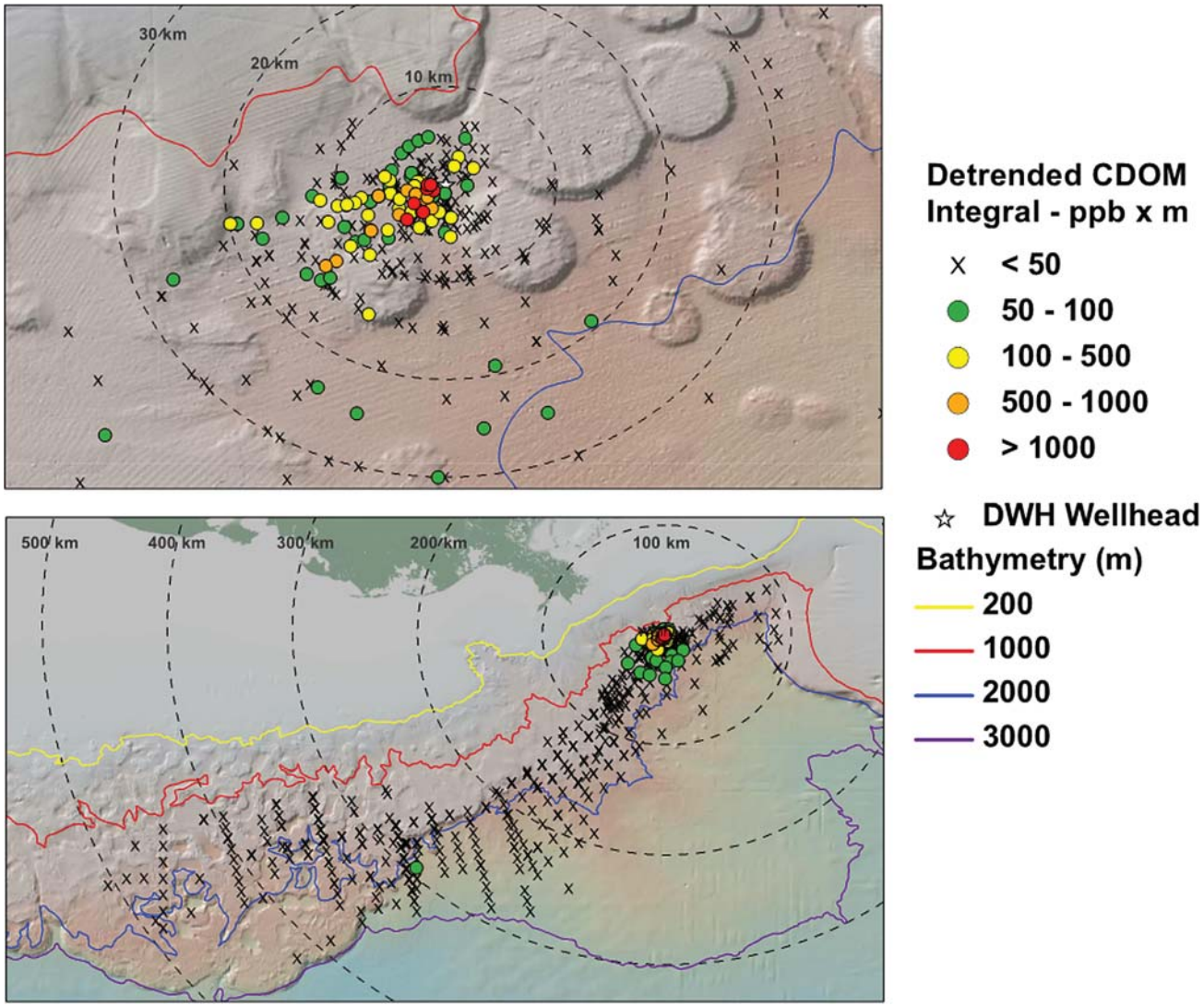

Figure 28. Normalized fluorescence as detected by CDOM fluorometers (mean 900–1300 m) vs. distance to wellhead.

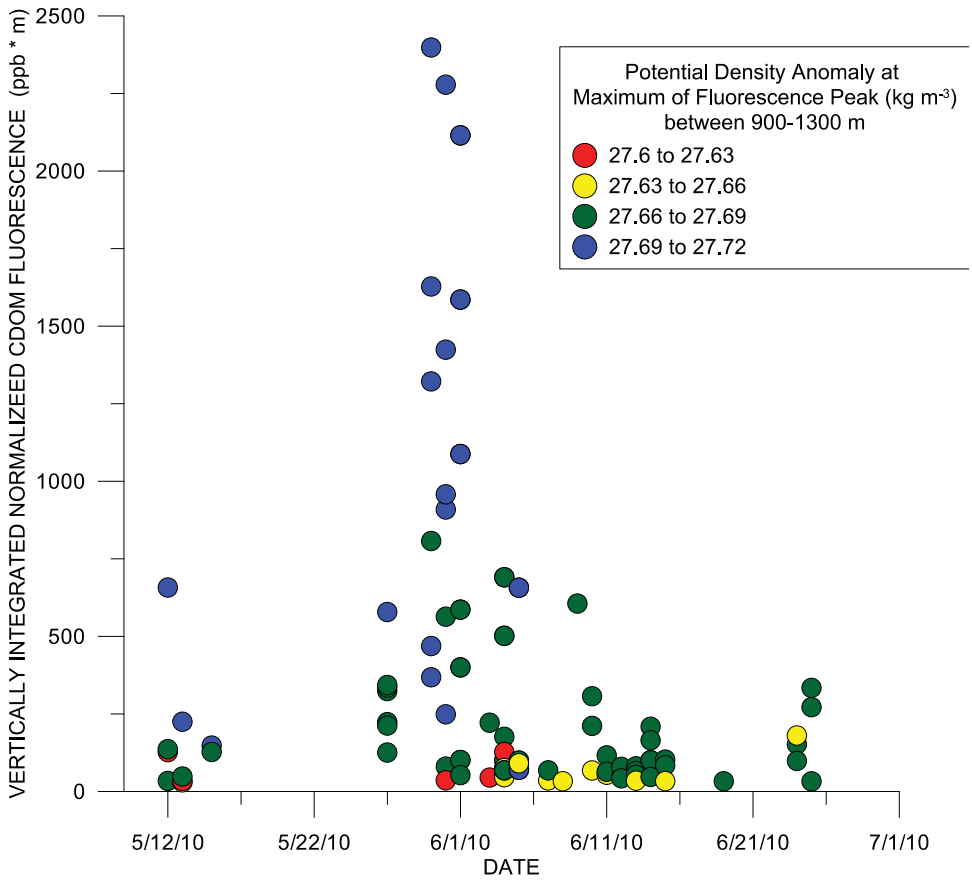

Figure 29. Changes in vertically integrated, normalized fluorescence detected by CDOM fluorometers as a function of water density and time. Colors correspond to the depth at which the maximum fluorescence peak occurred. These data were all collected within 10 km of the wellhead.

As entrained droplet and dissolved fractions moving away from the wellhead were dispersed, diffused, and degraded, the concentrations of detectable hydrocarbon fractions approached or fell below the CDOM fluorometer's detection level. The absence of a CDOM fluorescence signal does not necessarily indicate the absence of hydrocarbons.

Figure 30 shows the changes in the vertically integrated fluorescence signal from the AQUAtracka fluorometer with time as a function of distance from the wellhead. Figure 31 is a map of the AQUAtracka fluorometer signal plotted as distance from wellhead. The AQUAtracka fluorometer detected a signal up to 360 km southwest of the wellhead. Both the AQUAtracka and the CDOM fluorometers detected signals at 300 km. No calibration was carried out with the AQUAtracka fluorometer and MC252 oil at the time of sampling. Therefore, no conclusions could be drawn about concentrations of oil components that might have been present.

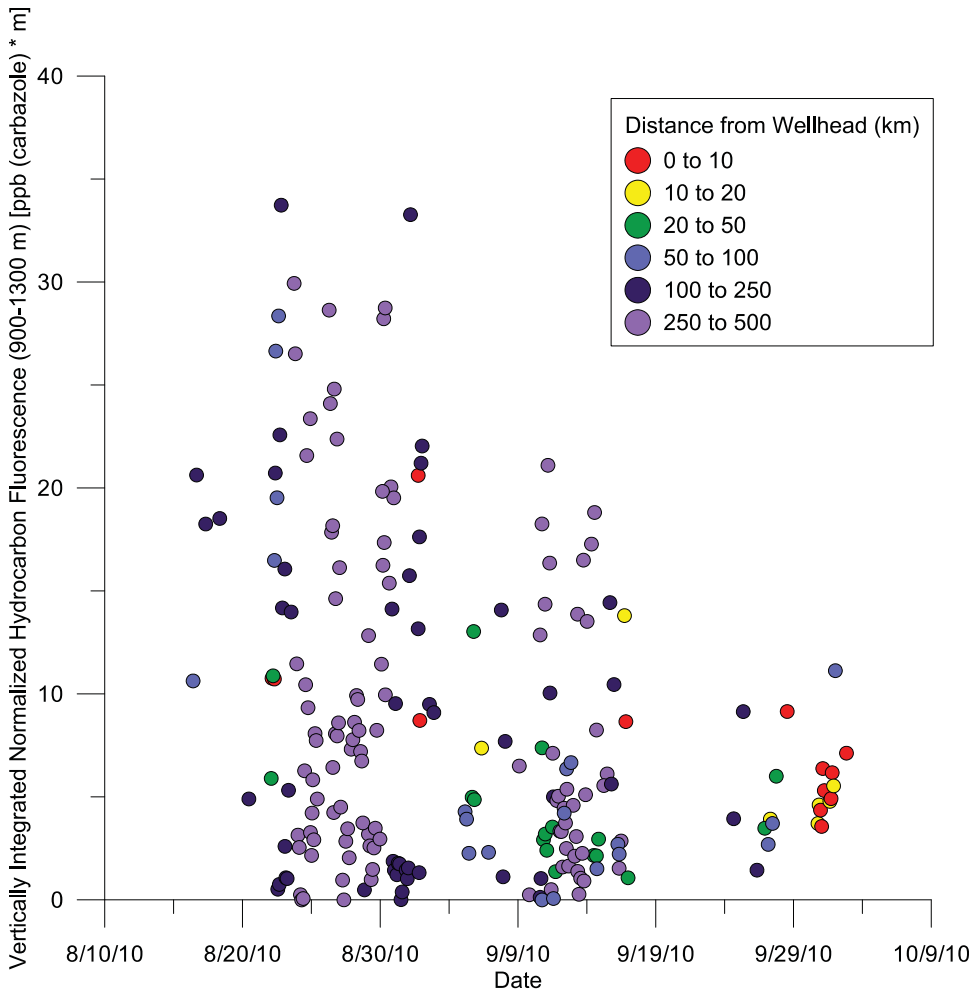

Figure 30. Changes in vertically integrated, normalized fluorescence detected by AQUAtracka fluorometers as a function of distance from the wellhead and time. Colors correspond to distance from the wellhead.

To help understand fluorometer sensor response to MC252 oil, experiments were later conducted at the Bedford Institute of Oceanography's (BIO) Center for Offshore Oil and Gas Environmental Research in Dartmouth, Nova Scotia to study the dynamic range, sensitivity, and response of in situ fluorometers to changing excitation or emission properties of fresh and weathered MC252 oil.[9] The experiments included the stepwise addition of oil and dispersant (DOR, dispersant-to-oil ratio of 1:25) to a wave tank while collecting in situ fluorescence and droplet-size distribution data, as well as coincident discrete samples for chemical analysis and EEM (excitation–emission matrices) analyses. The dataset from this experiment is expected to help to fully evaluate the fluorescence data collected during the oil-spill monitoring effort.

9 It is important to note that these preliminary data are used here for a general comparison of sensors and cannot be used to calibrate sensors as used during the response. A full report is expected to be released on the wave tank experiments in 2012 and will provide additional results for sensor detection limits, saturation, and performance.

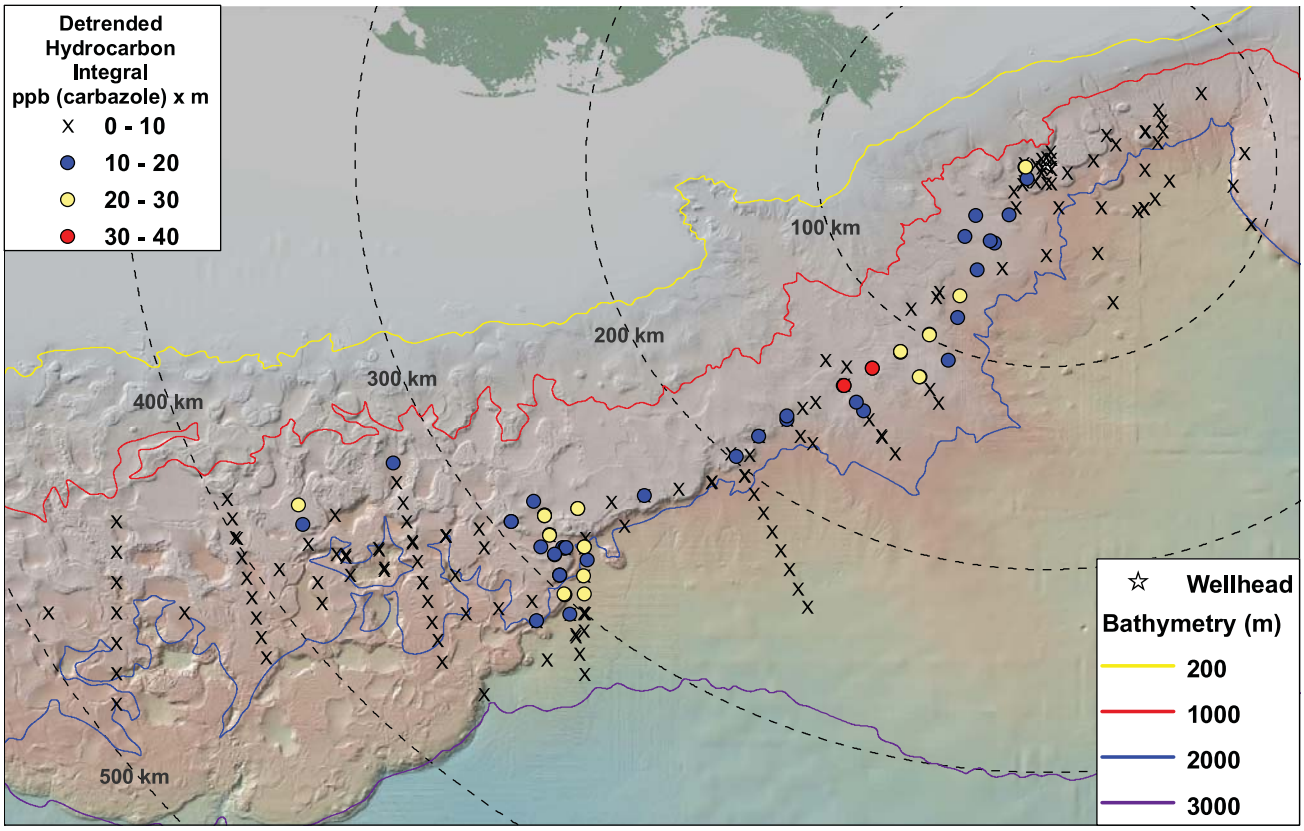

Figure 31. Vertically integrated, normalized AQUAtracka fluorescence.

Analyses of data from the BIO experiments are complete, but data synthesis efforts were ongoing at the time of this report. Preliminary results indicate that all the tested fluorometers were responsive to changes in oil concentration regardless of their wavelength configuration. Figure 32 (Robyn Conmy, pers. comm., U.S. EPA) shows the linear response of the WET Labs ECO, Turner Designs Cyclops and the Chelsea Technologies AQUAtracka fluorometers under varying oil concentration. The left panels of Figure 32 provide the response to the amount of oil added to the tank and right panels are for total petroleum hydrocarbons. Both are presented, as the low concentration additions (0 and 0.3 ppm) were below the detection limit for the total petroleum hydrocarbons analysis. This requires regressions based upon known volumes of oil added to the tank to demonstrate that lowest concentrations were in fact not below the detection limit of any sensor tested.

The experiments conducted at BIO demonstrated that all sensors exhibited a wide dynamic range of detection for MC252 oil and were capable of detecting oil at concentrations of approximately 300 ppb oil.[10] For the ECO CDOM fluorometer, 300 ppb is lower than the minimum detection limit found in an earlier calibration study conducted in 2010 (Joint Analysis Group, 2010b). This calibration found the minimum detection to be in the low parts-per-million range. Results from the 2010 calibration using small volumes within flasks indicated that ECO sensors deployed during MC252 monitoring were capable of detecting oil in relatively

10 It is important to note these preliminary data are used here merely for a general comparison of sensors and cannot be used to calibrate sensors used during the response at this time. A full report is expected to be released on the wave tank experiments in 2012 and will provide additional results for sensor detection limits, saturation, and performance. Principle funding for this work was provided by the National Oceanic and Atmospheric Administration, Fisheries and Oceans Canada, and the Alliance for Coastal Technology.

high concentrations, but might not be particularly sensitive to oil components found dissolved or as droplets below part-per-million concentrations. The differences in detection limit found by the two experiments might be explained by differences in the experimental design, scale, and the amount of physical dispersion (Robyn Conmy, pers. comm., U.S. EPA).

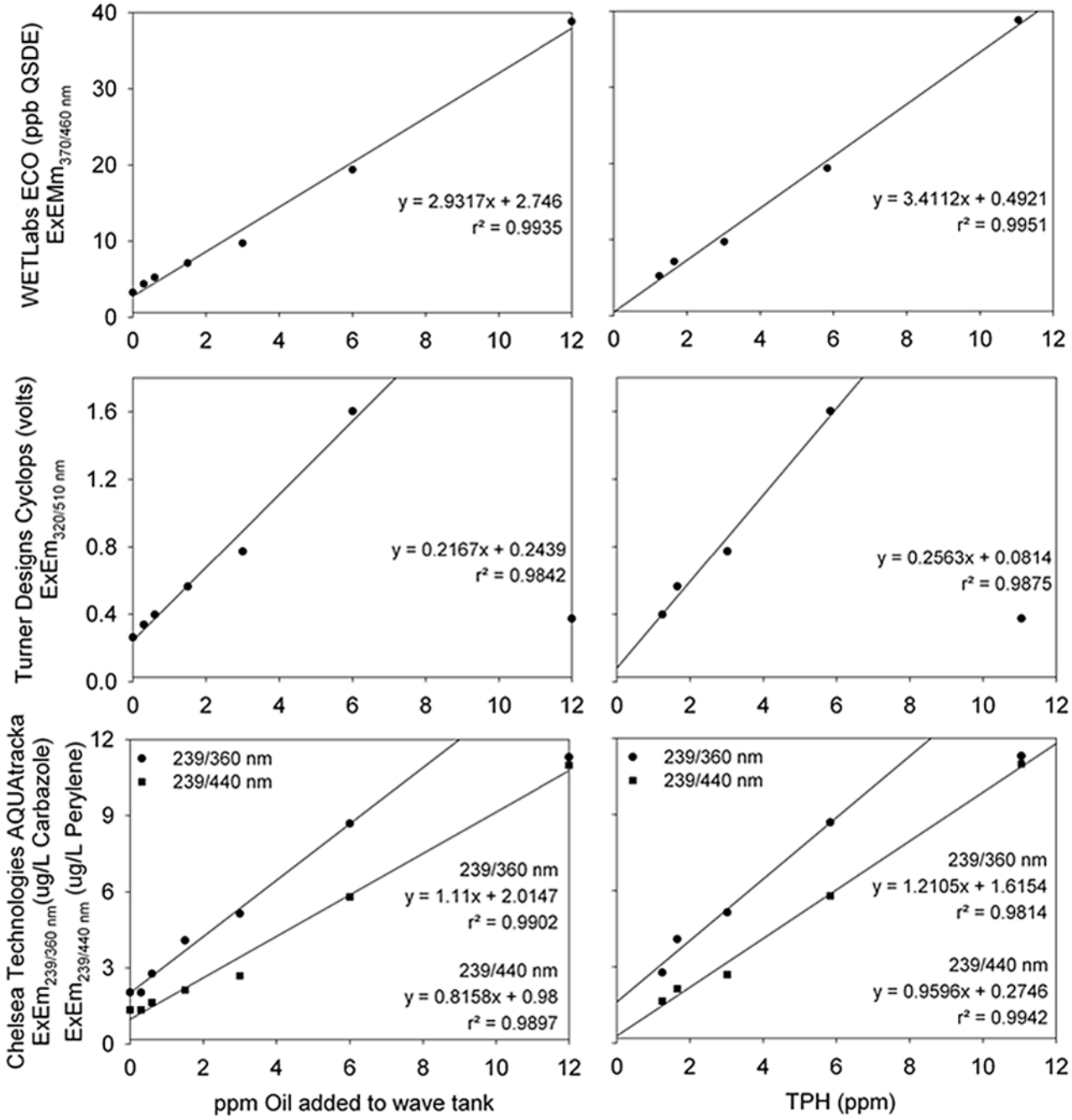

Figure 32. Preliminary calibration results from the May 2011 fluorescence sensor experiment held at the BIO wave tank facility in Halifax, Nova Scotia. Linear least-squares regressions are as shown in the plots and exclude the 12-ppm oil data point for the Turner and the AQUAtracka 239/360 nm due to sensor saturation.

4.3 Dissolved Oxygen Measurement and Results

4.3.1 Dissolved Oxygen Measurements

DO_2 levels were monitored from early in the response to address concerns about hypoxia. As oil measurements and water sample analyses became more limited as a way to detect MC252 hydrocarbons in real time, the affected water mass could be followed by examining depressions in DO_2. This report uses available monitoring data to examine where DO_2 concentrations were lower than expected at depth and whether hypoxic conditions existed over the period of these measurements. Hypoxia occurs when the concentration of DO_2 in the water falls to a level that impedes aquatic life. Hypoxic conditions are generally agreed to occur when DO_2 falls below 1.4 mL/L (also expressed as 2 mg/L),[11] although effects levels are species dependent. In this report, measured DO_2 values were compared to climatological norms described in Section 3.2 to determine if there was an anomalous depression attributable to deep subsurface dispersed hydrocarbons. With the exception of one observation, DO_2 were not observed to reach hypoxic levels in any areas investigated as part of this report.

Vertical profiles from a Sea-Bird Electronics, Inc., SBE 43 in situ sensor attached to a CTD sampling system make up the majority of the DO_2 data used in this report. The SBE 43 sensor used a Clark polarographic-type membrane for measuring DO_2, which captures readings at 2-second intervals as it is lowered and raised through the water column. The sensors were calibrated at the factory, but additional field calibrations were necessary to account for drift over time, systematic offsets, and to validate the measurements. The readings were processed using manufacturer-supplied software, taking into account the sensor response and susceptibility to pressure and temperature changes. The final data are presented at 1-m depth intervals.

In addition to calibration, these sensor systems are subject to a number of known issues that can affect data quality, including data transmission problems associated with the thousands of meters of conducting wire and related electrical connections, and can experience interference from contaminants in the sampled water. In addition, instrument setup, deployment, and post-processing software setting must be appropriate and consistent.

Automated Winkler chemical titration techniques using photometric or amperometric end-detection methods with proper sampling protocols are the most accurate method with the highest precision for measuring DO_2 at sea when they are performed by a trained operator using carefully prepared reagents and standards and with calibrated flasks following accepted protocols (e.g., (Dickson, 1995; Langdon, 2010).

Wanninkhof et al. (2011) examined Winkler oxygen measurements on NOAA Ships *Nancy Foster*, *Ocean Veritas*, *Brooks McCall*, *Henry B. Bigelow*, and *Pisces* during the spill response to assess the accuracy of the SBE 43 in situ DO_2 measurements. Overall, they found the SBE 43 measurements to be consistent to within approximately 2% (≈0.1 mL/L) for the Winkler data investigated, with a few exceptions as noted in the report. They concluded that SBE 43 measurements were a reliable indicator of DO_2 reductions due to oxidation of MC252 oil and gas. However, of the data in this report, only 15 cruises had Winkler oxygen measurements available for comparison to SBE 43 measurements.

The agreement between the CTD and DO_2 being within 2% is not necessarily applicable to all ships from which data are included in this report. Significant offsets, perhaps attributable to calibration differences, occur among some vessels and cruises and make direct comparisons of CTD data difficult. To mitigate this intercruise variation, this report integrates DO_2 anomaly values at depth, as determined from the SBE 43 sensor trace, over each CTD cast (described in Appendix 2C).

11 For DO_2, 1 mL/L is approximately equal to 1.43 mg/L.

DO_2 was also measured by means other than Winkler titrations in discrete water samples collected at specific depths with Niskin sample bottles during select cruises using different approaches. In these samples, the DO_2 was analyzed using chemical or electronic methods implemented in a variety of ways. Chemical measurements included commercial kits, such as the LaMotte and Hach DO_2 field-test kits. These kits are adaptations of the classic Winkler chemical titration method and are considered easier, but they are significantly less precise and accurate than the original Winkler procedure. Electronic DO_2 probes used on bottle samples on deck included an Extech membrane-based DO_2 probe, a YSI ProODO (optical probe), and a YSI Ecosense 200 (membrane probe).

On-deck measurement of DO_2 in bottle samples was complicated by the need to prevent sample contamination by atmospheric oxygen during the measurement. These methods can also be affected by sampling errors, reagent quality, operator inconsistencies, and interference from contaminants in sampled water. The DO_2 data from discrete water samples are not included in this report because they are not consistently available across cruises and, with the exception of the Winkler technique, are not considered as reliable as the in situ measurements.

4.3.2 Dissolved Oxygen Results

A DO_2 depression was consistently found in the waters between 900 m and 1300 m and, with one exception, did not reach levels considered to be hypoxic. Figure 33 shows SBE43 DO_2 data for the 1472 casts made between May 5, 2010, and October 19, 2010. Profiles were >200 m deep and had passed the quality-control procedures described in Appendix 2c. The majority of those casts do not show a significant variation from climatological norms described in Section 3.2. The wide band of DO_2 that is considered to be within the climatological norms results from cruise-to-cruise variations in instruments and also to regional variability in climatological norms (as discussed in Sec. 3.2).

The light-green dots on Figure 33 depict data from the R/V *Pelican* cruise in May 2010.[12] Profile 47A, taken on May 15 about 19 km west–southwest of the wellhead, shows a DO_2 anomaly observed between approximately 600 m and 800 m that fell below levels considered to be hypoxic. This DO_2 anomaly is one of the largest seen in the data.

12 CTD data from the R/V *Pelican* cruise were generously provided to the JAG by University of Southern Mississippi researchers. These data provide valuable information; however, additional supporting information (such as a chemical analysis of water samples) was not available to the JAG. Therefore, a comprehensive assessment of those data in the context of this report is not possible.

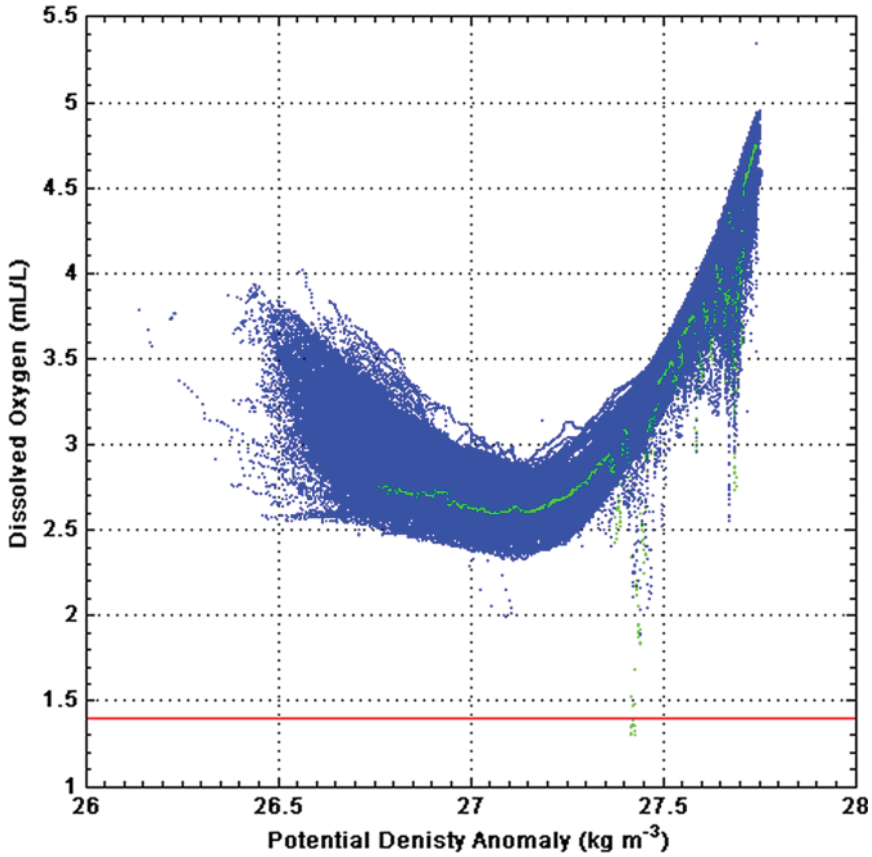

Figure 33. DO_2 data for 1472 casts measured with the SBE43 sensor. Only those that passed quality-control procedures described in Appendix 2C were used. The red line denotes the level below which DO_2 values are considered to be hypoxic. Light-green values are from the R/V *Pelican* cruise, where one cast had DO_2 values that fell below levels considered to be hypoxic.

A DO_2 depression in this 600 m to 800 m depth range can also be seen in R/V *Pelican* station 34 data taken about 2.6 km from the wellhead on May 12. Station 47A and 34 do not have corresponding fluorescence signals as measured by CDOM fluorometers associated with these DO_2 anomalies, unlike other stations where significant DO_2 depressions were seen. No corresponding water sample analyses were available to the JAG for these stations to help evaluate hydrocarbon levels. The JAG cannot determine why the anomaly was found in this depth range based on available data, but there is no reason to doubt the accuracy of these measurements. Specific information on this and other cruises from which data were derived can be found in Appendix 3, along with R/V *Pelican* station 47A and 34 profiles.

Figure 34 shows quality-controlled temperature and salinity data taken from the 1517 deep casts considered for this report. Gray dots indicate data that did not pass quality control checks. Black dots indicate data that passed quality control, approximately 96% of the individual depth points subjected to the quality-control checks. Red dots indicate the data space within the quality-controlled data for the anomalous DO_2 values. Anomalous is defined as the difference between the measured DO_2 values and the expected DO_2 value as determined by the methods described in Appendix 2c. Differences between measured DO_2 and the expected DO_2 values of 0.1 mol/m^3 or less are not considered.

Figure 35 shows the normalized-integrated DO_2 depression as a function of distance from the well and potential density. The largest DO_2 depressions are found within a relatively narrow density range independent of distance from the well. A spatial patchiness to the distribution of the DO_2 depression can be seen in these data.

DO_2 levels show a distinct depression with the first available data in mid-May, as seen in Figure 36, where casts with anomalous DO_2 values are plotted versus time. The hiatus in data for late June corresponds to the passage of Hurricane Alex, during which time sampling was suspended. DO_2 depressions decreased from initial intensity observed during early active release and continued to be observed as distinct depressions at comparable magnitudes until mid-September 2010, even at hundreds of kilometers from the wellhead as can be seen in Figure 37. These data likely captured the principal areas of DO_2 depressions associated with the MC252 release.

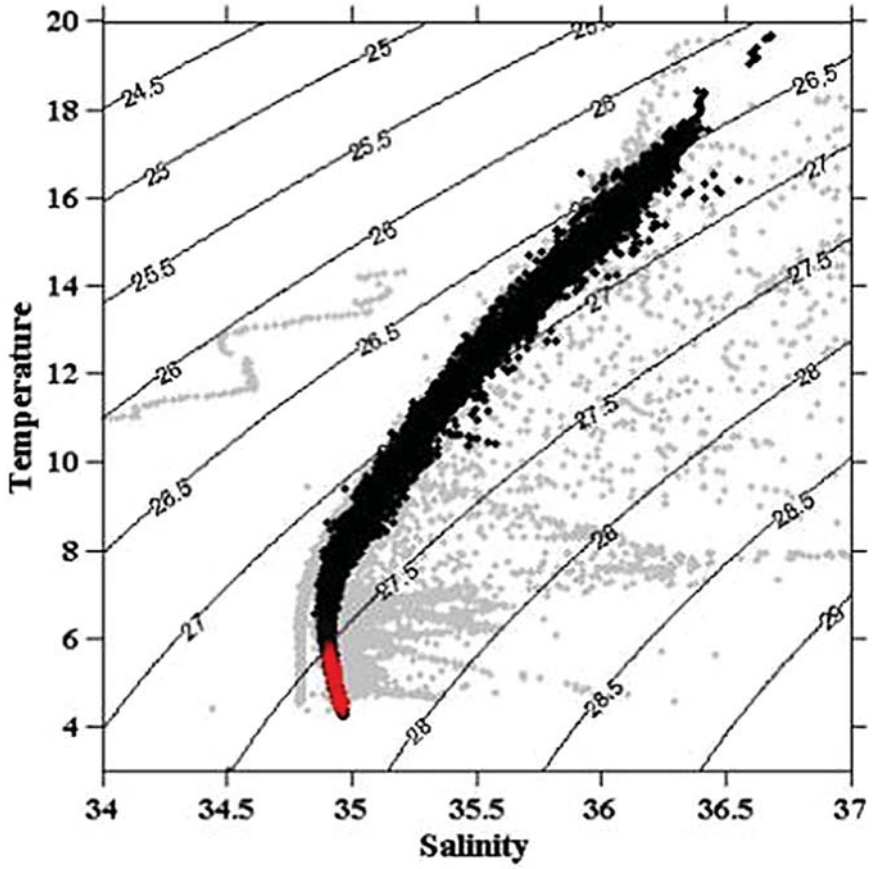

Figure 34. Results for quality-control analysis of SBE 43 sensor data from all cruises and casts considered in this report. Gray dots are casts that did not pass quality control tests; black and red dots did pass. Red dots indicate casts with anomalous DO_2 values within the depth range of 900–1300 m.

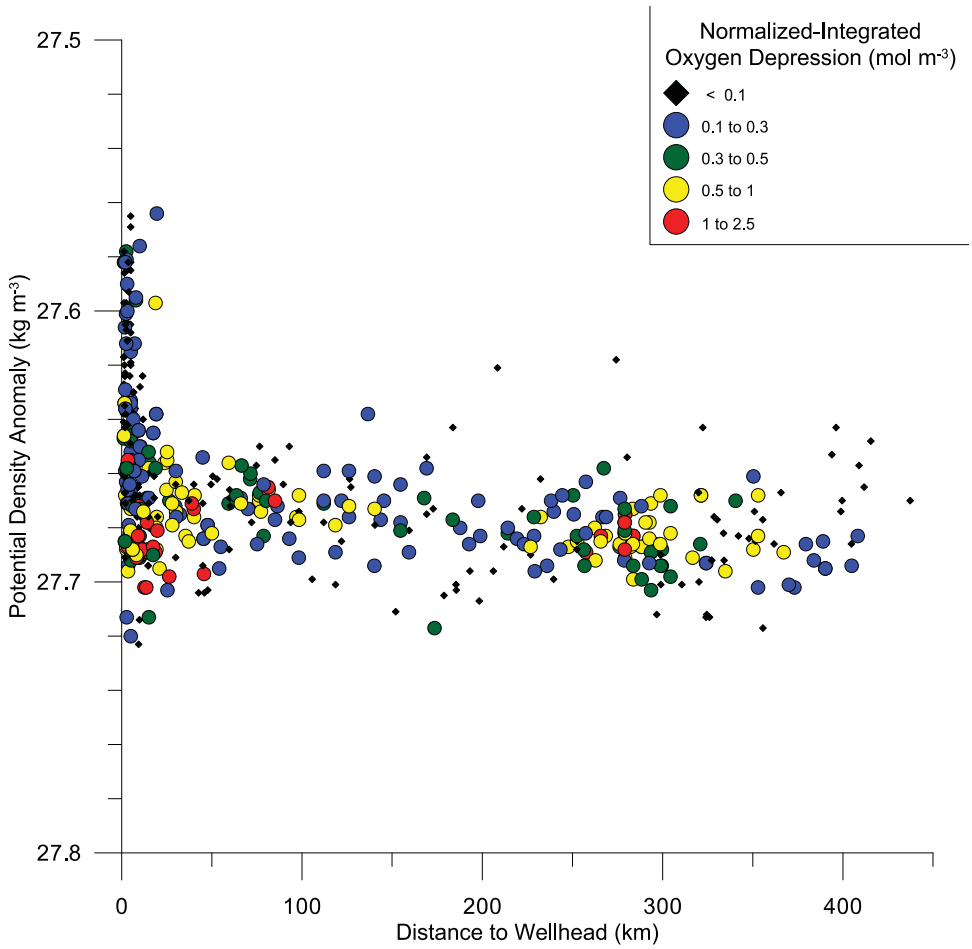

Figure 35. Normalized-integrated DO_2 levels in the 900- to 1300-m depth range that passed quality-control procedures as a function of distance from the well and potential density. Colors show the normalized integrated oxygen depression.

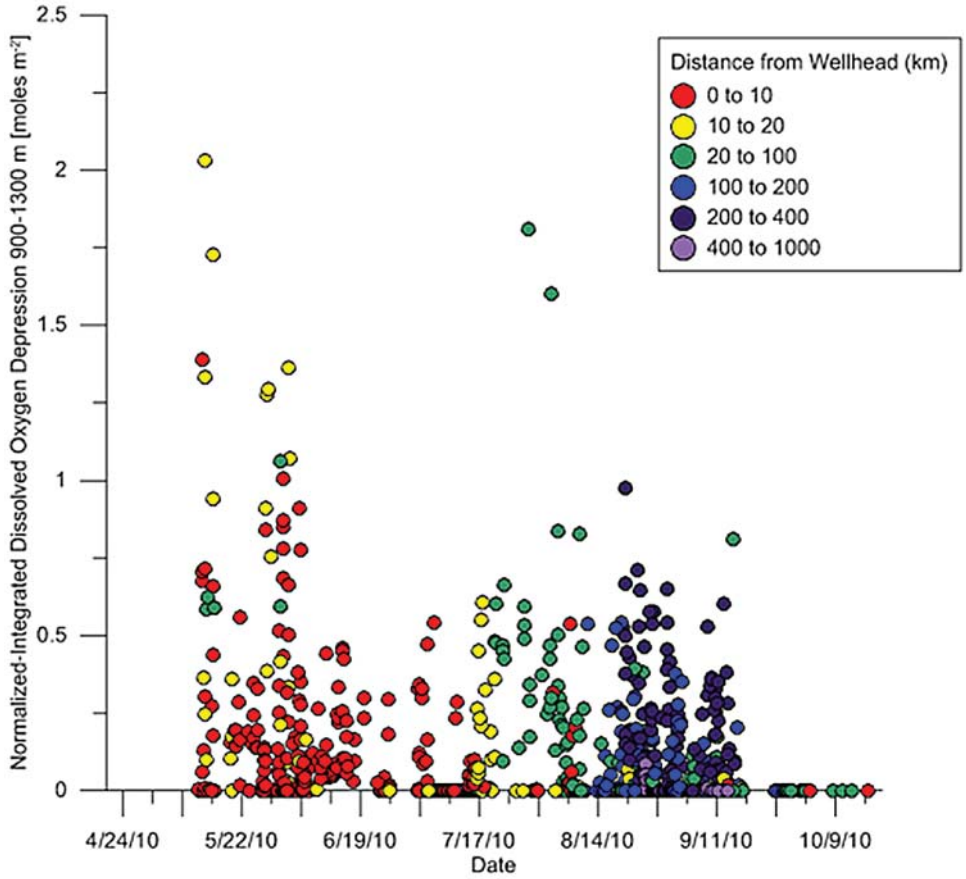

Figure 36. Normalized-integrated DO_2 levels in the 900- to 1300-m depth range that passed quality-control procedures as a function of time and distance from the wellhead. Colors denote distance from the wellhead.

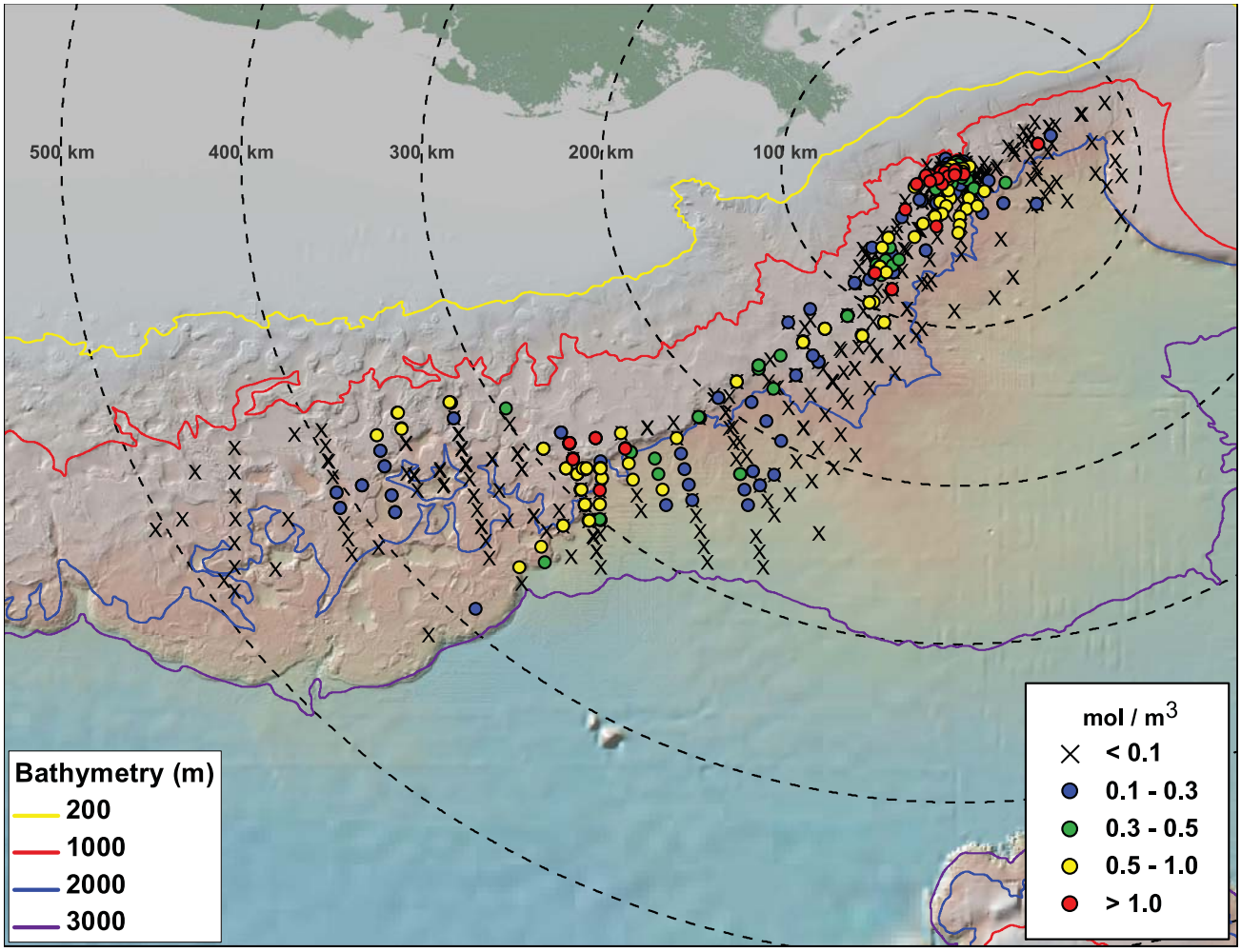

Figure 37. Map of normalized-integrated differences in DO_2 values. The differences between measured DO_2 and the expected DO_2 values of 0.1 mol/m² or less are not considered significant and are shown as an X. Depressed DO_2 values were measured about 400 km from the wellhead.

4.4 Ocean Current Measurements and Results

A number of platforms in the area collected ADCP data during the time that the data used in this report were being collected. Of the potential platforms that could have provided data along the deep subsurface dispersed oil pathway, five used 75-kHz ADCPs that did not penetrate deeper than 700 m; one reached 1000 m, but no deeper, and three production platforms did not collect data during the event, although they may have collected data before or after. MC252 was equipped with a 38-kHz Teledyne RDI ADCP instrument and transmitted data up to minutes before the explosion occurred on the platform.

Current observations in this report are based on ADCP data from the Ram-Powell, Development Driller 3, and Discoverer Enterprise platforms (Fig. 38). Development Driller 3, the drilling rig used to drill the relief well, was equipped with a 38-kHz ADCP, as was the Discoverer Enterprise rig used to bring oil and gas to the surface from the seafloor. Development Driller 3 was in place at the MC252 site and began collecting ADCP data on May 1, 2010. The Discoverer Enterprise was drilling 55 km to the south–southwest of the MC252 rig at the time it exploded. It remained there for 10 days before moving near the MC252 site on May 9, 2010 and began collecting ADCP data.

These two deployments of 38-kHz ADCPs, which penetrate to almost 1200-m water depth under good conditions, provided important information at the site of the spill during the time that oil was flowing. The ADCP captures a time history of the direction of currents affecting how hydrocarbons moved away from the wellhead site. An additional ADCP on the production platform Holstein, about 250km to the southwest of the MC252 site, provided information about the transport of the deep subsurface dispersed oil as it moved in that direction. The mean flow seen at platform Holstein was weaker, but in the same general direction as that seen closer to the well.

Figure 39 shows daily average current speed and direction information measured from the Development Driller 3 near the wellhead at 1152-m depth. The daily average currents (May 11–July 22) show the percent time the current flowed in a directional bin. Length of individual speed bin bars represents the number of occurrences that fall within the angular region defined by the bin size and speed. (Each directional bin can contain multiple speeds.) The flow direction during the measurement period was primarily to the southwest, following isobaths. The average current flow is between 2.0 and 4.0 cm/s, with velocities that ranged from 0 to 12.0–16.0 cm/s. Currents at platform Holstein had more of an offshore (southward) component than those measured near the well.

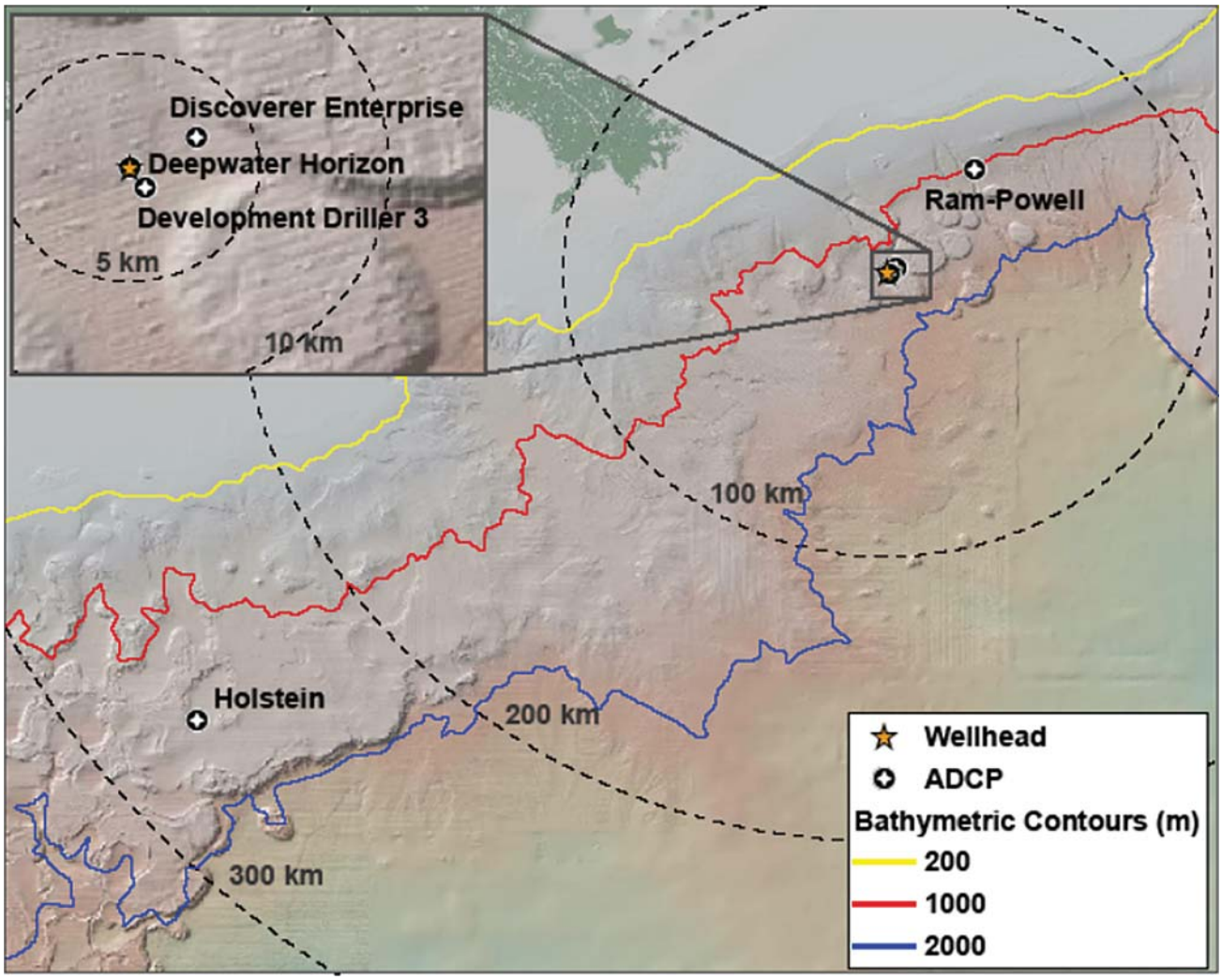

Figure 38. Location of ADCPs in the area of the MC252 well.

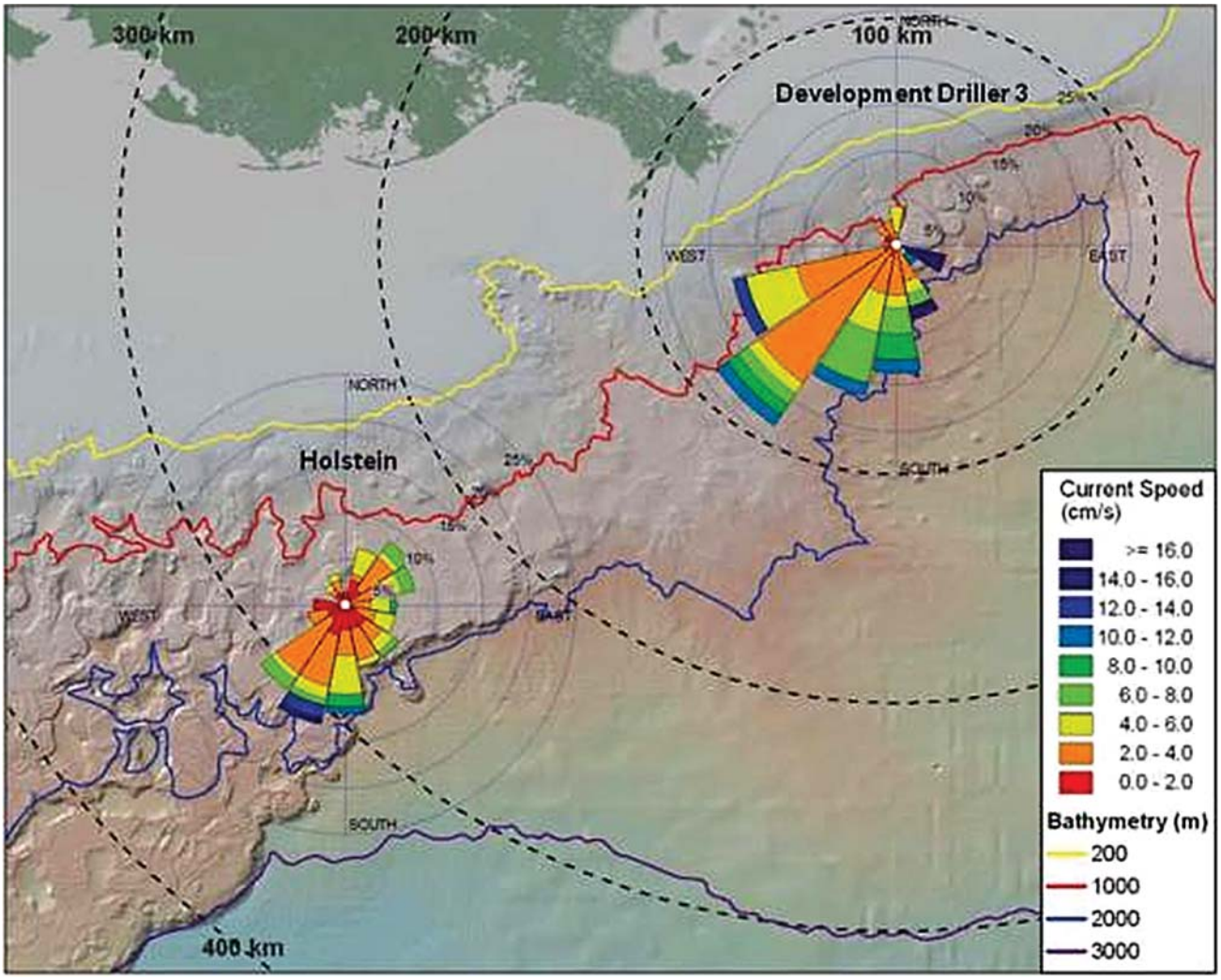

Figure 39. Current rose diagram of Acoustic Doppler Current Profiler currents.

Less frequent, but high-velocity events can be seen to the east-southeast. Some events to the north and northwest are also present. Easterly and northerly events could lead to water being recirculated back over the wellhead when currents reverted back to a southwest flow. The high-velocity, east-southeast event took place in mid-July during well-capping operations. At times those operations caused a loss of ADCP data. While no current flow to the northeast was measured, they could have occurred prior to the start of data collection on May 11. Topographic steering would be expected to control water movement away from the wellhead as a result of salt domes, particularly the Biloxi dome to the southwest.

4.5 Water Sample Analyses and Results

4.5.1 Chemical Methods of Analyses

This section describes the analytical chemistry methodologies used during the spill response to report analytical chemistry data for water samples collected with bottles as part of CTD casts. Chemical analyses were performed on 6493 water samples from 989 sampling stations. The samples were collected from 76 vessel cruises (listed in Appendix 3). The results of the analytical data were managed in two databases:

the EPA Scribe database; and the National Resource Damage Assessment (NRDA) Query Manager (QM) database.

The gasoline range volatile hydrocarbons were analyzed using the standard EPA SW-846[13] purge-and-trap analysis method 8260. Appendix 2 contains an in-depth discussion of the analytical methods used for analysis and Appendix 5 contains a complete list of analytes. Method detection limits for specific analytes were about 1μg/L. Specific method 8260 petroleum analytes results were summed to establish a concentration for each sample that represented the relative abundance of the more water-soluble fraction of the crude oil (tVOA). These concentrations were used to plot volatile petroleum hydrocarbons in figures and maps.

Semivolatile hydrocarbon analyses were performed by EPA SW-846 method 8270. Method detection limits for specific analytes were primarily below 1 μg/L. Method 8270 uses gas chromatography with mass spectroscopy. Modifications of 8270 were used to quantify semivolatile alkanes, biomarkers, and parent and alkylated PAHs, which were not normally analyzed by this method. To account for the bulk of the petroleum in this fraction for these samples, EPA SW-846 method 8015 was used to determine concentrations of the hydrocarbons in the semivolatile fraction (C9 to C44). This method used a gas chromatograph with flame ionization detection (GC/FID) and captured the large amount of saturate hydrocarbons that comprise the unresolved complex mixture often seen in hydrocarbon mixtures. Method detection limits for specific analytes were in the low μg/L range. To ensure that we have accounted for bulk of the hydrocarbon mass in this range, the results from method 8015 were added to those from the GC/MS 8270 analysis for each sample to determine the concentration for all the low water-soluble oil compounds (sTPH). These concentrations were used in figures and maps.

The analyses described above are protocols that yield individual petroleum hydrocarbon component concentrations. They are not designed for source identification chemistry. The source of highly weathered oil droplets can be identified only if that oil is in concentrations high enough to give reasonable ion chromatograms of biomarkers and fingerprint chromatograms. Except in areas close to the wellhead, where relatively high concentrations of oil droplets were present, source identification chemistry could not be effectively accomplished. At about 10 km from the wellhead, the sTPH concentrations dropped to the low parts per billion range, which precluded effective source identification using samples contained in this report. There are no analytical results in this report for natural gas components, including methane, condensates, and non-hydrocarbon gases released at the well.

The MC252 oil spill posed significant sampling challenges due to the size and extent of the spill. As a result, multiple sampling teams and sampling platforms were used on short notice, which might have resulted in differences in analytical results due to sampling rather than measured parameters. Laboratory quality control and quality assurance data were examined to identify potential systematic errors. Nothing has been found that would have invalidated the data, although few quality-control data were provided in the Scribe Database. Substantial quality-control data were provided in the QM Database. The EPA Analytical Protocols, as documented in each laboratory's standard operating procedures, dictated laboratory quality control/quality assurance. These standard operating procedures were, for the most part, guided by the SW 846 protocols, except that deviations were necessary to successfully detect and quantify the special list of oil hydrocarbons already identified.

The Scribe chemistry dataset is based on extractions from two of the databases: NOAADW (version 79, August 8, 2011) and the Environmental Standards database (version 72, August 23, 2011). Data used in this report from the QM Database was current as of August 18, 2011. The query consisted of all publicly releasable data as of that date. The participating analytical laboratories might continue to make minor changes

13 U.S. Environmental Protection Agency Publication SW-846 "Test Methods for Evaluating Solid Waste, Physical/Chemical Methods"

to data as part of data quality control, assurance, and validation activities after data were extracted for this report. The JAG is confident that these minor changes to chemical data will not substantially affect the conclusions that the present data support.

4.5.2 Chemistry Results

Analytical chemistry results are reported in two groups, tVOA and sTPH. As used in this report these fractions are defined as:

- tVOA - alkanes pentane (C5-C8) aromatic hydrocarbons, benzene, toluene, xylenes, ethylbenzene, through naphalene – EPA method 8260. This is the more readily water-soluble fraction.
- sTPH - heavier saturates (C9-C44 - EPA method 8015), biomarkers, and parent and alkyl substituted polynuclear hydrocarbons (i.e., heavier than naphthalene) – EPA method 8270. This is the less readily water-soluble fraction.

Separately reporting tVOA and sTPH allows differences in these fractions observed early in the spill to be distinguished. The differences (i.e., high tVOA totals, low sTPH totals in the same samples) are thought to be caused by a separation or fractionation of these hydrocarbon components in the water column due to rates of dissolution for the components of each fraction of the oil in general. Both were reported as part per billion concentrations. The tVOA and sTPH concentrations were binned into ranges (<1, 1–10, 10–100, 100–1000, and >1000 ppb) to help visualize data as it relates to oil concentrations.

The summary chemistry results represent analyses of 6308 whole water samples collected between the depths of 198 m and 2340 m from May 8, 2010 through November 12, 2010. Table 3 shows concentration ranges for both the tVOA and sTPH fractions analyzed. The levels of sTPH at depths of 900–1300 m were mostly quite low (1–10); the highest level in a water sample was 485 ppb found in a sample taken May 30, 2010 at *Brooks McCall* station 054, 1.2 km from the wellhead at 1194 m. More tVOA fractions were found in significantly higher concentration ranges than detected in sTPH fraction hydrocarbons. For the tVOA fraction, a maximum concentration of 2112 ppb was detected in the same sample as the highest sTPH value. Hydrocarbon levels above 10 ppb were mostly confined to within 20 km of the wellhead.

The concentrations of sTPH versus depth and time collected are plotted in Figure 40. Particularly evident in this figure is that most of the samples with the highest concentrations of sTPH were detected at depths between 900 m and 1300 m, consistent with fluorescence peaks and DO_2 depressions in this water layer. Figure 40 also shows concentration of sTPH vs. depth by month from May to October 2010. The highest concentrations of sTPH occurred in May, June, and July, decreasing through October. The sTPH values were detected at <23 ppb after July and 2 ppb after September. In October none of the samples collected yielded results above detection limits.

Table 3. Number of results in concentration ranges for samples collected between 198 m and 2340 m deep.

Concentration (ppb)	tVOA	sTPH
<1	4649	4557
1–10	305	909
10–100	302	158
100–1000	155	17
>1000	6	-
Max. Measured Concentration	2112	485

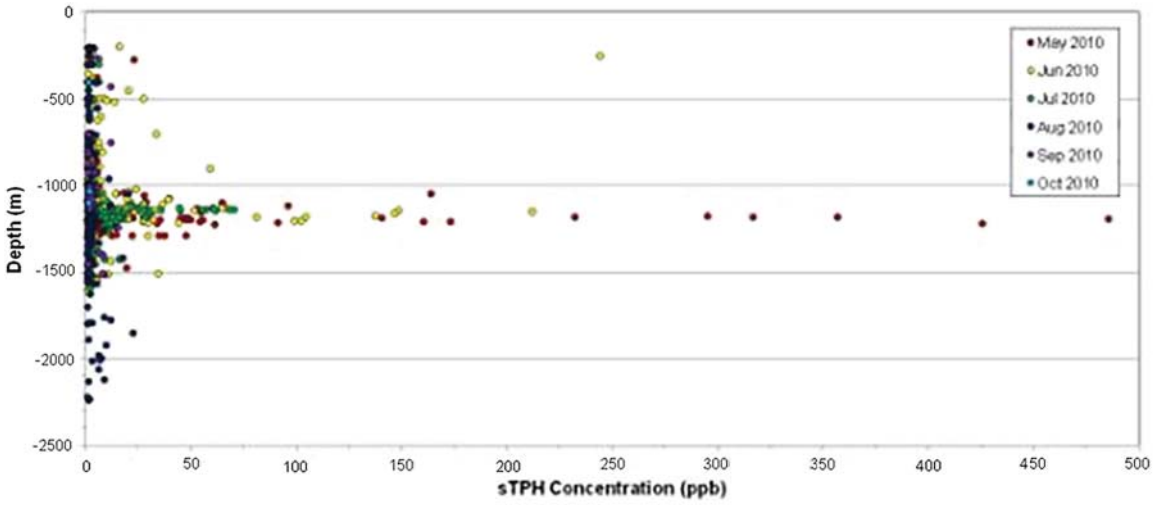

Figure 40. Concentration (>1 ppb) of sTPH vs. depth by month collected. Total samples ≥1 ppb: 849.

Figure 41 shows concentrations of sTPH vs. time and depth. The majority of sTPH concentrations above 10 ppb were detected at depths between 900 m and 1300 m; about a dozen samples above 10 ppb can be seen between 200 m and 700 m, particularly in May and June.

Figure 42 displays concentrations of tVOA vs. depth and time collected. As with the sTPH fraction, the great majority of samples with the highest concentrations of tVOA fraction were detected at depths between 900 and 1300 m.

The concentration of tVOA vs. time and depth from May to October 2010 is shown in Figure 43. Samples collected after the well was capped in July had relatively low tVOA concentrations. The tVOA concentrations detected in water samples collected after the well was capped did not fit into a distinct water layer. No clear signal of the deep subsurface dispersed oil as seen in tVOA analysis could be identified through chemical analysis of water samples collected after August 4 as part of this study.

Figure 44 displays concentrations of both tVOA and sTPH fractions over time. The data show that the concentrations of sTPH are typically lower, and sTPH persisted for a longer time, until early October, while tVOA were not detected after mid August.

Figure 45 displays the sTPH distribution around the wellhead. The sTPH fractions beyond 10 km from the wellhead could not be analytically attributed to MC252 oil because the low concentrations in these samples precluded chemical identification. A close-up view of the sTPH locations within approximately 30 km of the wellhead is plotted in Figure 46. Most of the samples with concentrations above 10 ppb were collected within 10 km of the wellhead. Figure 47 displays locations around the wellhead where samples contained tVOA. Figure 48 shows the tVOA locations within 100 km of the wellhead, where the samples contained tVOA concentrations >1 ppb.

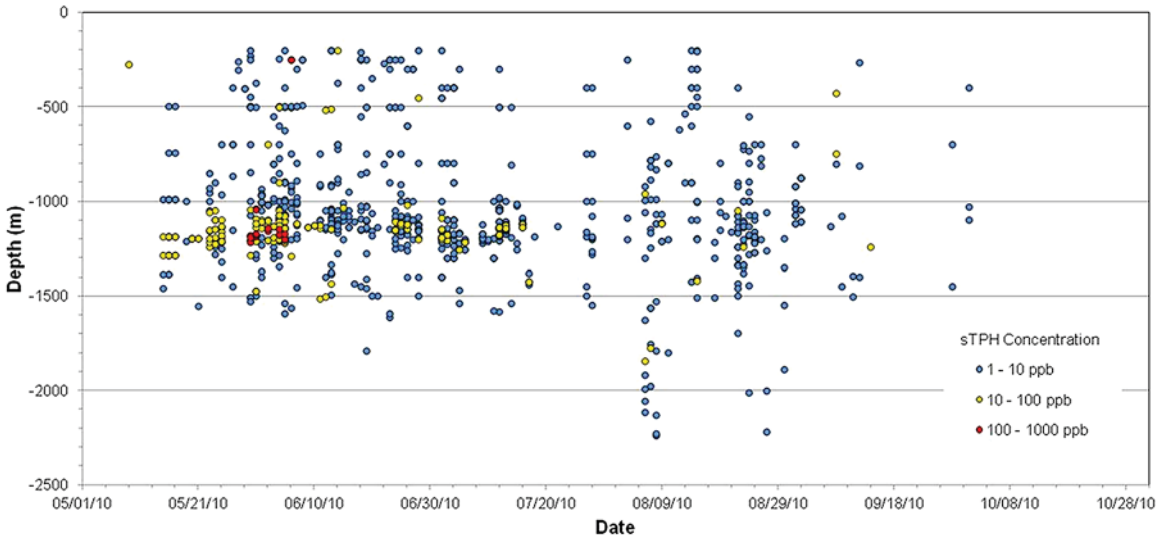

Figure 41. Concentration (>1 ppb) of sTPH vs. depth over time. Total samples >1 ppb: 849. Color circles show sTPH concentrations (ppb)

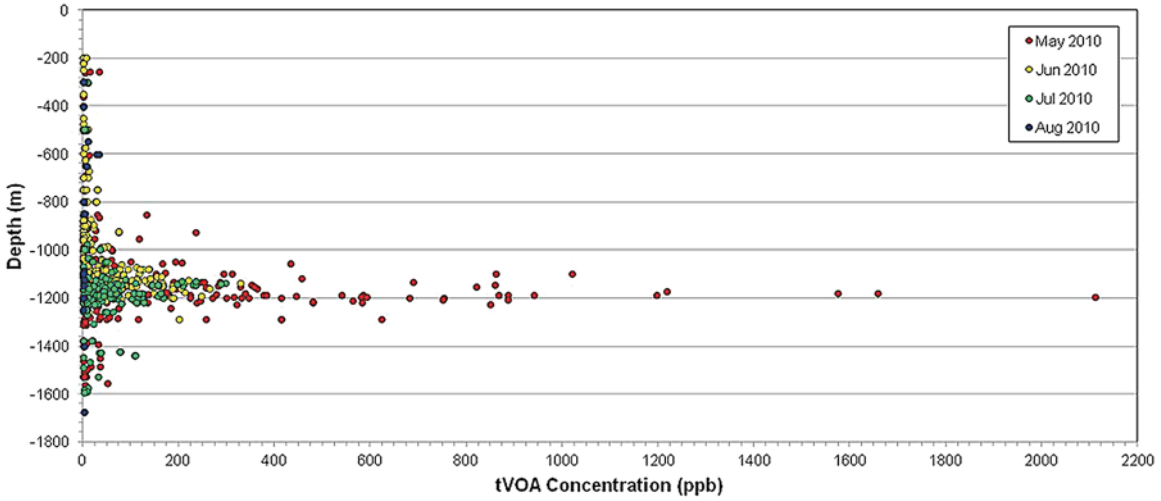

Figure 42. Concentration (>1 ppb) of tVOA vs. depth and time collected. Total samples >1 ppb: 768.

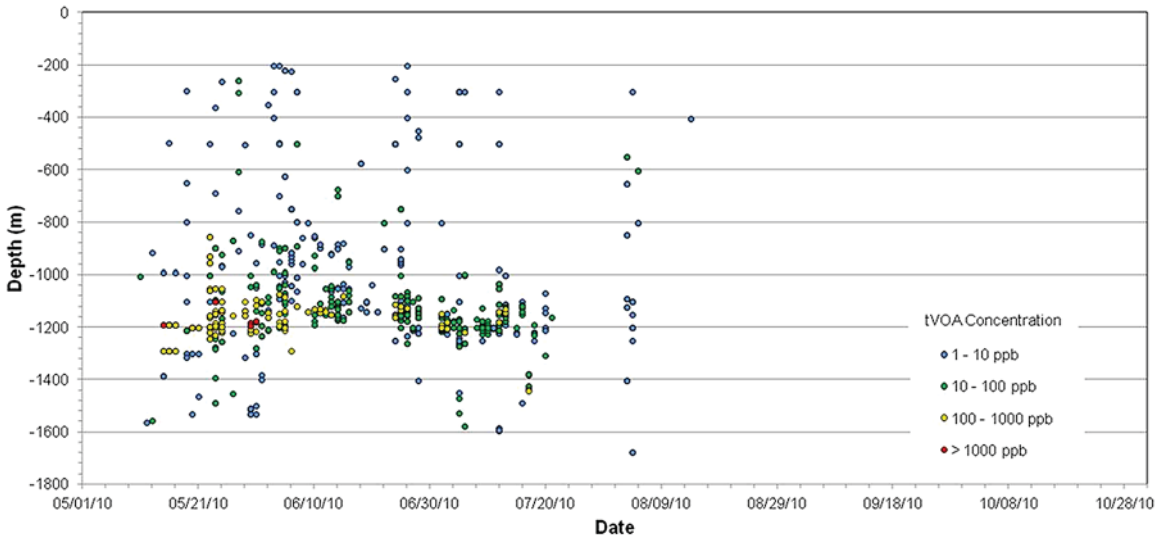

Figure 43. Concentration (≥1 ppb) of tVOA vs. depth over time. Total samples ≥1 ppb: 768. Color circles show tVOA concentrations (ppb)

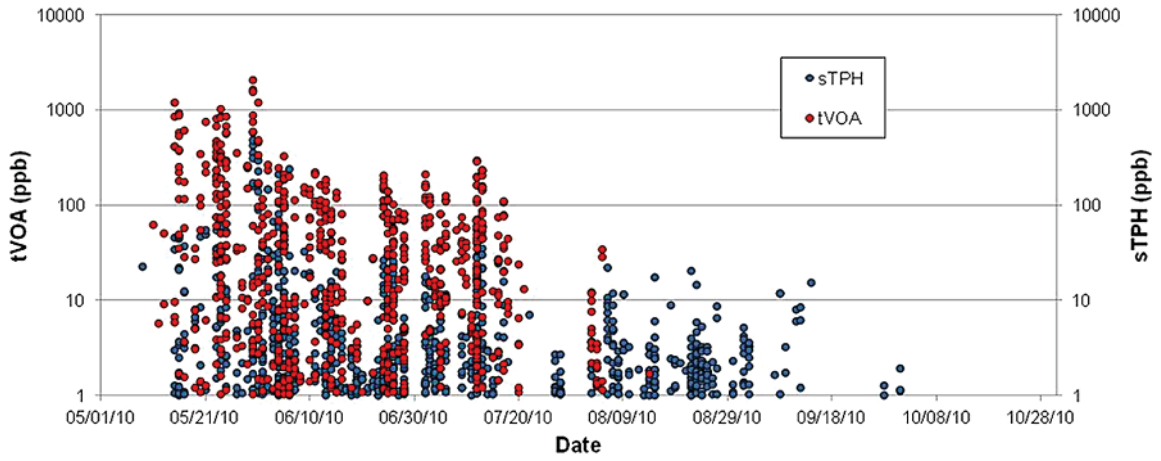

Figure 44. Concentrations (≥ 1 ppb) of the tVOA and sTPH fractions over time.

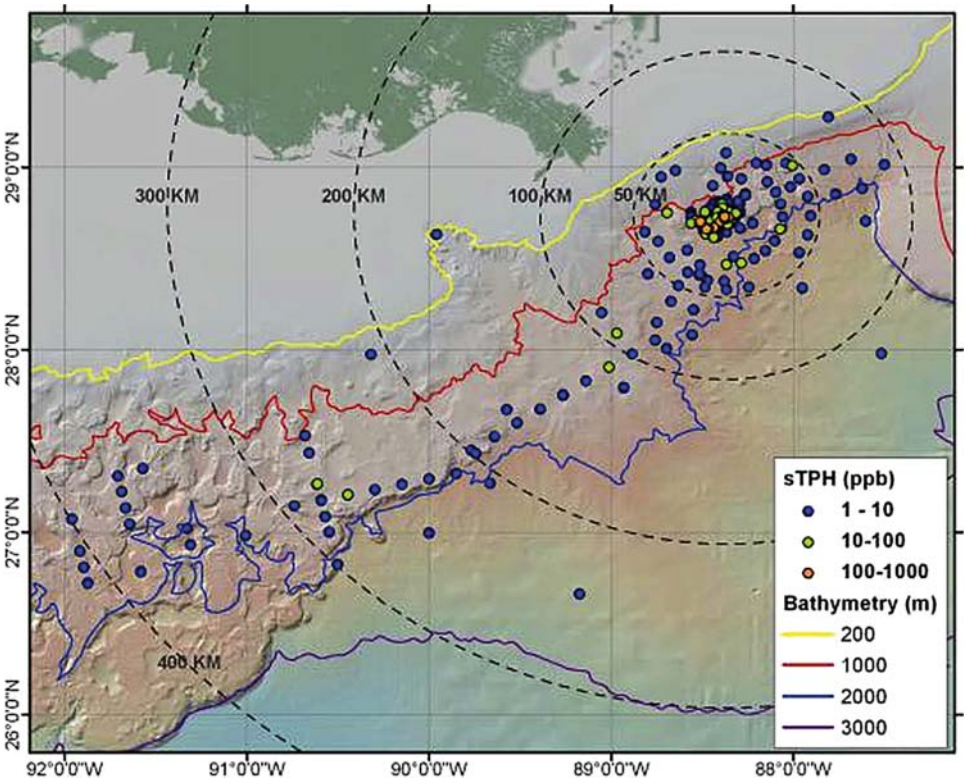

Figure 45. Color circles show sTPH around wellhead in concentration ranges 1–10, 10–100, and 100–1000 ppb.

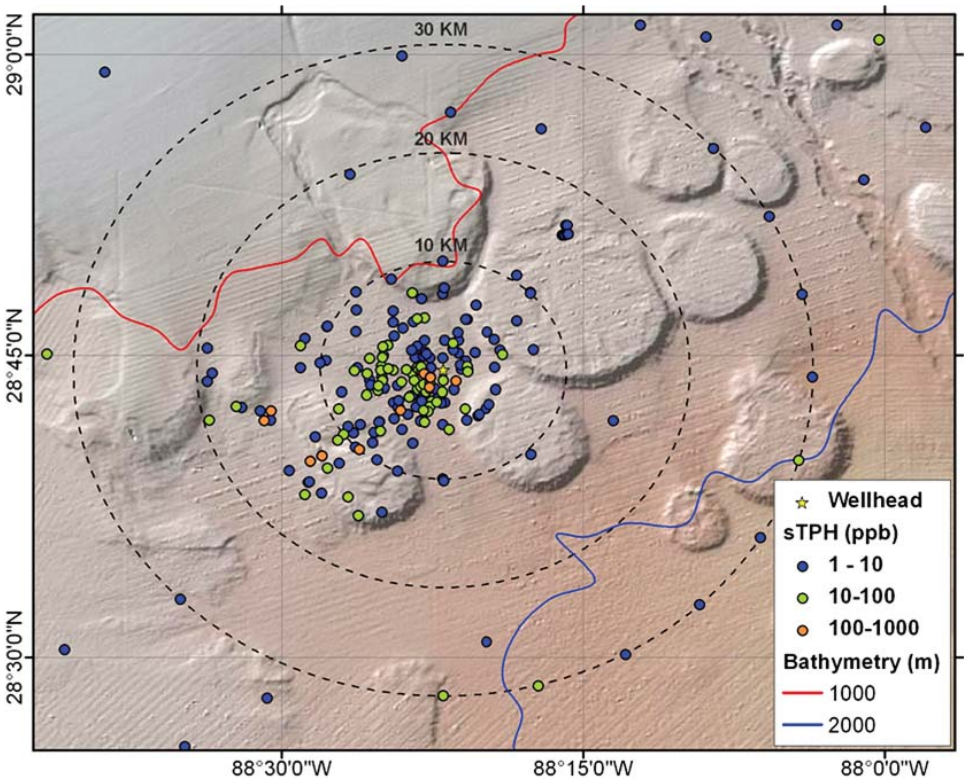

Figure 46. Locations within approximately 30 km of the wellhead where sTPH concentrations were ≥1 ppb. Total samples ≥1 ppb: 684. Color circles show sTPH concentrations (ppb)

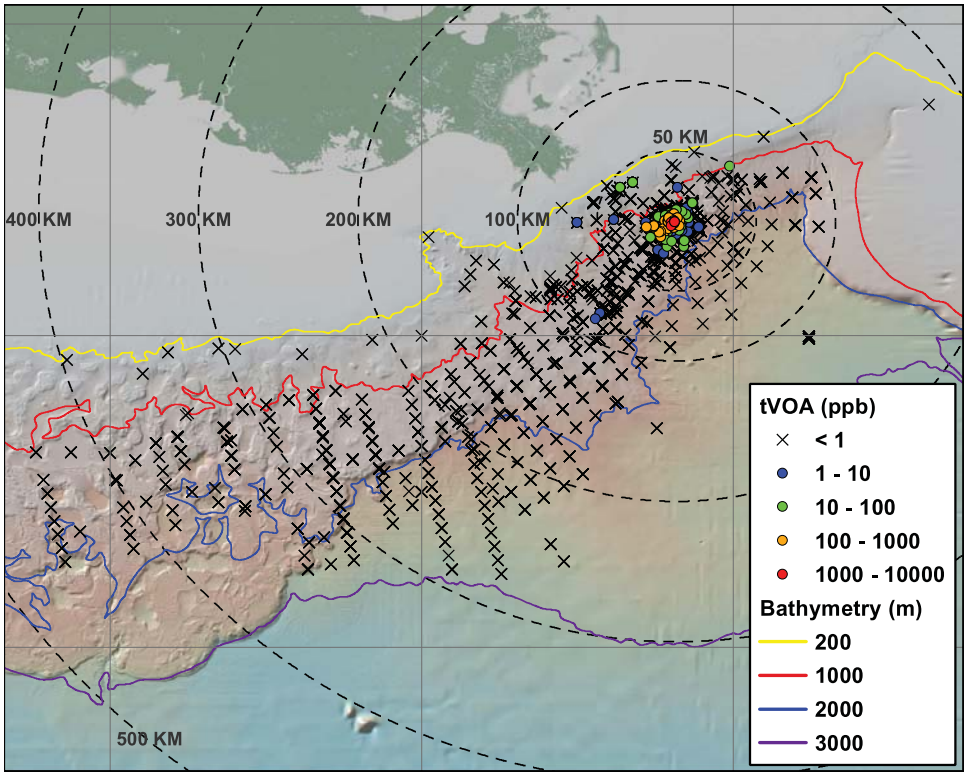

Figure 47. The tVOA sampling locations and tVOA concentrations around the wellhead. Total samples taken: 5399. Color circles show tVOA concentrations (ppb)

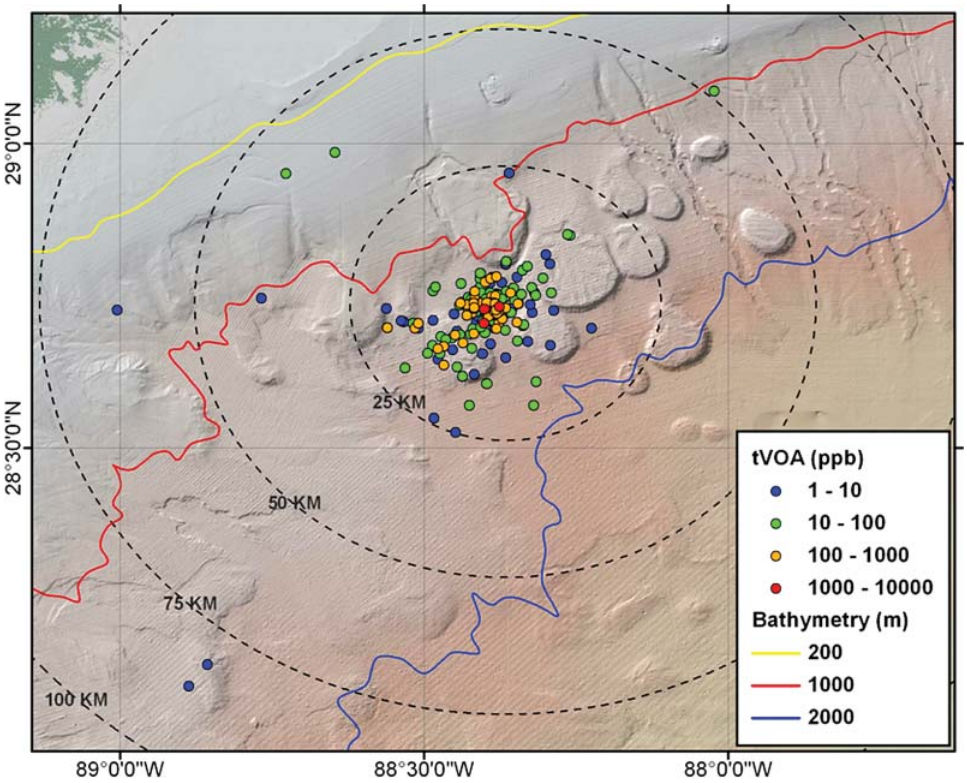

Figure 48. The tVOA locations within 75 km of the wellhead where samples contain tVOA concentrations of >1 ppb. Color circles show tVOA levels (ppb)

5 Conclusions and Key Findings

5.1 Character of the Deep Subsurface Dispersed Oil Field

Observations of five measures of dissolved oil and oil droplets presented in Chapter 4 provide information on the distribution and character of the deep subsurface dispersed oil feature that resulted from the MC252 spill:

1. Fluorescence as measured by CDOM fluorometers;
2. Fluorescence as measured by Chelsea AQUAtracka fluorometer;
3. Dissolved Oxygen;
4. sTPH concentrations from chemical analysis of discrete water samples; and
5. tVOA concentrations from chemical analysis of discrete water samples.

It is possible to develop a description of the deep dispersed oil that is consistent with all the observations despite the limitations that exist for each of the measures. This section strives to develop that consistent depiction to the greatest extent possible.

The aromatic fraction primarily detected by CDOM fluorometers would be the least likely to contribute to changes in oxygen concentration due to biodegradation. This is particularly true as the number of fused rings increases - the aromatics are persistent and are not as readily consumed by microorganisms. Additionally, these high molecular weight PAHs are not readily water-soluble and would be present primarily in droplets in the deep dispersed oil.

Laboratory analysis of discrete water samples showed that concentrations of petroleum hydrocarbons were at trace levels, primarily in the sTPH fraction; with virtually no observation of the tVOA, volatile fraction from August on to the end of the sampling period. Because, at the time of the spill, the Chelsea AQUAtracka fluorometer was thought to be more sensitive to petroleum hydrocarbons than the CDOM sensors, the Chelsea AQUAtracka fluorometer was deployed to detect the deep subsurface dispersed oil as it moved farther from the well. The Chelsea AQUAtracka fluorometer's spectral characteristics match those of the oil's fluorescing aromatic fraction (i.e., excitation/absorbance spectral characteristics). However, the fact that the concentration of the aromatic fraction was so low in MC252 oil probably contributed to findings that all of the fluorometer sensors yielded similar signals for MC252 oil as seen in Figure 32.

The Chelsea AQUAtracka fluorometers were able to measure fluorescence as the water in which the deep subsurface dispersed oil was found moved hundreds of kilometers in a southwesterly direction. Maximum intensities of the Chelsea AQUAtracka fluorometer's signal were small (maximum vertically integrated levels were in the range of 30-40 ppb Carbazole, Figs. 30 and 31) but were clearly related to the DO_2 depressions. However, no correspondence was found between the Chelsea AQUAtracka fluorometer-measured fluorescence and oil levels measured through chemical analysis of discrete water samples. It could not be determined from data available in this report if Chelsea AQUAtracka fluorometer-measured fluorescence was related to the spilled oil or to other fluorescence sources including those of biological origin.

The vertical extent of the deep subsurface dispersed oil between 900 and 1300 m depths was similar in all the measures of dissolved oil and oil droplets. The fluorescence profiles provided a continuous record from the ocean surface to the seafloor; signals associated with hydrocarbons were consistently seen between 900 and 1300 m depths. These depths correspond to a limited range of seawater potential densities, between 27.6 and 27.7 kg/m^3. The sTPH and tVOA concentrations peaked in this same layer (Figs. 40 and 42).

Peaks in fluorescence occurred at varying depths/densities within this layer, which led to the approach of integrating the fluorescence signal over this segment of the water column. Though the density of peak fluorescence as measured by CDOM fluorometers near the wellhead was seen to decrease after the riser was cut (Fig. 29), farther from the wellhead (tens of kilometers) there was no obvious change in the density at which the oil was found. This finding suggests that the deep subsurface dispersed oil did not experience significant buoyant rise or sinking after release, and instead behaved as neutrally buoyant particles or as dissolved materials in the water.

All of the measurements indicate that the majority of the deep subsurface dispersed oil was carried predominately to the southwest away from the wellhead by the prevailing currents at depths of 900–1300 m. The sTPH and tVOA and the CDOM fluorometer data indicate some deep subsurface dispersed oil up to 100 km northeast of the well; no similar signal was seen in the Chelsea AQUAtracka fluorometer data because these observations were made before the Chelsea AQUAtracka was deployed.

The horizontal geographic extent of the deep subsurface dispersed oil tended to be between the 1000-m and 2000-m isobaths. This horizontal distribution is consistent with the predominant currents in the region (Fig. 39) and suggests that the flow carrying the oil followed a constant depth and moved counterclockwise along the slope in the northern Gulf of Mexico, as has been observed in the past.

The description of the horizontal extent of the deep subsurface dispersed oil is based on the positions where the measured variables fell below minimum detectable levels. Some insight into where oil would be expected to be found can be gained by assuming that the mean current passively carries the oil. An estimate of the distance to which the oil was carried away from the well over time can be constructed. Figure 49 shows the distance from the wellhead of the leading edge (when the blowout first occurred on April 20) and the trailing edge (when the well was shut in on July 17) assuming a mean along-slope current of 2.7±0.7 cm/s (from the average value ±1 standard deviation at an 1100-m depth measured by the ADCP on the Development Driller).

The gray-shaded region between leading and trailing edges in Figure 49 is the expected position of the deep subsurface dispersed oil. The location and time of samples color-coded by the magnitude of oxygen depression are overlaid on Figure 49. Samples with detectable signal largely lie within the stippled region and support the notion that the flow field determined the oil's horizontal distance from the wellhead. Given the mean current speed and the release of oil over roughly 3 months, the feature is estimated to be at least 200 km long, but might be longer due to current reversals and mixing.

Figure 50 shows the measured concentration of DO_2 and sTPH fraction in water samples collected from the 70 stations circled in red on Figure 49 in the area considered to be the trailing edge of the deep subsurface dispersed oil. Only values from measurements taken since July 17, 2010 are shown.

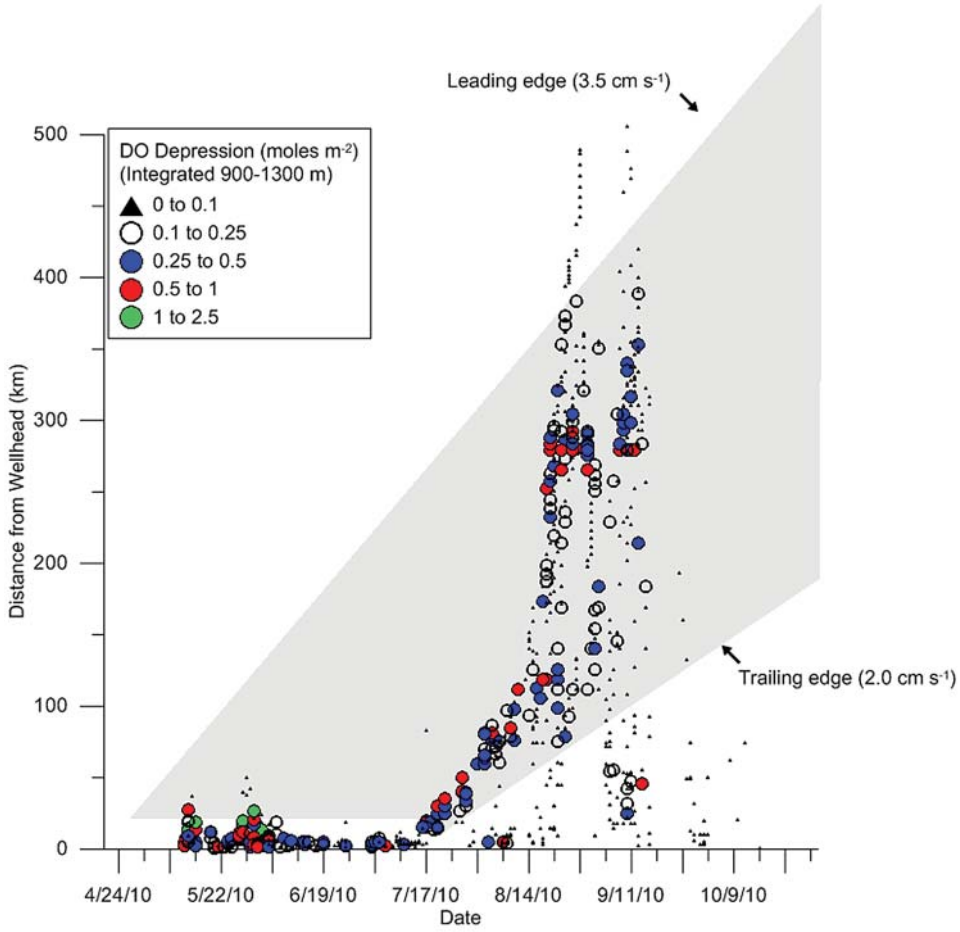

Figure 49. Estimated distance of the deep dispersed oil from the wellhead over time (stippled region) overlaid with the time and position of sampling locations. The color of the samples indicates the magnitude of the DO_2 depression observed.

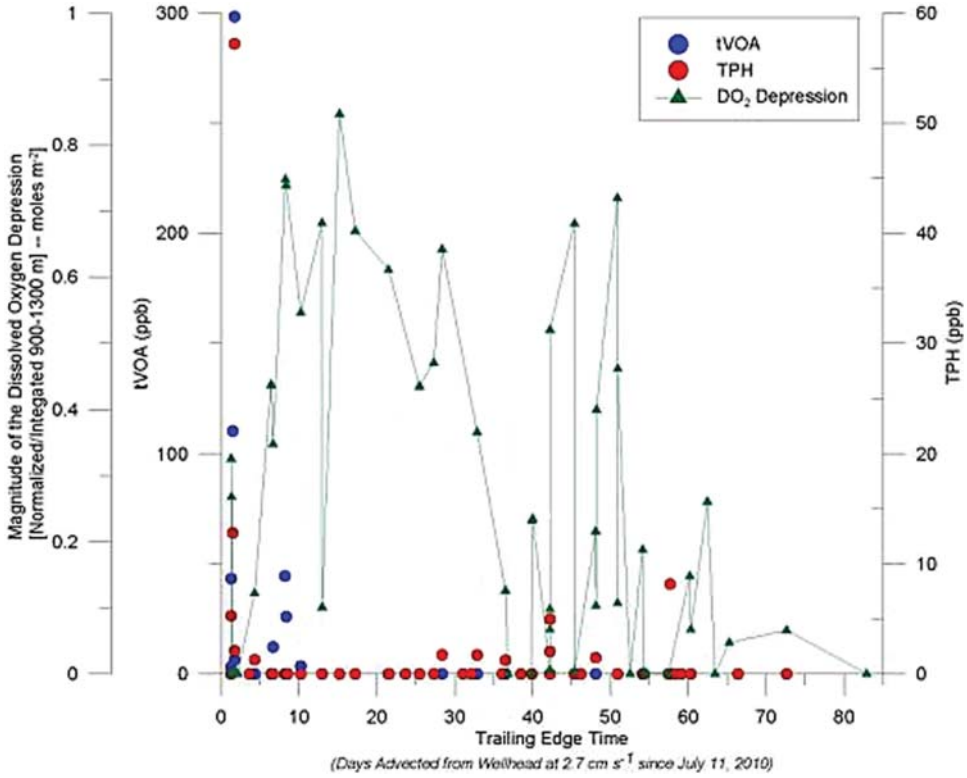

Figure 50. Concentrations of DO_2 and sTPH fraction in water samples collected on the estimated trailing edge of the water mass exposed to hydrocarbon releases from the MC252. The sTPH values are from cruises that had chemistry results corresponding to the oxygen values in the red circles in Figure 48. Samples with values <1 are not shown. The x-axis shows days elapsed since July 11.

Mixing would act to further spread out the deep dispersed oil through dilution with ambient seawater and result in decreased concentrations. As discussed in the conceptual model, horizontal (specifically along isopycnal) mixing rates are expected to be much greater than vertical (diapycnal) mixing rates in the deep stratified waters of the Gulf of Mexico. The lack of an obvious increase in time or distance of the range of isopycnals where oil was found attests to the weak vertical mixing rates. Horizontal mixing will increase the cross-stream breadth of the oil. The ability to quantify the breadth of the oil feature was impacted by the horizontal spacing of casts during surveys; for casts collected in August and September the spacing was 10–15 km (Figs. 24 and 25) so only a coarse measure of spread perpendicular to the mean current is possible. The AQUAtracka fluorometer data and sTPH fields (Figs. 31 and 45) provide some indication of breadth. In the AQUAtracka fluorometer data (Fig. 31), the feature is roughly 10–20 km across at distances 100 km from the well, and as much as 60 km in breadth at 300 km downstream. In the sTPH data (Fig. 45), the feature forms a band offshore of the 1000-m depth contour. For distances between 100 and 200 km, the feature is 15–30 km wide and at 250–300 km downstream, it is as much as 80 km wide.

The increase in breadth of the feature over time as it is carried away from the well by the mean current can be modeled with a constant horizontal mixing rate. In this case the spread is expected to increase as $(2*K_h*t)^{1/2}$, where the spread is interpreted as the standard deviation of a Gaussian-shaped distribution of the concentration in the cross-stream direction, K_h is the horizontal mixing rate and t is time. Assuming the breadth values above are four times the spread (i.e., that the measured breadth is 2 std dev on either side of the maximum) and that time is given by distance divided by the mean current speed, these values suggest horizontal mixing rates of 2 m^2/s to 18 m^2/s.

5.2 Changes in Measured Oil Concentrations

The chemical data in this report provide insight into the vertical and horizontal dimensions of the oil and concentration changes as oil moved away from the wellhead. These data cannot provide comprehensive explanations for changes in concentration because not all processes that influence concentration were measured. Valentine et al. (2012) developed a physical-metabolic modeling approach that identified the influences of circulation and biological processes as important factors influencing hydrocarbon and oxygen concentrations. The data in this report might be useful for modeling efforts, such as Valentine's.

Available analytical data provide evidence that the great majority of oil dispersed in the subsurface extended from the wellhead at depths between 900 and 1300 m (Figs. 40 and 42). The oil components in this water layer were dissolved, and most likely contained in small oil droplets. Some casts within 10 km of the wellhead showed high sTPH values at shallower depths. The elevated sTPH values at shallower depths may reflect oil droplets that migrated from the deep-water layer after the larger, more buoyant droplets had already risen to the surface. One exception is found in cast 241 taken by R/V *Ocean Veritas* where elevated TPH values were measured at 425 m (Fig. 44).

Figure 51 shows a wide range of sTPH and tVOA concentrations within 10 km of the well, an area with a very high density of sample stations. The sTPH levels at depths of 900–1300 m were predominantly quite low (1–10 ppb) at distances greater than 10 km from the well. Values in excess of tens of parts per billion sTPH were most frequently detected within 10 km of the wellhead; 485 ppb was the highest detected level. Higher levels of the tVOA fraction of hydrocarbons were detected in the water samples collected within 20 km of the wellhead, with 2100 ppb being the highest detected level. Beyond 20 km from the wellhead (equivalent to 8.5 days since leaving the wellhead assuming advection at the mean flow speed of 0.027 m/s) tVOA concentrations were below 100 ppb and no detectable values were measured beyond 100 km (43 days) from the wellhead. Measurable amounts of sTPH extended out to beyond 400 km (171 days) from the wellhead, with values above 10 ppb out to about 275 km (118 days).

Figure 51 illustrates the rapid drop-off of oil concentrations with distance from the wellhead for tVOA and sTPH fractions. The figure provides two scales of distance from the wellhead; where the lower figure is 0–10 km distance to help resolve the great number of samples collected for which values above 10 ppb in each fraction were observed. Also note the difference in relative concentration range for each fraction, which could possibly reflect the relative quantities of the fractions found in the original oil. The drop-off was faster in the tVOA fraction of hydrocarbons, which might be attributed to preferential biodegradation of this hydrocarbon fraction.

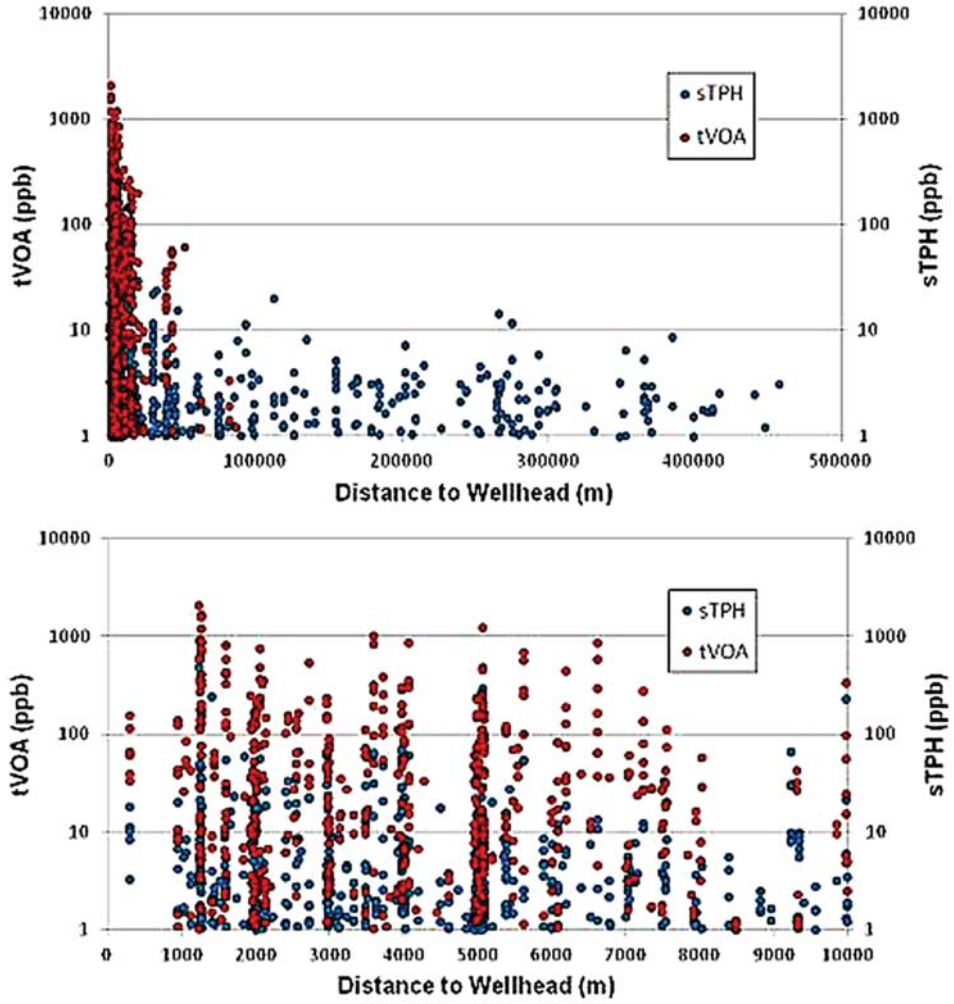

Figure 51. The concentration of tVOA and sTPH fractions as a function of distance from the wellhead. The figure provides two scales of distance from the wellhead. Values <1 are not plotted in this figure. Note that a log scale is used for concentration values.

Some evidence shows that the most easily degraded fractions of the oil—water-soluble tVOA fractions—were preferentially consumed. This fraction was present in higher concentrations in the water samples near the wellhead, but rapidly dropped off beyond about 20 km from the wellhead. The sTPH fraction also decreased while moving away from the wellhead, but decreased at a slower rate before reaching background concentrations.

The observed decrease in hydrocarbon concentration seen in sTPH, tVOA, and fluorescence signals was due to multiple factors, primarily dilution and biodegradation with other factors such as particulate adsorption also presumably contributing. A subset of samples, those depicted along the trailing edge in Figure 49 and as red circles in Figure 50 was extracted to examine whether the sampling was sufficient to estimate rates associated with these processes. Because these stations lie along an advective path of the feature (parallel to the trailing edge, hence in a Lagrangian frame of reference) the samples provide a time history of properties in the deep subsurface dispersed oil as it moved away from the wellhead. Unfortunately the sTPH values above background levels are too limited to permit estimates of rate changes over time but do highlight the rapid decrease in values as the feature moved away from the wellhead. The changes were also consistent with horizontal mixing rates of 2–20 m^2/s estimated from the change in breadth. Because this subsample began as the well was shut-in, tVOA values are largely at background levels. The rapid decline in the tVOA

concentration supports the notion that microbial degradation might preferentially remove this fraction, although (as previously discussed) biodegradation could not be differentiated from the more prominent dilution effect.

5.3 Changes in Dissolved Oxygen Depressions

Evidence of hydrocarbon-degrading bacteria—particularly those utilizing the more degradable components of the oil (e.g., butane, BTEX, etc.) in the deep dispersed oil—is supported by many profiles that showed simultaneous peaks in fluorescence and depressions in DO_2, as shown in earlier JAG reports and by other researchers, i.e., Kessler et al. (2011) and Hazen et al. (2010).

The depressions in DO_2 were observed over the same depth range as petroleum hydrocarbons between 900 m and 1300 m and over the same horizontal extent. The magnitude of the depression did not mirror the hydrocarbon changes, but instead reached a maximum some distance away from the wellhead and decreased more slowly than the hydrocarbon concentrations. Figure 50 shows the measured concentration of DO_2 in water samples collected from the 70 stations circled in red on Figure 49. Values reached maximum at 10 days after leaving the wellhead and maintained a fairly steady value of 0.5 mol/m^2 over 50 days.

The rapid increase in the magnitude of the DO_2 depression was observed over a similar timeframe as the rapid decrease in tVOA, and it is reasonable to assume that rapid oxidation of these more labile components of the oil fueled the bloom in hydrocarbon-consuming bacteria described by Hazen et al. and others. If this process served as the only cause of oxygen depletion, horizontal mixing would be expected to quickly replenish the oxygen returning it to ambient levels. The sustained depression suggests another source of oxygen demand. Hazen et al. suggested that the decomposition of the bloom could explain a sustained depression, and Valentine et al. suggested that the mixing may serve to reinoculate the bacteria community and lead to sustained biodegradation. If the more recalcitrant oil components, represented by sTPH in this study, were more slowly degraded, this too could explain the persistent DO_2 depression. Fortunately, the rates of DO_2 consumption by biodegradation and DO_2 replenishment by mixing were comparable, and a steady level of DO_2 depression was achieved well above levels considered hypoxic.

Sampling several hundreds of kilometers away from the wellhead, simultaneous DO_2 depression and anomalous Chelsea AQUAtracka fluorescence signals were consistently observed. No relationship between sTPH levels and the Chelsea AQUAtracka fluorescence signal was observed, but a relationship between vertically integrated fluorescence and DO_2 anomaly was observed. A subset of data from the NOAA Ship Pisces collected from August 6 to September 1, 2010, was examined for trends in comparing water sample chemistry results with other environmental data collected synoptically. Beginning August 22, the Pisces CTD was configured with a Chelsea AQUAtracka fluorescence sensor. No significant trends were observed among the environmental data (fluorescence as detected by CDOM fluormeters, DO_2, and Chelsea AQUAtracka fluorescence) and the water sample chemistry results (sTPH and tVOA). The left panel of Figure 52 relates between the Chelsea AQUAtracka fluorescence and the corresponding TPH analysis results at the sample depth. The right panel of Figure 52 relates the normalized, integrated Chelsea AQUAtracka fluorescence signal and the magnitude of the DO_2 depression normalized and integrated over the same depth region (900 to 1300 m). The correlation between these two parameters (R2=0.57) was evident, but the lack of correlation between the chemistry analysis and the environmental parameters indicated the complexity of the deep plume signal 1 month after the wellhead was capped. The source of the persistent fluorescence signal detected by the Chelsea AQUAtracka fluorometer is therefore unclear.

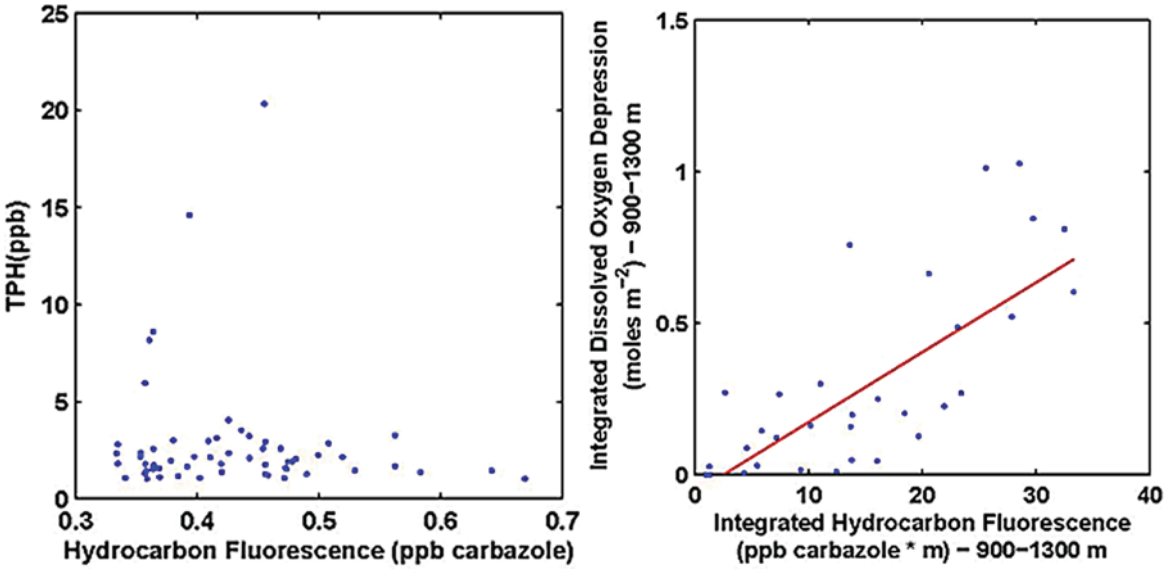

Figure 52. A subset of data from the NOAA Ship *Pisces* collected from August 6 to September 1, 2010. The left panel (a) relates between the Chelsea AQUAtracka fluorescence and the corresponding TPH analysis results at the sample depth. The right panel (b) relates the normalized, integrated Chelsea AQUAtracka fluorescence signal and the magnitude of the DO_2 depression.

Some areas of DO_2 depressions might not have been sampled, particularly before August when spatial sampling started. As an example, DO_2 depressions to the northeast might not have been sampled in that time period. DO_2 anomalies did not drop off as quickly as deep dispersed oil concentrations as indicated by both CDOM fluorescence (Section 4.2) and water sample analysis (Section 4.5). Later in September and October, both low DO_2 anomalies and oil concentrations were observed.

5.4 Summary

- The JAG is confident that the great majority of oil in the subsurface extended from the wellhead at depths between 900 and 1300 m. The oil components in this water layer were dissolved and most likely also contained in small oil droplets.
- The subsurface oil was mainly found to the southwest of the wellhead, consistent with the circulation in the Gulf of Mexico at these depths. Rough estimates of the increase in horizontal breadth of the feature suggest horizontal mixing rates of 2-18 m^2/s.
- Levels of semivolatiles at depths of 900–1300 m were predominantly quite low (1–10 ppb). Tens of parts per billion were detected in samples (the highest level of sTPH was 485 ppb).
- Volatile fraction of hydrocarbons (tVOA) were detected in water samples at significantly higher concentrations than sTPH. Relatively higher concentration levels of the tVOA fraction were found to be present in more samples nearer to the wellhead (within 25 km). A maximum tVOA concentration of 2112 ppb was detected in water between depths of 900 m and 1300 m.
- A faster drop-off was observed in the tVOA fraction than the sTPH hydrocarbons. This more labile fraction of hydrocarbons was likely preferentially biodegraded.
- The observed decreases in hydrocarbon concentrations were likely due to multiple factors, primarily dilution and biodegradation; other factors, such as particulate adsorption, also likely contributed. The observations and analysis conducted as part of this effort were not sufficient to provide a quantitative

estimate of the contribution that each process might have made to the observed changes in oil concentrations.

- As distance from the wellhead increased and time passed, a decrease in hydrocarbon concentrations concomitant with depressions in DO_2 concentrations was detected. These observations, together with the identification of active hydrocarbon-consuming bacterial communities by other investigations, suggested that biodegradation processes were actively consuming and mineralizing the hydrocarbons.
- The DO_2 depression persisted after laboratory analytical techniques no longer detected oil fractions above background levels. The steady level of the depression was considered to be the result of a balance between replenishment of DO_2 by mixing and consumption by DO_2 demand, but the source of the demand could not be conclusively identified.
- Chelsea AQUAtracka fluorescence and DO_2 depressions were observed at the same stations and in the same depth range hundreds of kilometers from the wellhead, but the source of fluorescence could not be defined with the data available in this report.
- The events associated with the MC252 oil-spill period do not represent how other subsurface spills might behave in the future. The dramatic variation in the Gulf of Mexico waters should be considered in future deepwater oil-spill planning. For example, the Loop Current position varies significantly in location and intensity among seasons and years (Sturges and Leben, 2000; Donohue et al. 2006; and Vukovich, 2007). Although the Loop Current was not as significant for transporting MC252 surface oil as was potentially possible (Barker, 2011), the Loop Current surface and deep expressions (e.g., Donohue et al., 2006; Hamilton et al., 2011) should be considered in discussing trajectories for the surface and subsurface for any future spill planning. Passage of a significant hurricane, such as Hurricane Katrina in 2005, can drive barotropic currents (currents that are constant from the sea surface to the seafloor) within the locus of the hurricane eye wall (Welsh et al., 2009). The associated downward propagation of energy could lead to increased mixing (Oey et al., 2008). Some areas in the Gulf of Mexico have lower DO_2 values than were found in the MC252 subsurface layer, so the potential for hypoxia in other spill circumstances and locations could vary from those found in this report.

6 Report Development

The Joint Analysis Group for Surface and Subsurface Oceanography, Oil and Dispersant Data was established as a standing workgroup within the National Incident Command on June 7, 2010.[14] The specific charge to the JAG was to develop data visualization products and analyses of data collected to monitor the deep subsurface dispersed oil from the MC252 well blowout. On March 11, 2011, the Federal On-Scene Coordinator gave approval for the JAG to complete a report summarizing what was learned about the deep subsurface dispersed oil. This approval extended previous efforts by examining unreported data.

Monitoring of the deep subsurface dispersed oil began when the EPA and the U. S. Coast Guard issued a joint directive to BP on May 10, 2010, as a requirement of deep-sea dispersant application. This directive required BP to implement a monitoring and assessment plan for subsurface and surface applications of dispersants as part of the BP oil-spill response (Environmental Protection Agency, 2010a). The initial plan required sampling to a depth of 550 m. On May 14, that directive was amended to require monitoring to a water depth of 1500 m (Environmental Protection Agency, 2010b). On July 23, 2010, that directive was further amended to require using a Winkler titration method to calibrate oxygen monitoring (Environmental Protection Agency, 2010c) due to concerns about the potential for hypoxia in the oil-affected waters.

Observations derived from the monitoring required by these directives formed the foundation of JAG reports through August 13, 2010. On August 18, the National Incident Commander's Strategic Plan For Sub-Sea and Sub-Surface Oil and Dispersant Detection, Sampling and Monitoring identified additional subsurface monitoring requirements (Unified Area Command, 2010a–c). Deep subsurface data were collected as part of those efforts through October 19, 2010.

The Subsurface Monitoring Unit of the Unified Area Command coordinated vessel-based operations conducted to support these response sampling and monitoring requirements. The Subsurface Monitoring Unit coordinated data from 23 vessels that conducted sampling during 93 cruises between May 9, 2010, and October 19, 2010.[15]

The JAG previously published reports and updates (Joint Analysis Group, 2010a–d) on various aspects of deepwater subsurface monitoring data collected under the oversight of the Subsurface Monitoring Unit. The JAG considered data from 657 stations[16] from which observations were successfully processed in previous reports. Other researchers have also studied deep subsurface dispersed oil and gas from MC252 (Camilli et al., 2010; Diercks et al., 2010); Hazen et al., 2010; Joye et al., 2011; Kessler et al., 2011; Kujawinski et al., 2011; Reddy et al., 2011; Socolofsky et al., 2011; Valentine et al., 2010; and Yvon-Lewis et al., 2011).

Three other National Incident Command teams provided information important to examining deep subsurface dispersed oil and gas. Information from the Flow Rate Technical Group (FRTG) provides the foundation upon which oil and gas flow rates and oil-release estimates are based. The FRTG's report (McNutt et al., 2011) provides insights into how petroleum hydrocarbons from MC252 were released into the ocean. Information from the Federal Interagency Solutions Group, Oil Budget Calculator Science and Engineering Team (Federal

14 The JAG is chaired by the National Oceanic and Atmospheric Administration and includes members from the U.S. Environmental Protection Agency, Bureau of Ocean Energy Management, Regulation, and Enforcement, and Office of Science and Technology Policy/Executive Office of the President.

15 With one exception, water sample analysis includes selected publicly available data collected as part of the government's Natural Resource Damage Assessment Efforts through November 12, 2010.

16 The first JAG report included data that subsequently did not meet quality-control tests. Therefore, those data points are not considered in the $D0_2$ analyses in this report, as noted in Table (1). Those raw data are available to the public as described in Appendix 2.

Interagency Solutions Group, 2010), provides the foundation for estimating the fraction of liquid petroleum naturally and chemically dispersed into the deep subsurface.

The OSAT reported on data collected under the National Incident Commander's "Sub-Sea and Sub-Surface Oil and Dispersant Detection, Sampling and Monitoring Strategy." The OSAT-1 report examined oil, as well as dispersant concentrations and toxicities, in water and sediment samples collected in three sampling zones: nearshore, offshore, and deepwater (OSAT, 2010).

The contents of this report were prepared by JAG members with information coordination and synthesis support as noted below.

6.1 Joint Analysis Group Members

6.1.1 National Oceanic and Atmospheric Administration

Dr. Robert Haddad, NOAA National Ocean Service, Silver Spring, MD (JAG Lead)

Dr. Carl Childs, NOAA Office of Response and Restoration, Seattle, WA (Deputy Lead)

Mr. Russell Beard, National Coastal Data Development Center, Stennis Space Center, MS

Dr. Richard L. Crout, National Data Buoy Center, Stennis Space Center, MS

Dr. Scott Cross, Regional Science Officer, National Coastal Data Development Center, Charleston, SC

Dr. Jim Farr, NOAA Office of Response and Restoration, Seattle, WA

Dr. Jerry Galt, Contractor, NOAA Office of Response and Restoration, Seattle, WA

Dr. Hernan Garcia, National Oceanographic Data Center, Ocean Climate Laboratory,

Silver Spring, MD

Dr. Jeffrey Napp, NOAA, National Marine Fisheries Service, Alaska Fisheries Science Center, Seattle, WA

Dr. Rost Parsons, National Coastal Data Development Center, Stennis Space Center, MS

Dr. Robert Pavia, Contractor, NOAA Office of Response and Restoration, Seattle, WA

Dr. Rik Wanninkhof, Atlantic Oceanographic and Meteorological Laboratory, Miami, FL

6.1.2 U. S. Environmental Protection Agency

Dr. Robyn N. Conmy, EPA, Land Remediation and Pollution Control Division, National Risk Management Research Laboratory, Office of Research and Development, Cincinnati, OH

Dr. Jan Kurtz, Office of Research and Development, National Health and Environmental Effects Research Laboratory, Gulf Breeze, FL

Dr. Albert Venosa, EPA, Land Remediation and Pollution Control Division, National Risk Management Research Laboratory, Office of Research and Development, Cincinnati, OH

Dr. Gregory Wilson, EPA, Office of Emergency Management, Washington, DC

6.1.3 Bureau of Ocean Energy Management

Dr. Rebecca Green, Office of the Environment, Bureau of Ocean Energy Management, Gulf of Mexico OCS Region

6.1.4 The White House

Dr. Jerry Miller, Office of Science and Technology Policy/Executive Office of the President

6.2 Information Coordination and Synthesis Provided by:

6.2.1 BP

Mr. Peter D. Carragher. Senior Scientific Advisor (consultant) to BP Gulf Coast Restoration Organization. Houston Texas

6.2.2 University of North Carolina

Dr. Harvey E. Seim, Department of Marine Sciences, UNC Chapel Hill

6.3 References

Atlas, R. M. and T. C. Hazen (2011). Oil Biodegradation and Bioremediation: A Tale of the Two Worst Spills in U.S. History. *Env. Science and Technol.* 45(16): 6709–6715. DOI: 10.1021/ES2013227.

Barker, C. H. (2011). An Early Long Term Outlook for the Deepwater Horizon Oil Spill. *In* Proc., 34th Arctic and Marine Ocean Pollution (AMOP) Conference, Banff, Alberta, Canada.

Beegle-Krause, C.J., Timothy P. Boyer, Hernan E. Garcia, Christopher H. Barker, Amy MacFadyen, and Debra Payton (2011). Deepwater Horizon MC252: Understanding the Spill Below the Surface. *In* Proc., 34th Arctic and Marine Ocean Pollution (AMOP) Conference, Banff, Alberta, Canada, 12 pp.

Broecker, Warren, Tsung-hung Peng, and Zonghong Beng (1982). *Tracers in the Sea*. Eldigio Press, Lamont-Doherty Geological Observatory, Columbia University, Palisades, N. Y., June, 690 pp.

Bugden, J. B. C., C. W. Yeung, P. E. Kepkay, and K. Lee. 2008. Application of ultraviolet fluorometry and excitation–emission matrix spectroscopy (EEMS) to fingerprint oil and chemically dispersed oil in seawater. *Mar. Poll. Bull.* 56: 677–685.

Camilli, R., C. M. Reddy, D. R. Yoerger, B. A. S. Van Mooy, M. V. Jakuba, J. C. Kinsey, and J. V. Maloney. (2010). Tracking Hydrocarbon Plume Transport and Biodegradation at Deepwater Horizon. *Science* 330(6001): 201–204. DOI: 10.1126/science.1195223.

Coastal Response Research Center. (2010). Deepwater Horizon Dispersant Use Meeting Report, May 26–27, 2010. University of New Hampshire. June 4, 2010. Revision 3.

Department of Energy (2010). Key Events Timeline. July 28, 2010. Accessed April 15, 2011. http://energy.gov/downloads/key-events-timeline.

Dickson, A. G. (1995). Determination of dissolved oxygen in sea water by Winkler titration. WOCE Operations Manual. WOCE Operations Manual. Part 3.1.3 Operations & Methods, WHP Office Report WHPO 91-1.

Diercks, A. R., R. C. Highsmith, V. L. Asper, D. J. Joung, Z. Z. Zhou, L. D. Guo,…, and S. E. Lohrenz (2010). Characterization of subsurface polycyclic aromatic hydrocarbons at the Deepwater Horizon site. *Geophys. Res. Lett.* 37. DOI: 10.1029/2010GL045046.

DiMarco, S. F., N. Walker, P. Chapman, W. J. Wiseman, Jr., S. P. Murray, and S. D. Howden (2007). Physical processes in the northern Gulf of Mexico and their influence on hypoxia of the Texas-Louisiana shelf. U.S. Environmental Protection Agency, Ref. Documents for the SAB Hypoxia Advisory Panel. http://yosemite.epa.gov/sab/sabhap.nsf/b3172537ac8bc12b85256dbf0056c462/ecc11213cae3f574852572650069f347/$FILE/DiMarco%20et%20al.,%202007.pdf.

Donohue, K., P. Hamilton, K. Leaman, R. Leben, M. Prater, D. R. Watts, and E. Waddell (2006). Exploratory study of the deepwater currents in the Gulf of Mexico. Volume II: Technical Report, U.S. Dept of the Interior, Bureau of Ocean Energy Management, Gulf of Mexico OCS Region, New Orleans, LA, OCS Study BOEM 2006-074.

Environmental Protection Agency (2010a). Dispersant Monitoring and Assessment Directive for Subsurface Dispersant Application, May 10, 2010.

Environmental Protection Agency (2010b). Dispersant Monitoring and Assessment Directive for Subsurface Dispersant Application, Addendum, May 14, 2010.

Environmental Protection Agency (2010c). Dispersant Monitoring and Assessment Directive for Subsurface Dispersant Application, Addendum 4, July 23, 2010.

Federal Interagency Solutions Group (2010). Oil Budget Calculator, Deepwater Horizon. Oil Budget Calculator Science and Engineering Team. http://www.restorethegulf.gov/sites/default/files/documents/pdf/OilBudgetCalc_Full_HQ-Print_111110.pdf.

Garcia, H. E., R. A. Locarnini, T. P. Boyer, J. I. Antonov, O. K. Baranova, M. M. Zweng, and D. R. Johnson (2010). *World Ocean Atlas 2009, Volume 3: Dissolved Oxygen, Apparent Oxygen Utilization, and Oxygen Saturation.* S. Levitus (Ed.), NOAA Atlas NESDIS 70, U.S. Government Printing Office, Washington, D.C., 344 pp.

Garcia, H. E., T. P. Boyer, S. Levitus, R. A. Locarnini, and J. I. Antonov (2005a). Climatological annual cycle of upper ocean oxygen content anomaly. *Geophys. Res. Lett.* 32, L09604, doi:10.1029/ 2004GL 022286.

Garcia, H. E., T. P., Boyer, S. Levitus, R. A. Locarnini, and J. Antonov (2005b). On the variability of dissolved oxygen and apparent oxygen utilization content for the upper world ocean: 1955 to 1998, *Geophys. Res. Lett. 32*, L09604. DOI:10.1029/2004GL022286.

Hamilton, P., K.A. Donohue, R.R. Leben, A. Lugo-Fernandez, and R.E. Green (2011) Loop Current observations during spring and summer of 2010: Description and historical perspective. In: Monitoring and Modeling the Deepwater Horizon Oil Spill: A Record-Breaking Enterprise, Geophysical Monograph Series 195, American Geophysical Union, 10.1029/2011GM001116.

Hazen, T. C., E. A. Dubinsky, T. Z. DeSantis, G. L. Andersen, Y. M. Piceno, N. Singh and O. U. Mason (2010). Deep-Sea Oil Plume Enriches Indigenous Oil-Degrading Bacteria. *Science* 8: 330(6001), 204–208. DOI: 10.1126/science.1195979.

Jochens, A. E., L. C. Bender, S. F. DiMarco, J. W. Morse, M. C. Kennicutt II, M. K. Howard, and W. D. Nowlin, Jr. (2005). Understanding the Processes that Maintain the Oxygen Levels in the Deep Gulf of Mexico: Synthesis Report. U.S. Dept. of the Interior, Minerals Management Service, Gulf of Mexico OCS Region, New Orleans, LA, OCS Study MMS 2005-032, 142 pp.

Johansen, Øistein (2003). Development and Verification of Deep Water Blowout Models. *Mar. Poll. Bull.* 47: 36–368.

Joint Analysis Group (2010a). Deepwater Horizon Oil Spill: Review of R/V *Brooks McCall* Data to Examine Subsurface Oil. National Oceanic and Atmospheric Administration, NOAA Technical Report NOS OR&R 24, June 2011, 68 pp.

Joint Analysis Group (2010b). Deepwater Horizon Oil Spill: Review of Preliminary Data to Examine Subsurface Oil in the Vicinity of MC252#1, May 19 to June 19, 2010. National Oceanic and Atmospheric Administration, NOAA Technical Report NOS OR&R 25, August 2011, 172 pp.

Joint Analysis Group (2010c). Deepwater Horizon Oil Spill: Review of Preliminary Data to Examine Oxygen Levels in the Vicinity of MC252#1, May 8 to August 9, 2010. National Oceanic and Atmos-pheric Administration, NOAA Technical Report NOS OR&R 26, June 2011, 106 pp.

Joint Analysis Group (2010d). Deepwater Horizon National Incident Command Joint Analysis Group. Initial Quality Control of Analytical Chemistry Data from Water Samples Taken in the Vicinity of MC252#1. http://ecowatch.ncddc.noaa.gov/JAG/files/Chemistry%20report_QA_QC_ Summary_V7.pdf.

Joye, S. B., I. R. MacDonald, I. Leifer, and V. Asper (2011). Magnitude and Oxidation Potential of Hydrocarbon Gases Released from the BP Oil Well Blowout. *Nature Geoscience* 4, 160–164. DOI: 10.1038/ngeo1067. http://www.nature.com/ngeo/journal/v4/n3/full/ngeo1067.html.

Keeling, R., and H. Garcia (2002). The Change in Oceanic O_2 Inventory Associated with Recent Global Warming. *Proc., U. S. Natl. Acad. Sci.* 99, 7848–7853.

Kessler, J. D., D. L. Valentine, M. C. Redmond, M. R. Du, E. W. Chan, S. D. Mendes, and T. C. Weber (2011). A Persistent Oxygen Anomaly Reveals the Fate of Spilled Methane in the Deep Gulf of Mexico. *Science 331*(6015), 312–315. DOI: 10.1126/science.1199697.

Kujawinski, E. B., M. C. Kido Soule, D. L. Valentine, A. K. Boysen, K. Longnecker, and M. C. Redmond (2011). Fate of Dispersants Associated with the Deepwater Horizon Oil Spill. *Environ. Sci. Technol.* 45(4): 1298–1306. http://pubs.acs.org/doi/abs/10.1021/es103838p.

Langdon, C. (2010). Determination of dissolved oxygen in seawater by Winkler titration using the amperometric technique. In *GO-SHIP Repeat Hydrography Manual: A Collection of Expert Reports and Guidelines*, B. M. Sloyan and C. Sabine (Eds.), IOC/IOCCP, Paris.

Ledwell, J. R., and A. Bratkovich (1995). A Tracer Study of Mixing in Santa Cruz Basin. *J. Geophys. Res.* 100: 20,681–20,704.

Ledwell, J. R., and B. M. Hickey (1995). Evidence for Enhanced Boundary Mixing in Santa Monica Basin. *J. Geophys. Res.* 100:20,665–20,680.

Ledwell, J. R., A. J. Watson, and C. S. Law (1993). Evidence for Slow Mixing across the Pycnocline from an Open-ocean Tracer-release Experiment. *Nature* 364: 701–703.

McNutt, M, R. Camilli, G. Guthrie, P. Hsieh, V. Labson, B. Lehr, D. Maclay, A. Ratzel, and M. Sogge (2011). Assessment of Flow Rate Estimates for the Deepwater Horizon/Macondo Well Oil Spill. Flow Rate Technical Group Report to the National Incident Command, Interagency Solutions Group, March 10, 2011, Appendix C.

Nowlin, W. D., A. E. Jochens, S. F. DiMarco, R. O. Reid, and M. K. Howard (2001). Deepwater Physical Oceanography Reanalysis and Synthesis of Historical Data: Synthesis Report. U.S. Department of the Interior, Minerals Management Service (now BOEMRE), Gulf of Mexico OCS Region, New Orleans, La. OCS Study MMS 2001-064, 528 pp.

O'Connor, B. M., R. A. Fine, and D. B. Olson (2005). A Global Comparison of Subtropical Underwater Formation Rates. *Deep-Sea Res. I*, 52: 1569–1590.

Obey, L.-Y.-, M. Inoue, R. Lai, X.-H. Lin, S. E. Welsh, and L. Rouse, Jr. (2008). Stalling of Near Inertial Waves in a Cyclone. *Geophys. Res. Lett.* 35: L12604. DOI: 10.1029/2088GL034273.

Operational Science Advisory Team (2010). Summary Report for Sub-Sea and Sub-Surface Oil and Dispersant Detection: Sampling and Monitoring. Deepwater Horizon MC252 Unified Area Command, 131 pp. http://www.restorethegulf.gov/sites/default/files/documents/pdf/OSAT_Report_FINAL_17DEC.pdf

Paluszkiewicz, T., L. P. Atkinson, E. S. Posmentier, and C. R. McClain (1983). Observations of a Loop Current Frontal Eddy Intrusion Onto the West Florida Shelf. *J. Geophys. Res.* 88(C14): 9639–9651. DOI:10.1029/JC088iC14p09639.

Rabalais, N. N., R. E. Turner, B. K. Sen Gupta, D. F. Boesch, P. Chapman, and M. C. Murrell (2007). Characterization and Long-term Trends of Hypoxia in the Northern Gulf of Mexico: Does the science support the action plan? *Estuaries and Coasts* 30: 753–772.

Reddy, C. M., J. S. Arey, J. S. Seewald, et al. (2011). Composition and Fate of Gas and Oil Released to the Water Column during the Deepwater Horizon Oil Spill. *In* Proc., National Academy of Sciences. July 18, 2011, DOI: 10.1073/pnas.1101242108.

Reid, J. L. and R. L. Lynn (1971). On the Influence of the Norwegian-Greenland and Weddell Seas Upon the Bottom Waters of the Indian and Pacific Oceans. *Deep-Sea Res.*18: 1063–1088.

Rivas, D., A. Badan, and J. Ochoa (2005). The Ventilation of the Deep Gulf of Mexico. *J. Phys. Oceanogr.* 35: 1763–1781.

Rosenberg, Eugene (2006). Hydrocarbon Oxidizing Bacteria. *Prokaryotes* 2: 564–577.

Sarmiento, J. L., T. M. C. Hughes, R. J. Stouffer, and S. Manabe (1998). Simulated Response of the Ocean Carbon Cycle to Anthropogenic Climate Warming. *Nature* 393: 245–249.

Schmitz, W. J., Jr., D. C. Biggs, A. Lugo-Fernandez, L.-Y. Oey, and W. Sturges (2005). A Synopsis of the Circulation in the Gulf of Mexico and on Its Continental Margins. *In* Circulation in the Gulf of Mexico: Observations and Models, American Geophysical Union, *Geophysical Monograph Series* 161: 11–29, 347 pp. ISSN: 0065-8448/ISBN: 978-0-87590-425-2.

Schmitz, W. J. and P. L. Richardson (1991). On the sources of the Florida Current. *Deep-Sea Research* 38 (Suppl.), 379–409.

Shedd, W., et al. (2011). BOEMRE Seismic water bottom anomalies map gallery. http://www. boemre.gov/offshore/mapping/SeismicWaterBottomAnomalies.htm.

Socolofsky, S. A., E. E. Adams, and C. R. Sherwood (2011). Formation Dynamics of Subsurface Hydrocarbon Intrusions following the Deepwater Horizon Blowout. *Geophys. Res. Lett.* 38: L09602. DOI:10.1029/2011GL047174.

Sturges, W., and K. E. Kenyon (2008). Mean Flow in the Gulf of Mexico. *J. Phys. Oceanogr.* 38(7): 1501–1514.

Sturges, W., and R. Leben (2000). Frequency of ring separations from the Loop Current in the Gulf of Mexico: A Revised Estimate. *J. Phys. Oceanogr.* 30:1814-1910.

Sundermeyer, M. A. and J. Ledwell (2001). Lateral dispersion over the continental shelf: analysis of dye release experiments. *J. Geophys. Res.* 106: 9603–9621.

Unified Area Command (2010a). Deepwater Horizon MC252 Response Unified Area Command (UAC). Implementation Plan for Sub-sea and Sub-surface oil and Dispersant Detection, Sampling, and Monitoring. Approved by Unified Area Command on September 13, 2010.

Unified Area Command (2010b). Deepwater Horizon MC252 Response Unified Area Command (UAC). Operational Annex for Execution and Management of Sub-sea and Sub-surface Detection, Sampling, and Monitoring Missions. Approved by Unified Area Command on October 1, 2010.

Unified Area Command (2010c). Deepwater Horizon MC252 Response Unified Area Command (UAC). 2010. Strategic Plan for Sub-sea and Sub-surface oil and Dispersant Detection, Sampling, and Monitoring, November 13, 2010. http://www.restorethegulf.gov/sites/default/files/documents/pdf/13_NOV_2010 _SMU_ Strategic_ Plan.pdf.

Valentine, David L., John D. Kessler, M. C. Redmond, C. J. Villanueva et al. (2010). Propane Respiration Jump-Starts Microbial Response to a Deep Oil Spill. *Science* 330(6001): 208–211. DOI: 10.1126/science.1196830.

Valentine, David L., Igor Mezićb, Senka Maćešićc, Nelida Črnjarić-Žicc, Stefan Ivićc, Patrick J. Hogand, Vladimir A. Fonoberove, and Sophie Loire (2012). Dynamic autoinoculation and the microbial ecology of a deep water hydrocarbon irruption. *In* Proc., Natl. Acad. Sci. DOI: 10.1073/pnas.1108820109.

Venosa, A. D., D. King, and G.A. Sorial (2002). The Baffled Flask Test for Dispersant Effectiveness: A Round Robin Evaluation of Reproducibility and Repeatability. *Spill Science Technol. Bull.* 7(5): 299–308(10).

Vukovich, F. M. (2007) Climatology of Ocean Features in the Gulf of Mexico using Satellite Remote Sensing. *J. Phys. Oceanogr.* 37: 689–707. DOI: 10.1175/JPO2989.1.

Walker, J. D. and R. R. Colwell (1975). Measuring Potential Activity of Hydrocarbon Degrading Bacteria. *Appl. Environ. Microbiol.* 31: 189–197.

Wanninkhof, R., G.-H. Park, and G. A. Berberian (2011). Oxygen Winkler Titrations by NOAA/AOML in Support of Deepwater Horizon Spill Monitoring. NOAA Technical Memorandum, OAR AOML-99, 15 pp.

Warren, B. A. (1981). Deep circulation of the world ocean. In *Evolution of Physical Oceanography: Scientific Surveys in Honor of Henry Stommel*, Bruce A. Warren and Carl Wunsch (Eds.). The MIT Press, 6–41.

Welsh, S. E., M. Inoue, L. J. Rouse, Jr., and E. Weeks (2009). Observations of the Deepwater Manifestation of the Loop Current and Loop Current Rings in the Eastern Gulf of Mexico. U.S. Dept. of the Interior, Bureau of Ocean Energy Management, Gulf of Mexico OCS Region, New Orleans, LA. OCS Study MMS 2009–050, 110 pp.

Worthington, L.V. (1981). The Water Masses of the World Ocean: Some Results of a Fine-scale Census. In: *Evolution of Physical Oceanography, Scientific Surveys in Honor of Henry Stommel*. Bruce A. Warren and Carl Wunsch (Eds.). The MIT Press, Cambridge, MA, pp. 42–69.

Yapa, P. D., L. Zheng, and K. Nakata (1999). Modeling Underwater Oil/Gas Jets and Plumes. *J. Hydraulic Eng.* 125: 481–491.

Yvon-Lewis, S. A., Lei Hu, and J. Kessler (2011). Methane Flux to the Atmosphere from the Deepwater Horizon Oil Disaster. *Geophys. Res. Lett.* 38: L01602. DOI:10.1029/2010GL045928, 2011.

Zukunft, Rear Admiral Paul (2010). Strategic Plan for Sub-Sea and Sub-Surface Oil and Dispersant Detection, Sampling, and Monitoring. Deepwater Horizon MC252 Response, Unified Area Command, U.S. Coast Guard, New Orleans, La., November 13, 2010.

Appendices

Appendix 1: Data Accessibility

Data collected in the Gulf of Mexico in response to the Deepwater Horizon incident are being catalogued, archived, and posted by the NOAA's National Oceanographic Data Center (NODC). This collection includes data collected by NOAA, other federal agencies, and academic partners' gulf science missions. This collection continues to expand as datasets are processed and validated. Chemical and physical oceanographic data that are used in this report are archived at: http://accession.nodc.noaa.gov/0087872.

This appendix is organized in two sections. Section 1A provides links to the primary datasets used by the Joint Analysis Group (JAG) in the development of this and the preceding JAG analysis reports. Some of the data collected during the MC252 Response Phase, particularly analytical chemistry data, continue to be processed and validated. These data will be made available on the NODC Incident Support for MC252 site when they become available. Additionally, these data will become part of the NODC permanent National Archive once quality assurance and quality control procedures are completed and validated metadata is available.

Section 1B provides links to the locations of additional data and information available concerning the Federal response to the MC252 incident.

1A: Data Used to Develop the Suite of JAG Reports

National Oceanographic Data Center Incident Support for Deepwater Horizon
http://www.nodc.noaa.gov/General/DeepwaterHorizon/support.html

The NODC Incident Support for MC252 includes a comprehensive archive of Deepwater Horizon data, climatology products, ocean currents data, resources on oil spills, response and restoration, coastal ecosystem maps, and ocean profile data. The data and information are available in a variety of formats, including OPeNDAP or THREDDS.

National Oceanographic Data Center Permanent National Archive
http://www.nodc.noaa.gov/General/getdata.html

The NODC manages the world's largest collection of publicly available oceanographic data. NODC holdings include in situ and remotely sensed physical, chemical, and biological oceanographic data from coastal and deep-ocean areas. NODC data holdings extend as far back as 100 years ago.

Through NODC archive and access services these ocean data are being reused to answer questions about ocean phenomena and management of coastal and marine resources, marine transportation, recreation, national security, and natural disasters. Once NODC MC252 data is processed to ensure that it meets quality assurance and quality control (QA/QC) and metadata standards, it is archived and made publicly available as part of the permanent data collection in the NODC Ocean Archive System.

National Data Buoy Center
http:www.ndbc.noaa.gov/obs.shtml
http://www.ndbc.noaa.gov/station_page.php?station=42916
http://www.ndbc.noaa.gov/station_page.php?station=42370

The National Data Buoy Center (NDBC) provides real-time, end-to-end capability beginning with the collection of marine atmospheric and oceanographic data and ending with its transmission, QC, and distribution. NDBC supports the mission of the National Weather Service and NOAA, promotes public safety, and satisfies the needs of a number of customers.

Deepwater Horizon Data Access Atlas
http://www.ncddc.noaa.gov/website/google_maps/DWHAtlas/mapsAtlas.htm

The NODC/National Coastal Data Development Center (NCDDC) MC252 Data Access Atlas provides data discovery and direct access using a Google map format. This atlas allows searches geographically, by data type, or by collection platform. Once data sets are identified and selected, the user is provided easy, direct access to the data, metadata, and related documents if available.

The Joint Analysis Group (JAG) for Surface and Sub-Surface Oceanography, Oil and Dispersant Data
http://ecowatch.ncddc.noaa.gov/JAG/data.html

The JAG Web site provides direct access to the JAG reports, links to other sources of data and information, and access to the EcoWatch THREDDS server that hosts the ocean profile data used in the JAG analyses.

1B: Additional Data and Information from the Federal Response to the MC252 Event

Data.Gov/RestoretheGulf
http://www.data.gov/restorethegulf/

Data.gov increases the ability of the public to easily find, download, and use datasets that are generated and held by the Federal Government. Data.gov provides descriptions of the Federal datasets (metadata), information about how to access the datasets, and tools that leverage government datasets. Data.gov is featuring data from the Department of Energy, EPA, NOAA, the Department of the Interior, and the states of Florida and Louisiana related to the Deepwater Horizon spill, its effects, and the cleanup effort.

NOAA Deepwater Horizon Archive
http://www.noaa.gov/deepwaterhorizon/

The Deepwater Horizon Archive is designed for many users, from scientists and researchers who are seeking data to citizens who want to learn more about the spill's impact on the Gulf.

GeoPlatform/gulfresponse
http://www.geoplatform.gov/gulfresponse/
http://www.restorethegulf.gov/release/2011/10/28/mapping-response-deepwater-horizon-oil-spill

GeoPlatform.gov/gulfresponse is an online tool that provides information about the response effort. Developed by National Oceanic and Atmospheric Administration (NOAA), with the Environmental Protection Agency (EPA), U.S. Coast Guard, and the Department of Interior, the site offers a "one-stop shop" for information using an interactive map format.

RestoretheGulf.gov
http://www.restorethegulf.gov/

RestoretheGulf.gov is the official website of the United States Government's response to the Deepwater Horizon Oil spill event.

Naval Oceanographic Office Special Support-GOMEX Mississippi Canyon 252 Oil Spill
http://ecowatch.ncddc.noaa.gov/JAG/Navy/

This page provides direct access to products and information from the Naval Oceanographic Office, including bathymetry, glider data, specialized imagery, model output, and satellite analysis.

EPA Response to BP Spill in the Gulf of Mexico
http://www.epa.gov/bpspill/

Environmental data, including air quality and water samples, will be posted and frequently updated on this site as it is collected and validated by EPA's response teams along the impacted coastlines.

NOAA Damage Assessment, Remediation & Restoration Program (DARRP)
http://www.darrp.noaa.gov/

NOAA Damage Assessment, Remediation & Restoration Program (DARRP) is coordinating data collection efforts with partners in five states (Louisiana, Mississippi, Alabama, Florida, and Texas) and the Department of the Interior (including the U.S. Fish and Wildlife Service, National Park Service, and Bureau of Land Management). BP is also participating in many of the data collection efforts.

Deepwater Horizon Oil Spill Research and Monitoring Activities Database
http://gulfseagrant.tamu.edu/oilspill/database.htm

This database, developed by NOAA, serves as a single location to upload and access information about research and monitoring activities related to the Deepwater Horizon oil spill. The database contains brief descriptions of activities but not raw data.

National Marine Fisheries Service (NMFS) Southeast Regional Office—St. Petersburg
http://sero.nmfs.noaa.gov/deepwater_horizon_oil_spill.htm

This page includes a map of fishery closure boundaries, fishery bulletin, current news, state closure information, fisheries, protected resources and habitat, and general information.

National Weather Service New Orleans/Baton Rouge Deepwater Horizon Decision Support Page
http://www.srh.noaa.gov/lix/?n=embriefing

This decision support page includes spot forecasts, top graphics, tropical weather, radar sites, forecasts/meteograms, offshore forecasts, wind forecast/analysis graphics, and wave forecast graphics.

NWS Mobile Deepwater Horizon Decision Support Page
http://www.srh.noaa.gov/mob/?n=oilspillsupportpage

This decision support page includes a 6-hour coastal thunderstorm outlook, regional radar summary, the latest special marine warning, the latest marine weather statements, tide information, and shoreline forecasts.

Air Resources Laboratory (ARL) Forecast Trajectory Maps for Gulf of Mexico
http://ready.arl.noaa.gov/READY_traj_gulfmex.php

The trajectories shown on this page represent where hypothetical atmospheric releases of material are predicted to be transported.

Appendix 2: Methods Used in Data Processing and Analysis

2A: General Profile,Temperature and Salinity Data Processing and Analysis

To provide consistency across different ships, sensors, and personnel, all conductivity-temperature-depth (CTD) profile data available to the JAG during the Federal Response to the Deepwater Horizon oil spill were reprocessed from raw instrument files. Seabird Electronics (SBE) manufactured all CTD instruments in the 23 ships that submitted profile data to the MC252 response. Binary data files (hex or dat) and configuration files (con) were obtained for all casts and reprocessed at National Oceanographic Data Center (NODC) using SBE data processing software. All fluorescence and oxygen data coincident with the CTD sensor observations in this report were collected and processed through the SBE CTD systems. During CTD processing, the recommended procedures following SBE Application Note 64-3 (SBE 43 Dissolved Oxygen [DO] Sensor—Hysteresis Corrections) were used as outlined under "Data conversion module when Winkler Bottle Data is NOT Available."

The profile data submitted to the Federal Response were processed with following considerations:

- Minimize digital filtering at all steps to ensure any unknown subsurface hydrocarbon effects remained in profile data.
- Provide documented, quantitative quality control and quality assurance (QA/QC) to meet Data Quality Act requirements and to provide data to the public as quickly as possible.
- Quick (24 h) turnaround of profiles for immediate analysis.
- Raw files (all scans) were initially plotted and visually examined for instrument response issues. Following that examination, the SBE processing routine "Wildedit" was used with to remove spikes in the temperature and salinity data based on statistics of blocks of individual scans. Data were then pressure-averaged files (1 dbar) for the downcast that were created and plotted for a quick-look review by the JAG members. Separate data files were created for comparing CTD observations to water-sample data collected concurrently using Niskin sampling bottles. These "bottle files" contained CTD observations extracted for the known depths of the Niskin bottle samples using both downcast and upcast data from the CTD.

Initial QC of the CTD casts was conducted following a subset of checks outlined in the Global Temperature and Salinity Profile Program (GTSPP) Real-Time Quality Control Manual (UNESCO, 2009). The following QC checks were done on all profiles

All parameters collected through the CTD system:

- Global Impossible Parameter

Temperature and Salinity Data:

- Spike
- Top and Bottom Spike
- Gradient
- Density Inversion
- Levitus Seasonal Statistics

QC flags were assigned to the individual observations following the Global Temperature and Salinity Profile Programme (GTSPP) procedures. GTSPP is a joint World Meteorological Organization (WMO) and Intergovernmental Oceanographic Commission (IOC) program, procedures and implements internationally

agreed QC standards. The CTD data and available bottle data (raw and processed) are located in the archive at NODC. Profile data are being subjected to additional QC checks as part of ingest into the World Ocean Database at NODC.

All CTD data were converted to a netCDF format (CF convention) for use by JAG members and public distribution.

In subsequent analyses, only observations that universally received a GTSPP QC flag of "1" (i.e., the element appears to be correct) at a given pressure level were considered (i.e., temperature, salinity, fluorescence, and dissolved oxygen (DO_2) data all had to receive QC flag 1 at same the pressure level to be included in any subsequent analysis).

2B: Color Dissolved Organic Matter Fluorescence Data (CDOM) Analysis

Various techniques were investigated to allow valid comparison of the data collected by the WET Labs open path CDOM fluorometers that were employed on the vast majority of deep (> 200 m) profiles during the response. The goal of this analysis was to isolate and analyze the characteristics of the fluorescence anomalies observed between 900 and 1300 m depth. Based on historical observations, the expected fluorescence profile shape for the northern Gulf of Mexico was linear down to 1000 m with values on the order of 1.5 Quinine Sulfate Units at 1000 m (pers. comm., Robert Chen University of Massachusetts Boston, July 6, 2010). Inspection of data collected during the response showed very similar profile characteristics to those expected with values at 1000 m on the order of units 2 ppb Quinine Sulfate Dihydrate Equivalent (QSDE) per the WET Labs calibration standard. However there was sufficient variation among the data collected by various ships and instruments that prevented accurate use of a canonical fluorescence profile to normalize the entire data set. Additionally, the profile shape below 1000 m did not remain linear and the fluorescence values tended to decrease slightly with depth. Not the subject of this analysis, this decreasing trend at depth could be attributed to naturally expected phenomena including the proximity to the ocean floor (pers. comm., Ian Walsh, WET Labs, May 16, 2012) and/or generally lower values that could be inferred for water masses at the deeper depths (North Atlantic Deep Water) (inference from Nelson et al., 2007).

In order to isolate fluorescence signals potentially associated with deep subsurface dispersed oil, a least-squares quadratic fit technique was applied to each individual profile using data points outside the region of interest (200-800 m and below 1300 m to the bottom of the profile). This fitted profile was used to normalize the entire profile below 200 m. Three additional quality control steps were also conducted prior to analysis. The quality of the fit (R2), comparison of gross profile shape (e.g. non-linear 200-800 m), and magnitude of the overall mean 200-800 m as compared to expected background values (order 2 ppb QSDE vice less than 1 ppb or greater than 6 ppb) were used to discard profiles prior to the analysis. A total of 774 stations met the criteria for this analysis (total profile depth > 1300 m, instrument type, and additional quality control). The normalized profiles were integrated over the depth range of 900–1300 m to estimate the magnitude of the overall fluorescence (CDOM) anomaly as measured by CDOM fluorometers on each profile.

To establish the baseline or the level of fluorescence considered to be the background threshold for these integrated values, means, maximums, and standard deviations were calculated on each of 68 profiles from 9 ships/instruments that had no indication of subsurface fluorescence anomalies in the region of 900-1300 m. The standard deviations of these "no signal above background" stations were very consistent (the standard deviation of the set of profiles was on the order of 0.01 ppb QSDE) as can be seen in Figure Appendix 2b 1. To provide confidence, two times average standard deviation was taken as the threshold for considering a fluorescence anomaly to be above background. The entire positive area was translated as the background integrated fluorescence value. This technique correspond to an background integrated fluorescence value of

48.60 ppb (QSDE) * m. A threshold of 50 ppb (QSDE) * m was therefore selected as the threshold for detect/non-detect time series and synthesized map and between all sensors/platforms (Figures 27b and 28).

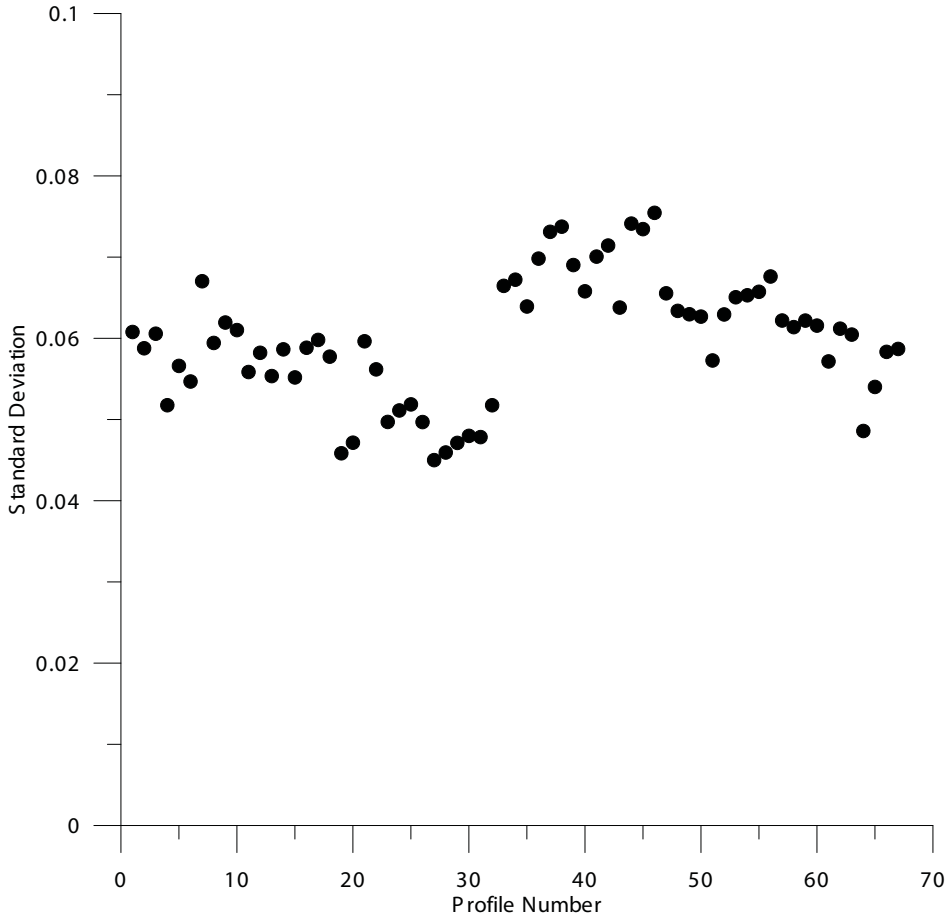

Figure 2b1. Standard deviation of fluorescence signals between 900 – 1300 m for 68 profiles.

2C:Profiles from SeaBird Electronics 43 Sensor

To examine a synthesis of all the oxygen profiles collected; all data that passed Global Impossible Value were plotted and examined. From the visual examination, additional profiles were excluded from the analysis based on documented or verified collection issues from the ship (e.g. cable electrical issue). Entire profiles that were outside at least 2 standard deviations of the mean oxygen profile were excluded and evaluated as gross calibration or other system errors (deemed to be not accurately sensing the environment) were also excluded. The following is a list of cruises and stations excluded from the Dissolved Oxygen analysis.

- *American Diver* (all casts)
- *Arctic* (all casts)
- *Gordon Gunther* Cruise 3 and 4
- *Walton Smith* Cruise 2 (all casts)
- *Ocean Veritas* Station 62

Figure 37 represents the remaining 813 profiles considered in the oxygen analysis. Basic statistics on the dissolved oxygen were calculated over the 900–1300 m range for each cast with a profile that extended to the

minimum depth of 1300 m. To examine the depressions observed in the dissolved oxygen profiles, a least-squares, second-order polynomial fit of the oxygen profile as function of seawater density between 1027.2 and 1027.75 kg $m^{-3}$was obtained. Coefficients for the polynomial fit were examined on a by-cast, by-cruise, by-ship basis to determine the overall quality of the profile fit. The difference between the polynomial fit and the actual profile determines the dissolved oxygen anomaly. The anomaly was converted back from density to pressure for further analysis. Oxygen concentration units were converted from mL/L to moles/m^3 to provide units with more consistent spatial dimensions prior to integrating. The anomalies were vertically integrated and the depressions analyzed in the 600–900 dbar and the 900–1300 dbar ranges (units moles/m^2).

2D: Chelsea Instruments AQUAtracka Fluorescence Data

Similar to dissolved oxygen, fluorescence data from the Chelsea Instruments AQUAtracka hydrocarbon fluorometer were initially processed through the SBE software. To analyze the observed peaks in the fluorescence profiles in the 900- to 1300-m layer, a least-squares, first-order polynomial fit of the fluorescence profile as function of seawater density between 1027.2 and 1027.75 kg m^{-3} was obtained. The difference between the polynomial fit and the actual profile determines the magnitude of the fluorescence peak anomalies. The vertical coordinate of the anomalies were converted back to pressure from density and integrated in the 900–1300 m range. Similarly to the CDOM fluorometer analysis, a baseline for distinguishing a positive anomaly in the integrated value was achieved by examining a subset of profiles where visually a hydrocarbon anomaly was not evident. The maximum integrated value in this subset was 9.926 ppb (carbezole) * m and therefore 10 ppb (carbezole) * m was selected as the baseline for a positive response in Figure 31.

2E: ADCP Ocean Current Data

In 2005, the former Minerals Management Service (now the Bureau of Ocean Energy Management and Bureau of Safety and Environmental Enforcement) issued a Notice to Lessees (NTL) requiring that ADCPs be deployed on drilling and production platforms in the northern Gulf of Mexico in water depths of >400 m. The data were to be transmitted to the National Data Buoy Center (NDBC), where it would be quality controlled, stored, and broadcast over the Global Telecommunications System. Previous reports describe the program and the quality control of the data (Crout and Conlee, 2007; Crout et al., 2006). The NTL has been extended several times, most recently in 2009, and data continue to be collected and transmitted.

QC at NDBC consists of range and comparison tests. The results are denoted by failed, suspect, and good data categories. Data that failed the NDBC quality tests were not included in the analysis. Several events interrupted the collection of ADCP data. Both Hurricane Alex and Tropical Storm Bonnie caused the drilling ships *Discoverer Enterprise* and *Development Driller III* to leave the Deepwater Horizon site for short periods. Activity near the seafloor (remotely operated vehicles and intense monitoring of the area using acoustics) also impacted the quality of the acoustic signal returned to the ADCP.

2F: Chemical Methods of Analysis

2F.1 Brooks McCall *Cruise 1 (5/8) to Cruise 5 (5/30),* Ocean Veritas *Cruise 1 (Starting 5/27)*

Early into the submerged oil plume investigation, it was thought that the concentrations of oil would be high and that screening methods for total petroleum hydrocarbons (TPH) could be used to locate the plume. Therefore, a UV/VIS spectrophotometric “screening” analysis was used to determine the concentration of the

semivolatile fraction of the oil. The method used was based on 40 CFR 300 (App. C sections 2.2.3, 2.4.2.1, and 2.5) except that preliminary testing of MC252 source oil samples determined that a 460-nm wavelength provided optimal resolution. Samples were extracted into methylene chloride, concentrated 10-fold and quantified by comparison to 6 different concentrations (1–100 mg/L) of MC252 oil. QC samples were run with the actual samples, including calibration check samples, method blanks, and matrix spike samples. Method detection limits were about 0.8 mg/L. TPH values were reported as TPH (µg/L) and represented the C-12 and higher alkanes, the isoprenoid or branched alkanes, and the polycyclic aromatic hydrocarbons (PAHs: 2, 3, 4, 5, and 6 ring aromatics), along with the rest of the hydrocarbon semivolatiles. All samples containing measurable amounts of petroleum hydrocarbons were further examined by gas chromatography/mass spectrometry (GC/MS) to verify that the petroleum was MC252 oil and to quantify the alkanes, biomarkers, and PAHs present in the sample.

The gasoline range volatile hydrocarbons were analyzed using the standard EPA SW-846[17] purge and trap analysis method 8260. The complete list of analytes can be found in Appendix 5. QC samples were run in accordance with EPA Method requirements. Method detection limits for specific analytes were about 1 µg/L. The sum of the gasoline range hydrocarbons components in each sample are reported as a tVOA concentration in this report.

2F.2 R/V Brooks McCall *Cruise 6 (6/5) to Cruise 13 (7/19), R/V* Ocean Veritas *Cruise 2 (6/2) to Cruise 10 (7/22)*

Subsurface concentrations of sTPH observed during the May cruises of the R/V *Brooks McCall* and R/V *Ocean Veritas* were lower than anticipated when sample analysis first began. Accordingly, starting with R/V *Brooks McCall* Cruise 6, EPA SW-846 method 8270 was used for semivolatile hydrocarbon analyses. Modifications of method 8270 were used to quantify semivolatile alkanes, biomarkers, and parent and alkylated PAHs that are not normally analyzed by this method. Method detection limits for specific analytes were primarily below 1 µg/L. The EPA SW-846 method 8015 was used to determine concentrations of the oil saturate fraction (C9 to C44). This method used a gas chromatograph with flame ionization detection (GC/FID) analysis. Method detection limits for specific analytes were in the low microgram per liter range. The results from method 8015 and 8270 analysis were added together for each sample and reported as an sTPH concentration in this report.

A complete list of analytes can be found in Appendix 5. QC samples were run in accordance with EPA method requirements. Methods for analyzing gasoline volatile range (tVOA) hydrocarbons were unchanged for these cruises.

2F.3 Subsequent Cruises and NOAA-managed Cruises

All subsequent cruises, including the "NOAA Cruises" data, appear in "The QM Database Summation of Chemistry Data as Fraction Analyzed." NOAA NOS Office of Response and Restoration. Query Manager DWH Response Database. http://querymanager.orr.noaa.gov/dr/aqua.fwx

2F.4 Summations of Petroleum Hydrocarbons

For the purpose of reporting chemistry data to the JAG, analytes for the fractions analyzed (see Appendix. 5) were summed. Therefore, all the volatile fraction (EPA method 8260) petroleum hydrocarbons were

17 U.S. Environmental Protection Agency Publication SW-846 "Test Methods for Evaluating Solid Waste, Physical/Chemical Methods"

summed to give a concentration for that fraction. The semivolatile fraction (EPA methods 8270 and 8015) was summed to obtain a single concentration. Both concentrations were reported in parts per billion. As these representations of the presence of petroleum hydrocarbons, they could be graphed and mapped for documenting the presence of oil.

2F.5 Quality Control, Quality Assurance, and Validation

QA/QC programs, procedures and samples are a cornerstone for any carefully conceived sampling and analysis plans. A spill-response effort places much pressure on the gathering of samples quickly at the risk of not necessarily gathering good representative data. MC252 posed a significant problem due to the size and extent of the spill, which required multiple sampling teams and sampling platforms to be utilized on short notice. Therefore, due to these factors many biases may have been created by the sampling teams. Biases can be introduced by two means: by sampling or by analytical work. Each bias, in its own way, can create a situation where the data must be rejected or at the least qualified.

2F.6 Sampling

Generally, a sampling plan will have many quality control samples associated with the overall plan. Trip Blanks and Sampling Blanks help determine various cross-contamination issues that might compromise analytical results from a sample. Field duplicates help to explain the homogeneity of the contaminant in the desired sampling medium.

For this report, very few of the aforementioned quality control sample data were available analytical data extracted from the Scribe Database. The only such data to be published in the Scribe Database were “field duplicate” samples collected as a duplicate and separate water subsample from the Niskin bottle. The results of the comparison of data from these duplicates are found in Appendix 6 and reflect reasonably good agreement between the results from the analysis of duplicates for dispersants and volatiles.

The exception was samples used for semivolatile fraction analysis. 124 samples used for these analyses had duplicates. Of these, 77 pairs have no significant differences in semivolatile concentrations, 47 pairs showed differences in semivolatile concentrations between duplicate analyses, with 31 of these exhibiting maximum average semivolatile concentrations in one sample pair, but no semivolatile concentrations in its duplicate. The degree to which this behavior could have affected the overall representativeness of the sampling effort is hard to determine. One possible cause for such differences between duplicate samples is that the Niskin bottle subsampling technique did not produce a homogeneous collection of oil within water samples. However, a full evaluation of this potential for sampling bias cannot be made on the basis of available data. Analysis of field duplicates pairs also took place at different laboratories introducing another potential source of variability.

Quality control sample results were better reported in the NOAA Cruises represented in the Query Manager (QM) Chemical Database. Most of these cruises were in support of Natural Resource Damage Assessment (NRDA) activities.

Duplicate field sampling results appear in both Scribe and QM databases. These samples were collected and split from the same Niskin bottle sample and are related by the station number and depth at which the sample was collected. From there, the samples took parallel paths because the samples were carried to different laboratories and were analyzed with slightly different standard operating procedures (SOP). For the most part, agreement is reasonable among these sample results. However, a number of samples had quite significant differences that were observed between the two field duplicate results. In a number of samples, the sTPH data in the Scribe database were lower than in QM. The reason for this bias is unknown at this time. Either a

systematic bias was a result of sampling technique or a particular problem occurred in the analytical standard methods. The problem could not be isolated, and corrected for this report.

2F.7 Laboratory Quality Assurance

Laboratory QA/QC was dictated by the EPA Analytical Protocols and where outlined in each specific laboratory's SOPs. These SOPs were, for the most part, guided by the SW 846 protocols, except that deviations were necessary for the "special" list of oil hydrocarbons already identified.

2F.8 Data Validation

The purpose of data validation is to determine the quality of the data by detecting and correcting laboratory errors. Effective data validation procedures are usually completely independent of the procedures of the initial data collection. Moreover, it is advisable that the individuals responsible for data validation not be directly involved with data collection. Data validation is necessary to identify data with errors, biases, and physically unrealistic values before they are used for any purpose, such as for modeling or release to the public. In addition to the laboratory QA review, datasets were evaluated and validated by experienced personnel for the following reasons:

- Conformance with requested testing requirements;
- Completeness;
- Reporting accuracy (including hardcopy of electronic data downloads);
- Confirming receipt of requested items.

2F.9 Traceability, Sensibility, and Usability of the Data

In addition to the above criteria, the data were validated with guidance from an EPA publication, "U.S. EPA Contract Laboratory Program National Functional Guidelines for Superfund Organic Methods Data Review, EPA-540-R-08-01 (June 2008)." It should be noted that these guidelines are not completely applicable to the EPA and SW-846 methods used in the Federal Response; consequently, professional judgment was used to evaluate data usability.

Data acquired by subsurface and subsea monitoring and sampling efforts are considered to be validated upon completion of QA/QC procedures. All laboratories conformed to all levels of QA reporting for the purpose of the planning sampling and analyses. One exception to the validation was data analyzed from the early stages of the Federal Response at the Louisiana State University laboratory in Baton Rouge, Louisiana. These data were not validated because some sample documentation lacked information pertaining to chain of custody or laboratory SOPs for preparation and analyses of samples. These data also had higher than normal method-detection limits (1000 ppb).

Currently, the data validation process is still ongoing. This effort will continue because of the large amount of data to be reviewed. As a result of these reviews, corrections may be made to the Scribe Database in the future. In fact, issues were raised about the VOA EPA 8260 analyses from one contract laboratory that will require changes to the minimum detection limits reported for the analytes. We are, however, confident that the major supporting chemical data will not change the JAG's conclusions that the current data supports.

The QM database prior to reporting goes through a complete third-party data validation process; therefore, all data results were validated.

2F.10 Official Databases (Scribe and QM)

The official databases for managing the subsurface analytical data for the subsurface response were EPA's Scribe and NOAA's QM. Scribe currently stores information about subsurface water column data primarily analyzed from several laboratory sources, including BP and its representatives, as well as State and Federal partners. Sampling data collected during the subsurface monitoring efforts followed data management protocols established by either the Subsurface Monitoring Unit or the data collector. The NODC serves as the official database and archive for oceanographic data collected aboard vessels.

2F.11 Qualifications on the Data—Lab Qualifiers Presently in Results Database (Scribe/QM)

Appendix 6 provides brief explanations of the qualifiers assigned to results in the Scribe and QM database for the Deepwater Horizon Federal Response. However, it should be remembered that these flags were dropped for the summation work, data reduction that the JAG elected to do. As mentioned, the summations of individual components of the oil were made by fraction analyzed, i.e., volatile fraction, tVOA, and sTPH. Readers should be reminded that, if going to the Scribe database, the following qualifiers apply only to the individual components analyzed for any given method.

2F.12 Data Flow

During the early period of the Federal Response and for most of its timeframe, data flowed from directions given by the two primary Incident Command Posts in Houma, Louisiana, and in Mobile, Alabama. From these posts, sampling plans were devised, field procedures defined, analyses outlined, and laboratories selected as needed. Data tended to flow as follows.

After collecting individual samples onboard vessels or collecting individual samples in the field onshore, samples were transferred to the Sample Receiving Office in Houma or in Mobile. Samples received at the Sample Receiving Office were unpacked, subjected to several QC checks, and repacked for shipment to the appropriate laboratory(ies) for analysis.

After analysis, reports were issued to parties identified on the Analytical Request Form or as otherwise communicated to the laboratory and electronic data, and deliverables were sent to the designated entity. For BP, the data were sent to Environmental Standards for uploading into the Equis database or to the Center for Toxicology and Environmental Health before publishing to Scribe. Data for other entities were sent to the appropriate agency (Federal or State) for uploading into their appropriate database.

Following successful loading, the data were subsequently published to Scribe. The appropriate entity was charged with performing a data validation, and in the case for much of JAG's Chemistry Data, the third-party validation is currently ongoing. The JAG then retrieved the data from Scribe and did the data reduction summation of petroleum hydrocarbon analyses. The QM Database has been fully validated, and the same process of retrieval "summation" was performed on the QM database.

References

Crout, R. and D. Conlee (2007). National Data Buoy Center (NDBC) Processing, Display, and Observation of Near-Bottom Currents Acquired by Oil and Gas Companies in the Northern Gulf of Mexico. *In* Proc., IEEE/MTS Oceans 2007 Conference, Vancouver, Canada, 5 pp.

Crout, R., D. Conlee, D. Gilhousen, R. Bouchard, M. Livington, M. Garcia, C. Cooper, and R. Raye (2006). Real-time Oil Platform Ocean Current Data in the Gulf of Mexico: An IOOS Industry Partnership Success Story. 22nd International Conference on Interactive Information and Processing Systems for Meteorology, Oceanography, and Hydrology, January 29–February 2, 2006.

Nelson, N.B., D.A. Siegel, C.A. Carlson, C. Swan, W.M. Smethie, Jr., and S. Khatiwala, 2007: Hydrography of chromophoric dissolved organic matter in the North Atlantic. *Deep-Sea Research*, Part I, 54, 710-731

Appendix 3. List of Cruises with Water Chemistry Data and Associated Databases

Cruise Identifier	Database Resource	
	Scribe	QM
05-08-2010_BrooksMcCall	X	
05-09-2010_JackFitz		X
05-15-2010_BrooksMcCall	X	X
05-19-2010_BrooksMcCall	X	X
05-21-2010_JackFitz		X
05-23-2010_BrooksMcCall	X	X
05-26-2010_OceanVeritas	X	X
05-27-2010_GordonGunter		X
05-30-2010_BrooksMcCall	X	X
06-01-2010_OceanVeritas	X	
06-01-2010_WaltonSmith	X	
06-03-2010_ThomasJefferson		X
06-03-2010_WaltonSmith	X	
06-04-2010_BrooksMcCall	X	X
06-07-2010_OceanVeritas	X	
06-10-2010_BrooksMcCall	X	X
06-11-2010_JackFitz		X
06-13-2010_OceanVeritas	X	X
06-15-2010_ThomasJefferson		X
06-16-2010_BrooksMcCall	X	X
06-17-2010_Endeavor		X
06-19-2010_OceanVeritas	X	X
06-22-2010_BrooksMcCall	X	X
06-25-2010_OceanVeritas	X	X
06-29-2010_OceanVeritas	X	X
07-04-2010_BrooksMcCall	X	X
07-07-2010_OceanVeritas	X	
07-09-2010_SewardJohnson		X
07-10-2010_BrooksMcCall	X	X
07-13-2010_OceanVeritas	X	X
07-15-2010_Ferrel	X	
07-16-2010_BrooksMcCall	X	
07-17-2010_AmericanDiver		X
07-19-2010_OceanVeritas	X	
07-26-2010_Ferrel	X	
07-26-2010_OceanVeritas	X	X
07-28-2010_BrooksMcCall	X	
07-28-2010_HenryBigelow		X
07-29-2010_AmericanDiver		X
07-30-2010_Ferrel	X	
07-31-2010_OceanVeritas	X	
08-02-2010_GordonGunter		X
08-03-2010_BrooksMcCall	X	
08-03-2010_Ferrel	X	
08-05-2010_Pisces		X
08-06-2010_OceanVeritas	X	
08-09-2010_BrooksMcCall	X	
08-12-2010_OceanVeritas	X	
08-13-2010_Ferrel	X	
08-13-2010_HenryBigelow		X
08-15-2010_BrooksMcCall	X	
08-17-2010_BunnyBordelon	X	
08-17-2010_WesBordelon	X	
08-18-2010_Ferrel	X	
08-18-2010_JackFitz	X	
08-18-2010_OceanVeritas	X	
08-18-2010_Pisces		X
08-21-2010_BrooksMcCall	X	
08-23-2010_Ferrel	X	
08-25-2010_HOSDavis		X
08-25-2010_OceanVeritas	X	
08-29-2010_BrooksMcCall	X	
08-30-2010_OceanVeritas	X	
09-02-2010_BrooksMcCall	X	
09-03-2010_OceanVeritas	X	
09-06-2010_WaltonSmith		X
09-07-2010_BrooksMcCall	X	
09-07-2010_OceanVeritas	X	
09-08-2010_SpecialtyDiver		X
09-09-2010_Pisces		X
09-11-2010_OceanVeritas	X	
09-16-2010_RyanChouest	X	
09-22-2010_OceanVeritas	X	
09-23-2010_RyanChouest	X	
09-25-2010_WaltonSmith		X
10-07-2010_RyanChouest	X	
11-01-2010_Arctic		X

Appendix 4: MC252 Reservoir Oil Composition

Sample Inventory and History

PENCOR ID No.	Sample Depth (Ft. MD)	Sample Source	Reservoir Condition (psia / °F)		Sample Date	Sample Type	Opening Condition (psia / °F)		Restoration Time (Hours)	Restoration & Transfer Condition (psia / °F)		Transfer Date	Original Sample Volume (cc)
36126-01	N/A	Active Mud pit	N/A		4/10/2010	Drilling Mud	N/A		N/A	N/A		N/A	3,500
36126-01	N/A	Active Mud pit	N/A		4/10/2010	Drilling Mud	N/A		N/A	N/A		N/A	3,500
36126-39	18,142	MRSC-147	11,856	236	4/12/2010	Reservoir Fluid	6,030	68	12	14,000	170	4/14/2010	750
36126-40	18,142	MRSC-147	11,856	236	4/12/2010	Reservoir Fluid	6,030	68	12	14,000	170	4/14/2010	750
36126-41	18,142	MRSC-147	11,856	236	4/12/2010	Reservoir Fluid	6,030	68	12	14,000	170	4/14/2010	750
36126-42	18,142	MRSC-147	11,856	236	4/12/2010	Reservoir Fluid	6,030	68	12	14,000	170	4/14/2010	750
36126-43	18,142	MRSC-147	11,856	236	4/12/2010	Reservoir Fluid	6,030	68	12	14,000	170	4/14/2010	750
36126-44	18,142	MRSC-147	11,856	236	4/12/2010	Reservoir Fluid	6,030	68	12	14,000	170	4/14/2010	750
36126-45	18,142	MRSC-147	11,856	236	4/12/2010	Reservoir Fluid	6,030	68	12	14,000	170	4/14/2010	750
36126-46	18,142	MRSC-147	11,856	236	4/12/2010	Reservoir Fluid	6,030	68	12	14,000	170	4/14/2010	750
36126-47	18,142	MRSC-147	11,856	236	4/12/2010	Reservoir Fluid	6,030	68	12	14,000	170	4/14/2010	750
36126-48	18,142	MRSC-147	11,856	236	4/12/2010	Reservoir Fluid	6,030	68	12	14,000	170	4/14/2010	750
36126-49	18,142	MRSC-147	11,856	236	4/12/2010	Reservoir Fluid	6,030	68	12	14,000	170	4/14/2010	750
36126-50	18,142	MRSC-147	11,856	236	4/12/2010	Reservoir Fluid	6,030	68	12	14,000	170	4/14/2010	750
36126-51*	18,142	MRSC-147	11,856	236	4/12/2010	Atmospheric Oil	6,030	68	12	14,000	170		425
36126-52*	18,142	MPSR-3810	11,856	236	4/12/2010	Reservoir Fluid	5,875	66	120+	14,000	170	4/22/2010	360
36126-53	18,142	MPSR-3547	11,856	236	4/12/2010	Reservoir Fluid	5,720	66	120+	14,000	170	4/22/2010	355
36126-54*	18,142	MPSR-1268	11,856	236	4/12/2010	Reservoir Fluid	5,950	66	120+	14,000	170	4/22/2010	360
36126-55	18,142	MPSR-1181	11,856	236	4/12/2010	Reservoir Fluid	6,645	66	120+	14,000	170	4/22/2010	360
36126-56	18,142	MPSR-3980	11,856	236	4/12/2010	Reservoir Fluid	6,500	66	120+	14,000	170	4/26/2010	350
36126-57*	18,142	MPSR-4065	11,856	236	4/12/2010	Reservoir Fluid	6,270	66	120+	14,000	170	4/22/2010	365

Sample Validation Data

PENCOR ID No.	Laboratory Opening Pressure	Saturation Pressure	Laboratory Analyses										Remaining Pressurized Sample
			G / L Ratio	API Gravity	Drilling Fluid	Gas Gravity	Liq Analysis	CCE	Diff Lib	Vis	MSF	ASTM Tests	
	(psia / °F)	*(psia / °F)*	*(scf / stb)*	*(API)*	*(wt % STO)*	*(Air = 1.000)*							*(cc)*
36126-44**	6,030 / 68		2,840	35.0	< 1.0	0.785	x						750
36126-53	5,720 / 66	6,504 / 243	2,819	35.2	< 1.0	0.807	x	x	x	x	x	x	0
36126-54*	5,950 / 66		2,802	35.2	< 1.0	0.808	x						0
36126-57*	6,270 / 66									x			259

* Samples from these ID numbers were shipped to other laboratories as requested by BP
** Results presented are from mobile laboratory testing that was performed onsite.

Reservoir Fluid Summary PENCOR ID No. 36126-53

Reservoir Summary

Sample Depth	18,142	Ft. MD
Reservoir Pressure	11,856	psia
Reservoir Temperature	243	°F

Stock Tank Oil Properties

Drilling Fluid Content	< 1.0	wt% STO
Drilling Fluid Type	Rheliant	
API Gravity (from R0F)	35.2	°API at 60 °F (water free)
Paraffin Content	1.8	wt%
Asphaltene Content	0.4	wt%
Sulfur Content	0.27	wt%
Wax Appearance Temp. (CPM)	89	°F
Pour Point	< -30	°F
Mini-Reid Vapor Pressure	2.86	psi
Total Acid Number	< 0.1	mg KOH / g

Fluid Properties at Reservoir Pressure & Temperature

Reservoir Pressure	11,856	psia at 243 °F
Density	0.587	g/cm3
Density	36.6	lb/ft3
FVF (from MSF)	2.131	Pres bbl/stb
Viscosity	0.168	cP
Compressibility	N/A	Dvol/vol/Dpsi x 106

Fluid Properties at Saturation Pressure & Temperature

Saturation Pressure	6,504	psia at 243 °F
Density	0.528	g/cm3
Density	33.0	lb/ft3
FVF (from MSF)	2.367	Psat bbl/stb
Viscosity	0.162	cP
Compressibility	28.50	Dvol/vol/Dpsi x 106

Flash Comparison

Experimental Procedure	GOR (SCF/stb)	FVF (Psat bbl/stb)	Gas Gravity	API at 60 °F
Reservoir Oil Single-Stage Flash	2,819	2.564	0.807	35.2
Differential Liberation at Reservoir Temperature	4,057	3.459	1.050	31.8
Multi-Stage Separator Test	2,554	2.367	0.740	38.2

Reservoir Fluid Composition	
Component	**Mole %**
N2	0.444
CO2	0.919
H2S	0.000
C1	65.467
C2	6.418
C3	4.572
iC4	0.951
nC4	2.177
iC5	0.890
nC5	1.081
C6	1.409
C7	2.010
C8	2.157
C9	1.529
C10	1.282
C11	0.944
C12	0.789
C13	0.753
C14	0.674
C15	0.564
C16	0.547
C17	0.436
C18	0.425
C19	0.360
C20	0.311
C21	0.253
C22	0.225
C23	0.203
C24	0.182
C25	0.149
C26	0.135
C27	0.141
C28	0.125

Reservoir Fluid Composition	
Component	**Mole %**
C29	0.111
C30	0.102
C31	0.096
C32	0.086
C33	0.074
C34	0.073
C35	0.060
C36	0.055
C37	0.053
C38	0.050
C39	0.043
C40	0.042
C41	0.031
C42	0.034
C43	0.031
C44	0.029
C45	0.027
C46	0.023
C47	0.025
C48	0.021
C49	0.019
C50+	0.393
C50+ Mole Wt	950.71
C50+ Sp Gr	1.148

Reservoir Fluid Composition PENCOR ID No. 36126-53

Flash Summary (14,000 psia and 170 °F to atmospheric pressure and 80 °F)

Gas-Liquid Ratio	2,819	scf/stb	Vapor Gravity	0.807	(Air = 1.00)
FVF	2.564	Vsat/Vstd	API Gravity	35.2	°API at 60 °F (Water Free)
			Water Content	0.02	weight %

Component (Symbol/Name)		Atmospheric Vapor (mole %)	Atmospheric Liquid (mole %)	Atmospheric Liquid (weight %)	Molecular Weight	Specific Gravity (Water = 1.0)	Reservoir Fluid (mole %)	Reservoir Fluid (weight %)
N_2	Nitrogen	0.528	0.000	0.000	28.01	0.809	0.444	0.237
CO_2	Carbon Dioxide	1.092	0.000	0.000	44.01	0.818	0.919	0.770
H_2S	Hydrogen Sulfide	0.000	0.000	0.000	34.08	0.801	0.000	0.000
C1	Methane	77.781	0.003	0.000	16.04	0.300	65.467	19.994
C2	Ethane	7.597	0.148	0.021	30.07	0.356	6.418	3.674
C3	Propane	5.346	0.456	0.097	44.10	0.507	4.572	3.838
iC4	i-Butane	1.080	0.263	0.073	58.12	0.563	0.951	1.052
nC4	n-Butane	2.406	0.958	0.268	58.12	0.584	2.177	2.408
iC5	i-Pentane	0.880	0.943	0.327	72.15	0.624	0.890	1.222
nC5	n-Pentane	0.995	1.536	0.533	72.15	0.631	1.081	1.484
C6	Hexanes	0.926	3.977	1.648	86.18	0.664	1.409	2.312
C7	Heptanes	0.824	8.318	3.747	93.13	0.707	2.010	3.564
C8	Octanes	0.392	11.541	5.960	106.90	0.733	2.157	4.390
C9	Nonanes	0.104	9.103	5.250	119.93	0.764	1.529	3.490
C10	Decanes	0.049	7.837	5.048	134.28	0.779	1.282	3.277
C11	Undecanes		5.965	4.215	147.00	0.790	0.944	2.643
C12	Dodecanes		4.982	3.855	161.00	0.801	0.789	2.417
C13	Tridecanes		4.754	4.000	175.00	0.812	0.753	2.507
C14	Tetradecanes		4.254	3.886	190.00	0.815	0.674	2.436
C15	Pentadecanes		3.563	3.528	206.00	0.826	0.564	2.212
C16	Hexadecanes		3.455	3.688	222.00	0.826	0.547	2.312
C17	Heptadecanes		2.755	3.139	237.00	0.839	0.436	1.968

Component (Symbol/Name)		Atmospheric Vapor (mole %)	Atmospheric Liquid (mole %)	Atmospheric Liquid (weight %)	Molecular Weight	Specific Gravity (Water = 1.0)	Reservoir Fluid (mole %)	Reservoir Fluid (weight %)
C18	Octadecanes		2.685	3.240	251.00	0.839	0.425	2.031
C19	Nonadecanes		2.274	2.874	263.00	0.847	0.360	1.803
C20	Eicosanes		1.963	2.594	275.00	0.854	0.311	1.627
C21	Heneicosanes		1.599	2.237	291.00	0.868	0.253	1.402
C22	Docosanes		1.421	2.083	305.00	0.873	0.225	1.306
C23	Tricosanes		1.281	1.959	318.00	0.878	0.203	1.228
C24	Tetracosanes		1.149	1.827	331.00	0.882	0.182	1.146
C25	Pentacosanes		0.938	1.555	345.00	0.886	0.149	0.975
C26	Hexacosanes		0.850	1.467	359.00	0.890	0.135	0.920
C27	Heptacosanes		0.892	1.603	374.00	0.894	0.141	1.005
C28	Octacosanes		0.791	1.474	388.00	0.897	0.125	0.925
C29	Nonacosanes		0.704	1.361	402.00	0.900	0.111	0.853
C30	Triacontanes		0.642	1.283	416.00	0.903	0.102	0.805
C31	Hentriacontanes		0.607	1.255	430.00	0.907	0.096	0.787
C32	Dotriacontanes		0.543	1.159	444.00	0.910	0.086	0.727
C33	Tritriacontanes		0.470	1.035	458.00	0.913	0.074	0.649
C34	Tetratriacontanes		0.458	1.039	472.00	0.915	0.073	0.652
C35	Pentatriacontanes		0.379	0.885	486.00	0.918	0.060	0.555
C36	Hexatriacontanes		0.346	0.832	500.00	0.920	0.055	0.521
C37	Heptatriacontanes		0.333	0.823	514.00	0.923	0.053	0.516
C38	Octatriacontanes		0.316	0.802	528.00	0.925	0.050	0.503
C39	Nonatriacontanes		0.273	0.712	542.00	0.927	0.043	0.446
C40	Tetracontanes		0.268	0.717	556.00	0.929	0.042	0.449
C41	Hentetracontanes		0.195	0.534	570.00	0.931	0.031	0.335
C42	Dotetracontanes		0.217	0.610	584.00	0.932	0.034	0.382
C43	Tritetracontanes		0.194	0.557	598.00	0.934	0.031	0.350
C44	Tetratetracontanes		0.186	0.548	612.00	0.936	0.029	0.343
C45	Pentatetracontanes		0.169	0.508	626.00	0.938	0.027	0.319
C46	Hexatetracontanes		0.146	0.450	640.00	0.941	0.023	0.282

Component (Symbol/Name)		Atmospheric Vapor (mole %)	Atmospheric Liquid (mole %)	Atmospheric Liquid (weight %)	Molecular Weight	Specific Gravity (Water = 1.0)	Reservoir Fluid (mole %)	Reservoir Fluid (weight %)
C47	Heptatetracontanes		0.160	0.503	654.00	0.942	0.025	0.315
C48	Octactetracontanes		0.135	0.434	668.00	0.944	0.021	0.272
C49	Nonatetracontanes		0.123	0.402	682.00	0.945	0.019	0.253
C50+	Pentacontanes Plus		2.482	11.355	950.71	1.148	0.393	7.112
Total		100.000	100.000	100.000			100.000	100.000
Calculated Mole Weight		23.28	208.03				52.53	
Measured Mole Weight			208.03					

See following pages for Liquid Analysis parameters, Different Compositional Groupings, Oil-Based Mud Calculations, Liberated gas properties, etc.
Compositional groupings based on normal to normal carbon distribution.
Pristane is included as C_{17} and Phytane is included as C_{18}.

Compositional Groupings of Reservoir Fluid

Group	Mole %	Weight %	MW	SG	Tb
Total Fluid	100.000	100.000	52.53	0.576	N/A
C7+	15.673	63.009	211.19	0.851	N/A
C10+	9.977	51.565	271.51	0.882	1,144
C20+	3.203	27.959	458.56	0.951	1,436
C30+	1.368	16.571	636.21	1.007	1,629
C50+	0.393	7.112	950.71	1.148	1,922

*Tb by Correlation

Appendix 5: Methods Used to Analyze Specific Compounds

8015 M - Tot Sat. HC - GC/FID	8260 M - PIANO VolHC - GC/MS	8270 M - Alkylated PAHs	M8270
Nonane (C9)	Benzo(b)thiophene	cis/trans-Decalin	Naphthalene
Decane (C10)	Naphthalene	C1-Decalins	C1-Naphthalenes (methyl)
Undecane (C11)	1-Methylnaphthalene	C2-Decalins	C2-Naphthalenes (ethyl)
Dodecane (C12)	2-Methylnaphthalene	C3-Decalins	C3-Naphthalenes (propyl)
Tridecane (C13)	Nonane (C9)	C4-Decalins	C4-Naphthalenes (butyl)
2,6,10 Trimethyldodecane (1380)	Decane (C10)	Benzo(b)thiophene	Fluorene
Tetradecane (C14)	Undecane (C11)	C1-Benzo(b)thiopenes	C1-Fluorenes (methyl)
2,6,10 Trimethyltridecane (1470)	Dodecane (C12)	C2-Benzo(b)thiophenes	C2-Fluorenes (ethyl)
Pentadecane (C15)	Tridecane (C13)	C3-Benzo(b)thiopenes	C3-Fluorenes (propyl)
Hexadecane (C16)	2-Methylbutane	C4-Benzo(b)thiopenes	Anthracene
Norpristane (1650)	1-Pentene	Naphthalene	Phenanthrene
Heptadecane (C17)	2-Methyl-1-butene	C1-Naphthalenes (methyl)	Dibenzothiophene
Pristane	Pentane	C2-Naphthalenes (ethyl)	C1-Dibenzothiophenes (methyl)
Octadecane (C18)	2-Pentene (trans)	C3-Naphthalenes (propyl)	C2-Dibenzothiophenes (ethyl)
Phytane	2-Pentene (cis)	C4-Naphthalenes (butyl)	C3-Dibenzothiophenes (propyl)
Nonadecane (C19)	Tertiary butanol	Biphenyl	Fluoranthene
Eicosane (C20)	Cyclopentane	Dibenzofuran	Pyrene
Heneicosane (C21)	2,3-Dimethylbutane	Acenaphthylene	Naphthobenzothiophene
Docosane (C22)	2-Methylpentane	Acenaphthene	C1-Naphthobenzothiophenes
Tricosane (C23)	Methyl-Tert-Butyl Ether	Fluorene	C2-Naphthobenzothiophenes
Tetracosane (C24)	3-Methylpentane	C1-Fluorenes (methyl)	C3-Naphthobenzothiophenes
Pentacosane (C25)	1-Hexene	C2-Fluorenes (ethyl)	Benzo(a)anthracene
Hexacosane (C26)	Hexane, n-	C3-Fluorenes (propyl)	C1-Chrysenes (methyl)
Heptacosane (C27)	Diisopropyl ether	Anthracene	C2-Chrysenes (ethyl)
Octacosane (C28)	Ethyl Tertiary Butyl Ether	Phenanthrene	C3-Chrysenes (propyl)
Nonacosane (C29)	2,2-Dimethylpentane	C1-Phenanthrenes/ anthracenes	C4-Chrysenes (butyl)
Triacontane (C30)	Methylcyclopentane	C2-Phenanthrenes/ anthracenes	Benzo(b)fluoranthene
Hentriacontane (C31)	2,4-Dimethylpentane	C3-Phenanthrenes/ anthracenes	Benzo(e)pyrene
Dotriacontane (C32)	1,2-Dichloroethane	C4-Phenanthrenes/ anthracenes	Benzo(a)pyrene
Tritriacontane (C33)	Cyclohexane	Retene	Perylene

8015 M - Tot Sat. HC - GC/FID	8260 M - PIANO VolHC - GC/MS	8270 M - Alkylated PAHs	M8270
Tetratriacontane (C34)	2-Methylhexane	Dibenzothiophene	Indeno(1,2,3-c,d)pyrene
PentaTriacontane (C35)	Benzene	C1-Dibenzothiophenes (methyl)	Dibenzo(a,h)anthracene
HexaTriacontane (C36)	2,3-Dimethylpentane	C2-Dibenzothiophenes (ethyl)	Benzo(g,h,i)perylene
HeptaTriacontane (C37)	Thiophene	C3-Dibenzothiophenes (propyl)	Decane (C10)
OctaTriacontane (C38)	3-Methylhexane	C4-Dibenzothiophenes (butyl)	Undecane (C11)
NonaTriacontane (C39)	tert-Anyl methyl ether	Benzo(b)fluorene	Dodecane (C12)
Tetracontane(C40)	1-Heptene/1,2-DMCP (trans)	Fluoranthene	Tridecane (C13)
Total Extractable Matter (C9-C44)	Isooctane	Pyrene	Tetradecane (C14)
	Heptane	C1-Fluoranthenes/pyrenes	Pentadecane (C15)
	Methylcyclohexane	C2-Fluoranthenes/pyrenes	Hexadecane (C16)
	2,5-Dimethylhexane	C3-Fluoranthenes/pyrenes	Heptadecane (C17)
	2,4-Dimethylhexane	C4-Fluoranthenes/pyrenes	Pristane
	2,2,3-Trimethylpentane	Naphthobenzothiophene	Octadecane (C18)
	2,3,4-Trimethylpentane	C1-Naphthobenzothiophenes	Phytane
	2,3,3-Trimethylpentane	C2-Naphthobenzothiophenes	Nonadecane (C19)
	2,3-Dimethylhexane	C3-Naphthobenzothiophenes	Eicosane (C20)
	3-Ethylhexane	C4-Naphthobenzothiophenes	Heneicosane (C21)
	2-Methylheptane	Benzo(a)anthracene	Docosane (C22)
	3-Methylheptane	Chrysene + Triphenylene	Tricosane (C23)
	Toluene	C1-Chrysenes (methyl)	Tetracosane (C24)
	2-Methylthiophene	C2-Chrysenes (ethyl)	Pentacosane (C25)
	3-Methylthiophene	C3-Chrysenes (propyl)	Hexacosane (C26)
	1-Octene	C4-Chrysenes (butyl)	Heptacosane (C27)
	Octane	Benzo(b)fluoranthene	Octacosane (C28)
	1,2-Dibromoethane	Benzo(j+k)fluoranthene	Nonacosane (C29)
	Ethylbenzene	Benzo(a)fluoranthene	Triacontane (C30)
	2-Ethylthiophene	Benzo(e)pyrene	Hentriacontane (C31)
	Xylene, m,p-	Benzo(a)pyrene	Dotriacontane (C32)
	1-Nonene	Perylene	Tritriacontane (C33)
	Styrene	Indeno(1,2,3-c,d)pyrene	Tetratriacontane (C34)
	Xylene, ortho-	Dibenzo(a,h)anthracene	PentaTriacontane (C35)
	Cumene	Benzo(g,h,i)perylene	
	Propylbenzene, n-	Carbazole	
	1-Methyl-3-ethylbenzene	4-Methyldibenzothiophene	
	1-Methyl-4-ethylbenzene	2/3-Methyldibenzothiophene	
	Benzene, 1,3,5,-trimethyl	1-Methyldibenzothiophene	
	1-Decene	3-Methylphenanthrene	

8015 M - Tot Sat. HC - GC/FID	8260 M - PIANO VolHC - GC/MS	8270 M - Alkylated PAHs	M8270
	1-Methyl-3-isopropylbenzene	2/4-Methylphenanthrene	
	1,2,4-Trimethylbenzene	2-Methylanthracene	
	Butylbenzene, sec-	9-Methylphenanthrene	
	Methylpropylbenzene	1-Methylnaphthalene	
	4-Cymene	2-Methylnaphthalene	
	1-Methyl-2-isopropylbenzene	2,6-Dimethylnaphthalene	
	2,3-dihydroindene	1-Methylphenanthrene	
	1-Methyl-3-propylbenzene	2,3,5-Trimethylnaphthalene	
	1-Methyl-4-propylbenzene	Hopane	
	Butylbenzene, n-		
	4-Ethyl-1,2-dimethylbenzene		
	1,2-Diethylbenzene		
	1-Ethyl-2-methylbenzene		
	2-Ethyl-1,4-dimethylbenzene		
	1,3-Dimethyl-4-ethylbenzene		
	1,3-Dimethyl-5-ethylbenzene		
	2-Ethyl-1,3-dimethylbenzene		
	1-Ethyl-2,3-dimethylbenzene		
	1,2,4,5-Tetramethylbenzene		
	Pentylbenzene		
	Methylcymantrene		

Appendix 6: Results of Comparisons of Field Duplicates from Scribe Databases

TOTAL NUMBER OF WATER SAMPLES	**400 pairs**
Total number of water samples analyzed for dispersants	112 pairs
Number of identical duplicate analyses	111 pairs
Number of different duplicate analyses	1 pair
Total number of water samples analyzed for semivolatiles	124 pairs
Number of identical duplicate analyses	77 pairs
Number of different duplicate analyses	47 pairs
Total number with max difference = 1	31 pairs
Numbers that differ because of a TIC	0 pairs
Total number with max difference between 0.1 and 1	6 pairs
Numbers that differ because of a TIC	2 pairs
Total number with max difference between 0 and 0.1	10 pairs
Numbers that differ because of a TIC	0 pairs
Total number of water samples analyzed for volatiles	119 pairs
Number of identical duplicate analyses	96 pairs
Number of different duplicate analyses	23 pairs
Total number with max difference = 1	4 pairs
Number that differ because of a TIC	0 pairs
Total number with max difference between 0.1 and 1	7 pairs
Numbers that differ because of a TIC	7 pairs
Total number with max difference between 0 and 0.1	12 pairs
Numbers that differ because of a TIC	3 pairs